AD NUMBER

AD866147

NEW LIMITATION CHANGE

TO

Approved for public release, distribution unlimited

FROM

Distribution authorized to U.S. Gov't. agencies and their contractors; Critical Technology; FEB 1970. Other requests shall be referred to Air Force Aero Propulsion Laboratory, Attn: APIP-3, Wright-Patterson AFB, OH 45433.

AUTHORITY

AFAPL ltr, 12 Apr 1972

NICKEL HYDROXIDE ELECTRODE RESEARCH

First Interim Technical Report

January - December 1969

Contract No. F33615-69-C-1312

Project No. 3145

Prepared for

DEPARTMENT OF THE AIR FORCE
HEADQUARTERS AERONAUTICAL SYSTEMS DIVISION (AFSC)
AIR FORCE AERO PROPULSION LABORATORY
WRIGHT-PATTERSON AIR FORCE BASE, OHIO

Attn: APIP-3

Prepared by

General Electric Company
Research and Development Center
Schenectady, New York

and

Battery Business Section
Gainesville, Florida

S-70-1025

NOTICES

When Government drawings, specifications, or other data are used for any purpose other than in connection with a definitely related Government procurement operation, the United States Government thereby incurs no responsibility nor any obligation whatsoever; and the fact that the Government may have formulated, furnished, or in any way supplied the said drawings, specifications, or other data, is not to be regarded by implication or otherwise as in any manner licensing the holder or any other person or corporation, or conveying any rights or permission to manufacture, use, or sell any patented invention that may in any way be related thereto.

This document is subject to special export controls and each transmittal for foreign governments or foreign nationals may be made only with prior approval of the Headquarters Aeronautical Systems Division (AFSC), Air Force Aero Propulsion Laboratory, Wright-Patterson Air Force Base, Ohio 45433.

The distribution of this report is limited because it contains technology identifiable with items on the strategic embargo lists excluded from export or re-export under U.S. Export Control Act of 1949 (63 Stat. 7), as amended (50 U.S.C. App. 2020, 2031) as implemented by AFR 400-10.

Copies of this report should not be returned unless return is required by security considerations, contractual obligations, or notice on a specific document.

NICKEL HYDROXIDE ELECTRODE RESEARCH

First Interim Technical Report

January - December 1969

Contract No. F33615-69-C-1312

Project No. 3145

Prepared for

DEPARTMENT OF THE AIR FORCE
HEADQUARTERS AERONAUTICAL SYSTEMS DIVISION (AFSC)
AIR FORCE AERO PROPULSION LABORATORY
WRIGHT-PATTERSON AIR FORCE BASE, OHIO

Prepared by

General Electric Company
Research and Development Center
Schenectady, New York

and

Battery Business Section
Gainesville, Florida

FOREWORD

This First Interim Technical Report covers work performed from 1 January 1969 to 2 February 1970 under Contract No. F33615-69-C-1312, Project No. 3145, "Nickel Hydroxide Electrode Research." It was prepared by the General Electric Research and Development Center, Schenectady, New York and the General Electric Battery Business Section, Gainesville, Florida for the Department of the Air Force Headquarters Aeronautical Systems Division (AFSC), Air Force Aero Propulsion Laboratory, Wright-Patterson Air Force Base, Ohio. The program monitor is Mr. J.E. Cooper, APIP-3.

Dr. H. A. Christopher, the technical coordinator of the Physical Chemistry Laboratory of the Research and Development Center is Program Manager. The program is a joint effort of two General Electric Departments, with Dr. D.H. Kröger of the Blectronic Capacitor and Battery Department, Battery Business Section, as Project Engineer.

The following personnel have contributed to this program in the areas indicated:

Program Management

Dr. H. A. Christopher

Study of Additives

Dr. J. L. Weininger
Mr. J.G. Ruzzo

Substrate Evaluation

Dr. H. A. Christopher
Dr. R. F. Thornton
Mr. P.J. Moran

Ideal Structure Analysis

Dr. H. A. Christopher
Dr. R. F. Thornton

Plate Fabrication and Pretest Evaluation

D. R. F. Thornton
Dr. A. A. Catherino
Mr. J. G. Ruzzo
Mr. P.J. Moran

Memory Analysis

Dr. H. H. Kröger

Literature Survey and Evaluation

Dr. J. L. Weininger

The information and assistance received from the following contributors is gratefully acknowledged:

Research and Development Center	--	Dr. W. N. Carson
Battery Business Section	--	Mr. A J. Catotti
Battery Business Section	--	Mr. C. Rampel
Battery Business Section	--	Mr. P.R. Voyentyie

TABLE OF CONTENTS

LIST OF ILLUSTRATIONS

LIST OF ILLUSTRATIONS (Cont'd)

LIST OF TABLES

LIST OF TABLES (Cont'd)

Section 1

INTRODUCTION AND APPROACH

This report covers work performed during the first year of a three-year program aimed at developing an improved nickel hydroxide electrode for use in rechargeable alkaline batteries for aerospace applications. The improvements sought in this study were primarily concerned with achieving a higher nickel electrode performance capability from the standpoint of energy density, charge efficiency and capacity reproducability in nickel-cadmium, nickel-zinc or nickel-iron cell systems. The specific objectives of this program were, therefore, the development of nickel hydroxide electrodes:

- With a minimum capacity of eight ampere-hours per inch^3 when discharged at the five-hour rate at room temperature
- With a charge efficiency of 98% when charged at room temperature at the five-hour rate
- With a capacity uniformity of $\pm$ 1% after a minimum of 200, 50% depth-of-discharge cycles at the five-hour rate at room temperature
- By a process offering maximum ease of fabrication and formation while still complying with the above objectives

It was decided at the outset of this program that the best approach to meeting these objectives would be through a research program in which the first year would be devoted to a critical examination of the electrode structure, alternative fabrication techniques, and the role of additives. When the characteristics of the most promising electrode design and fabrication technique have been sufficiently identified through this examination, efforts will be devoted to advanced electrode testing, further electrode and process development refinements, and production on a pilot-line basis to produce 20 ampere-hour, sealed nickel-cadmium cells for final evaluation.

In order to efficiently perform the various analytical and experimental investigations required, five independent tasks were established for the present reporting period. The scope of each of these tasks is briefly outlined below:

1. Additive Study. An experimental study to assess the various effects of cobalt and other additives to the active electrode material was conducted, and included a determination of the extent and effect of zinc oxide absorption in nickel hydroxide electrodes when coupled with zinc-negative plates. Chemical, physical, crystallographic and electrochemical aspects of the electrode were considered in an effort to better understand the possible mechanisms associated with the operation of the electrode and the role of additives in general.

2. Substrate Evaluation. A corrosion-resistance evaluation of various candidate substrate materials as a means for meeting the capacity reproducability goal was conducted. Since it is known that pure nickel will corrode to some extent during cycling (leading to a possible increase in the amount of active material present), practical alternatives to conventional nickel substrate materials were examined.

3. Ideal Structure Analysis. A theoretical analysis to identify and characterize the "ideal" structure in terms of the effects of pore size porosity plate thickness and the relative amounts of conductor and active material on the available electrode energy density was conducted. These results could also provide useful assistance in the experimental work of the fabrication task.

4. Fabrication Evaluation. Experimental work in which electrodes were prepared by various methods and electrochemically and chemically analyzed to determine the optimum plate fabrication and active material loading technique with respect to the overall goals of this program was conducted. Conventional electrode preparations as well as electrodeposited and pasted processes were examined in the course of this work. In conjunction with the ideal structure analysis, experiments were made to determine the effects of substrate pore size and general configuration on the active material utilization and associated electrode behavior. The most promising plate structures were subjected to pretesting under sealed-cell conditions. The test used nickel-positive plates of a size suitable for 20 ampere-hour cells and commercially available cadmium counter electrodes.

5. Memory Analysis. An experimental task in which a systematic sequence for cycling and for electrically and chemically analyzing a series of commercially available "sub-C" cells was established to determine the extent and site of cell capacity loss with cycling. Particular attention was focused on the nickel electrode to determine whether it is the contributing factor to such memory effects commonly experienced in rechargeable nickel-cadmium battery applications.

Literature pertinent to the work of the overall program has been evaluated and discussed in the appropriate technical sections of this report. Additional references, with titles, which were not cited in the present report have been arranged according to the subject matter and are presented in the Appendix I, "Bibliography."

The major conclusions and corresponding recommendations based on the present results of this program are presented at the end of each of the technical sections of this report and are briefly summarized in Section 7.

Section 2

THE EFFECT OF ADDITIVES ON THE $Ni(OH)_2$ ELECTRODE

INTRODUCTION

For a discussion of the effect of additives on the $Ni(OH)_2$ electrode, it is first necessary to understand the mechanism of the electrode itself without any additive. This involves not only the chemical transformations of the electrode reactions, but also extremely intricate structural changes of the polycrystalline $Ni(OH)_2$ active mass during the course of charge and discharge. The complexity of the electrode mechanism arises from the physical and chemical nature of a system that is heterogeneous, highly disordered, and subject to irreversible or highly hindered reactions under the driving force of an electric field, particularly with respect to the effect of additives.

It is, therefore, not surprising to find a large amount of literature filled with contradictory statements. Examples of a general treatment of the whole field of nickel/cadmium batteries are the comprehensive works of Milner and Thomas (Ref. 1) and Falk and Salkind (Ref. 2). In addition to these two works, it may be best to select different schools of work for review of the literature; a selection of works in which different aspects of the problem have been studied extensively, and in which many of the conclusions have stood the test of time.

Briggs, Wynne-Jones and their co-workers (Refs. 3 and 4) may have been the first to recognize the crucial importance of the connection between an electrode reaction mechanism and crystal morphology. They proposed a structural model of mixed-layer lattices with large surface areas. The crystalline shape was generally laminar, permitting the penetration into the spaces between layers by ionic species and water molecules. Concomitant changes in electrical conductivity were also recognized.

The structure of $Ni(OH)_2$ in its various aspects was further elucidated by Bode and co-workers (Refs. 5, 6, and 7) and by Tuomi (Refs. 8 through 11), among others. Basic to this structure is the layer structure of the active mass through which Lukovtsev (Refs. 12 through 14) articulated what Wynne-Jones and co-workers anticipated, namely, proton diffusion. Bode established the existence of different crystal structures, notably a hydrated hydroxide, α - $3Ni(OH)_2 \cdot 2H_2O$. It is oxidized to γ - NiOOH which, in concentrated alkali, converts to the form common in battery application, β - $Ni(OH)_2$ with brucite structure. Both α and γ phases contain water of hydration. α - $Ni(OH)_2$ also has a lattice structure in which the water molecules are assigned definite locations in a hexagonal structure, with unit cell value of the c-axis as c = 8.09 angstroms. Such wide spacing of layer lattices obviously makes for greater ion and water mobility. On exposure to battery conditions, this structure is

irreversibly changed to β - $Ni(OH)_2$, also reflecting a change in density from α-to β-phase from 2.50 to 3.85 g/cm³. Tuomi (Ref. 9) obtained the γ-phase in its oxidized form by overcharging the $Ni(OH)_2$ electrode, but he chooses to call it α - hydroxide, citing precedence of a previous publication (Ref. 8). He concluded that, on the basis of extensive x-ray diffraction studies, the oxidation-reduction process is described inadequately by a proton diffusion process (Ref. 11). Alkali ions, hydroxyl ions, and water molecules contribute significantly to the reaction mechanism.

The evolution of oxygen, the oxidation state of nickel, and its relative stability in the charge and overcharge condition are of particular importance in battery operation. These factors, relating to charge acceptance and retention, have been studied by Conway and co-workers (Refs. 15 through 22) and most recently by Scarr (Ref. 23) and MacArthur (Ref. 24). Many different reaction paths are suggested for the overall oxidation of $Ni(OH)_2$ and OH^- to NiOOH and O_2. The question of the ultimate oxidation state of nickel on overcharge is still unanswered. It is certainly larger than three, but there is no concrete evidence for even a relatively stable +4 state under battery conditions, so that a value higher than three could be attributed to absorbed or otherwise occluded oxygen atoms in the irregular active battery mass. It is fundamental that under standard conditions the oxidation of $Ni(OH)_2$

$$Ni(OH)_2 + OH^- = NiOOH + H_2O + e^-$$

has a potential (versus Hg/HgO) of $E^\circ = 0.414$ v, as compared with the oxygen evolution,

$$4\,OH^- = O_2 + 2\,H_2O + 4\,e^- \text{ at } E^\circ = 0.307$$

In spite of the favorable thermodynamic values favoring oxygen evolution, the nickel electrode in secondary battery systems is a reality because of the much higher overvoltage of the oxygen evolution process on charging the nickel electrode. Herein lies the importance of the study of additives to $Ni(OH)_2$. They may contribute to the distortion or perfection of crystal lattice structure, thereby helping or hindering beneficial or detrimental processes. The additives may also contribute to an increased overvoltage of the oxygen reaction and to a decrease in the self-discharge of active mass directly through the change in crystal structure, from surface modification, or from chemical bulk effects.

The above was recognized and, for the first time, systematically attacked by Doran in a series of studies on the addition of cobalt, magnesium, manganese, and cadmium to the nickel hydroxide positive electrode (Refs. 25 and 26) Later on he added scandium to this list (Ref. 27). The literature up to about 1962 was summarized by Casey and co-workers (Ref. 28). Figure 1 indicates (in the form of a periodic table) the extensive testing of different cation additions to the $Ni(OH)_2$ lattice. The circled symbols of berium, silicon, and lead indicate that in later work by Harivel and associates these three elements were the only additional new ones tested (Refs. 29 through 32).

	I	II	III	IV	V	VI	VII	VIII
2	Li	Be	B					
3	Na	Mg	Al	Si				
4	K / Cu	Zn	Sc		As	Cr	Mn	Fe Co
5	Rb / Ag	Cd		Sn	Sb	Mo		
6	Cs	Ba / Hg	RARE EARTH	Pb	Bi	W		

Figure 1. Tests of Additives to $Ni(OH)_2$ Reported in Literature. (Circles Indicate New Additives After Casey's Review in Reference 27. Squares Indicate Present Investigation.)

In spite of the many insights into the structural complexity of the nickel hydroxide electrode in Casey's own work as well as in his review, he still considered the status of the problem confused in 1962. So, it remains today. This may well be attributed to the difficulty of reproducing original electrode conditions from one experiment to the next, especially from one laboratory to another. The positive results of Casey's study referred to the enhancement and maintenance of electrode capacity at high temperature (55°C) by the addition of lithium ions to $Ni(OH)_2$. Mention of a beneficial effect of Al (III) was also made. This was studied systematically by Harivel et al (Ref. 30).

Harivel and Laurent (Ref. 29) determined by x-ray analysis that $Co(OH)_2$ and $Ni(OH)_2$ were isomorphous, forming solid solutions. By observing the decomposition of the higher oxides, they were led to believe that the role of cobalt was to stabilize the hydroxide lattice by blocking oxygen diffusion. In the study of aluminum addition, nickel aluminate (Ref. 30), $NiAlO_2$ was found to have a structure similar to γ-NiOOH so that the aluminum addition may tend to maintain the desirable γ structure over the β-phase. Harivel's thesis (Ref. 32) contains a comprehensive overview of the structural factors, and distinguishes clearly between α-, β- and γ-$Ni(OH)_2$. In addition to general information on the crystal structure induced by foreign ions, it also presents magnetochemical evidence for a nickel +4 oxidation state. Yet, in a detailed performance analysis of $Ni(OH)_2$ electrodes with many different additives (Refs. 30 and 31) the results are as conflicting as in Casey's earlier review. Harivel employed the following two criteria for electrochemical characterization of the electrodes.

- Electrode capacity after the fifth formation cycle
- The capacity after open-cell stand for 15 days at 50°C in 7N KOH, following a sixth recharge

A clear distinction of the effect on crystal structure, β-versus γ-phase, was found, but the effect of additives on capacity was inconclusive and tended more nearly to indicate an adverse result. Previous reports of beneficial effects, such as those of Doran (Refs. 25 through 27), were attributed to the more lightly impregnated sintered nickel plates of Doran's work as compared with the commercial plates used by Harivel.

EXPERIMENTATION

A major part of this work was the elucidation of the effect of additives on $Ni(OH)_2$ electrodes. This work effort was to be done by an experimental, voltametric method in which electrodes were subjected to slow linear sweep voltametry. The structure of the electrodes was varied in a direction of increasing physical complexity from anodized plain polycrystalline nickel foils to commercially impregnated sintered plates. The former would most clearly yield results showing the electrochemical factors of the electrode reaction, whereas the latter would have these results changed by the structural factors introduced in the design of a practical nickel/cadmium cell.

Cell Design

The basic cell design for the additive study is shown in Figure 2 and consists of a three-inch outer diameter cast acrylic (or PTFE) tank into which the nickel test electrode, the cadmium counter electrode, and a reference electrode are immersed. For the initial experiments, the nickel electrodes were 99.99% pure, 0.005-inch thick foil with an area of approximately 1 cm^2. Both platinum and cadmium electrodes were used as counter electrodes. They gave equivalent results so that, for most of the work, a sintered-plate type cadmium electrode with a surface of 4 cm^2 was used. The reference electrode was a mercury-mercury oxide electrode housed in 5-mm Pyrex glass tubing. Gas bubbles maintained an argon atmosphere above the electrolyte solution.

Test Circuit

Following previous work (Refs. 33 and 34), the multipulse circuit of Figure 3 was used to study the anodized $Ni(OH)_2$ films. In this circuit, the test electrode was subjected to a series of programmed, constant-potential steps prior to potentiostatic or galvanostatic voltage sweeps. The object was to prepare the nickel electrode by cleaning the surface electrochemically, adding cobalt or other impurities in a controlled manner, then oxidizing the surface in alkali to a state corresponding to a discharged battery plate ($Ni(OH)_2$). Finally, this was followed by alternately charging and discharging the electrode between the Ni(II) and Ni(III+) states.

The potential sequence is shown in Figure 4, which also gives a typical voltamogram resulting from the triangular voltage sweep. In later parts of the program, when the active electrode material consisted of formed $Ni(OH)_2$ (either by cathodic precipitation or by impregnation of a sintered matrix), the preliminary potential steps were no longer applicable. Thus, electrodes were cycled in a triangular manner immediately on immersion in the electrolyte solution. In this case, it became important to observe the first and early cycles.

The current/voltage curve of the triangular voltage sweep (Figure 4) is the basis of this study. The oscilloscope trace has an oxidation step corresponding to the anodic process Ni(II) → Ni(III), which occurs with a capacity (charge) Q_A. At a sweep rate of dE/dt, it reaches an anodic peak current i_a and peak voltage E_a. An inflection point is noted when a second anodic process, the evolution of oxygen, becomes noticeable. Similarly, the cathodic step has a discharge capacity, Q_C, and peak values of E_C and i_c.

Voltametric Cycling

As mentioned previously, experiments were successively performed on structurally more complex electrodes. These are listed in Table 1, in sequence with respect to the electrode and the additive used, to the electrolyte, and to the temperature.

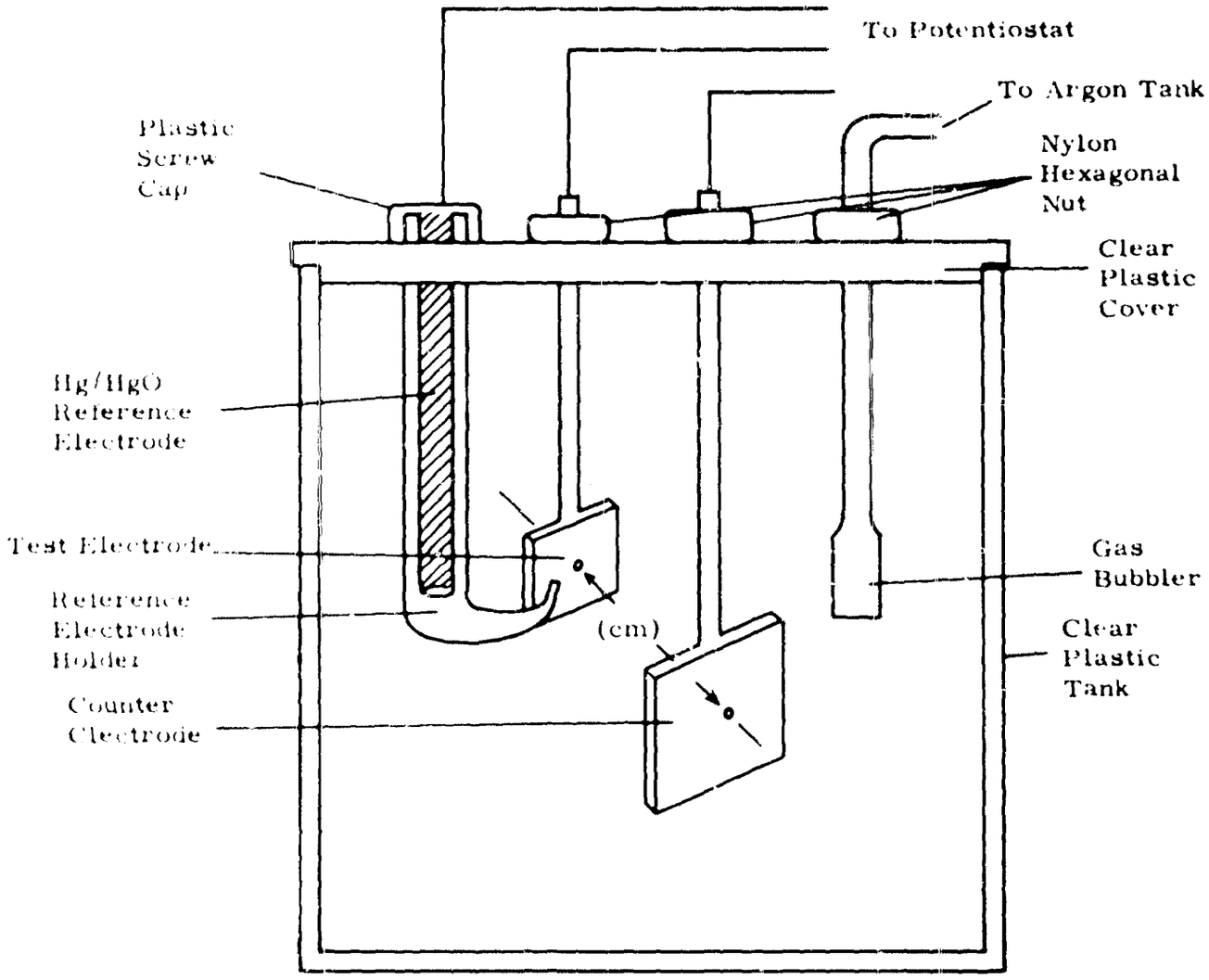

Figure 2. Cell for Additive Study

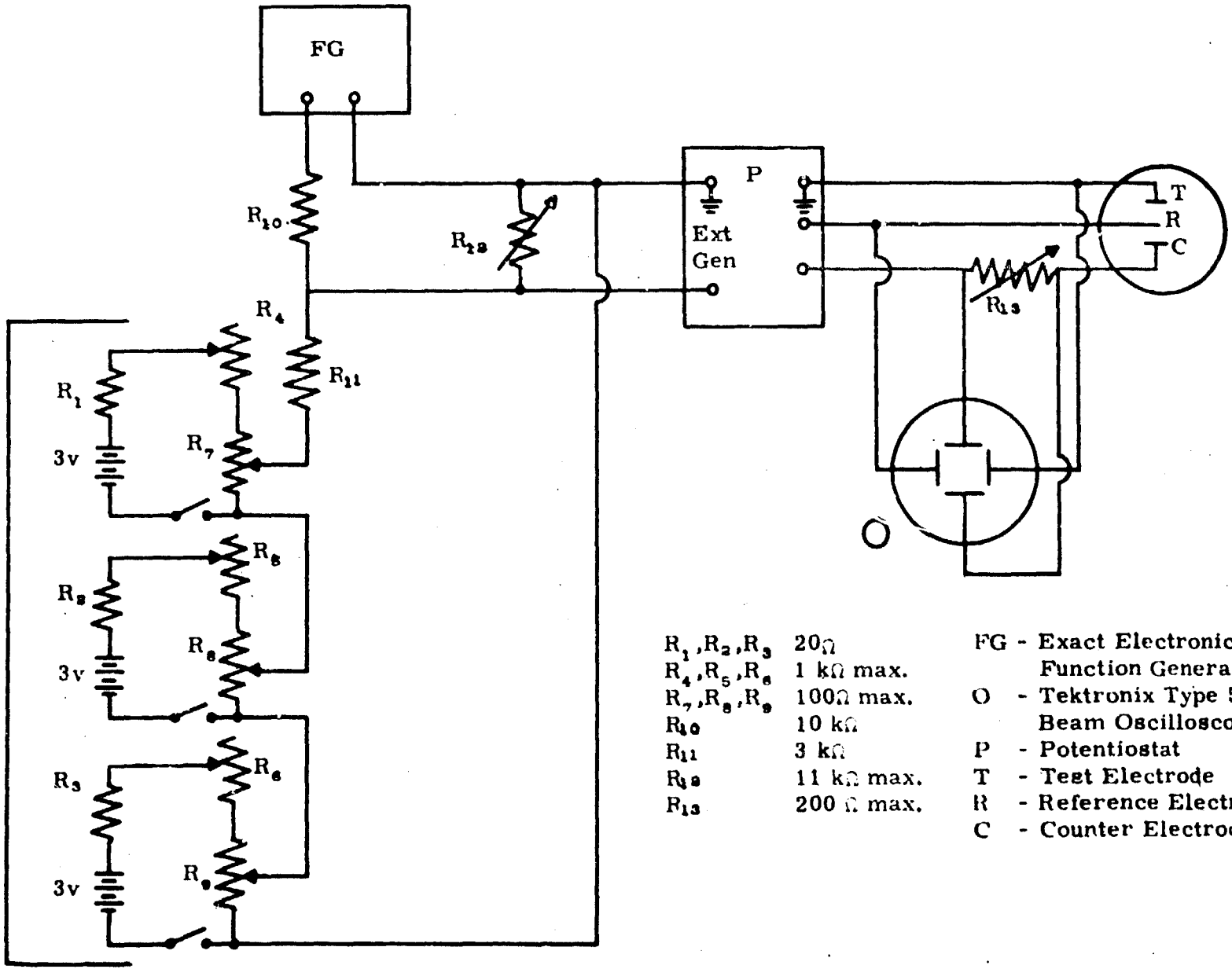

R_1, R_2, R_3	20Ω	FG	- Exact Electronics Type 255 Function Generator
R_4, R_5, R_6	1 kΩ max.		
R_7, R_8, R_9	100Ω max.	O	- Tektronix Type 502 Dual Beam Oscilloscope
R_{10}	10 kΩ		
R_{11}	3 kΩ	P	- Potentiostat
R_{12}	11 kΩ max.	T	- Test Electrode
R_{13}	200 Ω max.	R	- Reference Electrode
		C	- Counter Electrode

Figure 3. Test Circuit for Additive Study

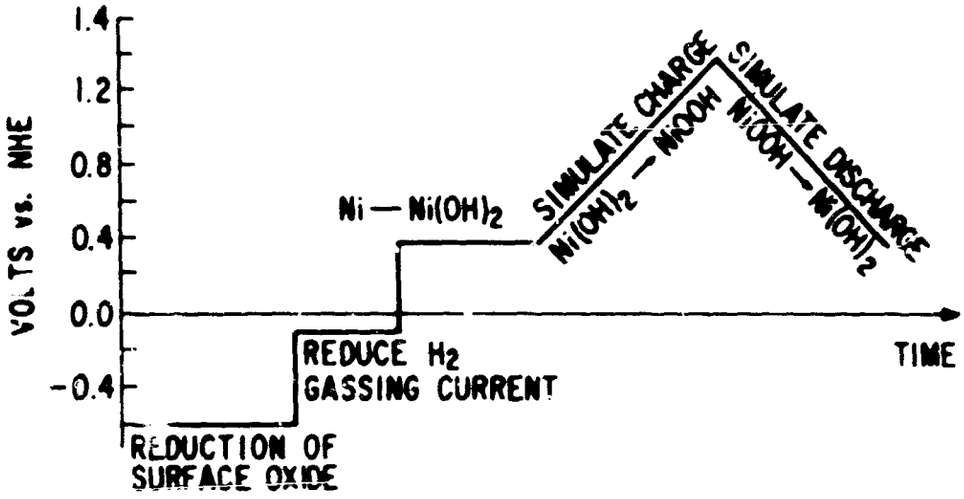

POTENTIAL SEQUENCE

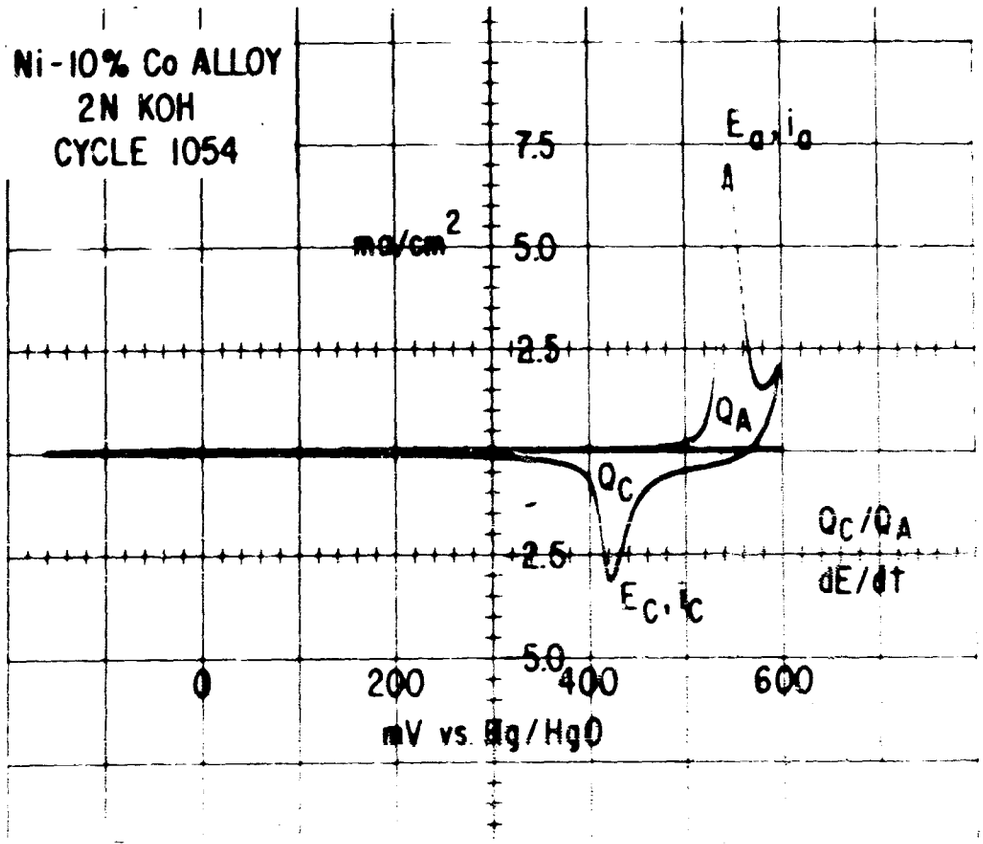

TYPICAL CYCLIC i vs. E CURVE FOR NICKEL

Figure 4. Potential Sequence and Typical Voltamogram

Table 1

SUMMARY OF VOLTAMETRIC EXPERIMENTS

	Electrode	Electrolyte	Temperature (°C)
a	Polycrystalline nickel foil	0.2N, 2N, and 6N KOH	23*
b	Nickel and cobalt, co-deposited on nickel foil	0.2N KOH	23
c	89.8% nickel, 10.2% cobalt alloy	2N, 6N KOH	23
d	Cathodically precipitated hydroxides		
	100% Nickel	6N KOH	23 and 45
	10% Cobalt**	6N KOH	23 and 45
	100% Cobalt	2N KOH	23
	5% Zinc	6N KOH	23
	100% Nickel	6N KOH containing 10g/1 ZnO	23
	5% Zinc	6N KOH containing 10g/1 ZnO	23 and 45
	5% Aluminum	6N KOH	23 and 45
	5% Cadmium	6N KOH	23 and 45
	100% Nickel	4.3N KOH + 1N LiOH	23 and 45

*Room Temperature

**Percent of cations, remainder nickel

Experimental Procedure for Planar Electrodes

All nickel electrodes were chemically polished before testing in a solution of 50 ml HOAC, 30 ml HNO_3, 10 ml H_2SO_4, and 10 ml H_3PO_4 at 90°C. The samples were then rinsed in distilled water free of dissolved oxygen and immersed in the test cell at a potentiostatically controlled cathodic potential

to reduce the small amount of surface oxide formed during the polishing and immersing operation. At cathodic potentials, there was also concurrent gassing of hydrogen. Subsequent potential steps were used to further cleanse the surface, to reduce the hydrogen gassing current, and to oxidize nickel to $Ni(OH)_2$. A triangular potential sweep was then used to simulate charge/discharge cycling. The potential sequence used in these preliminary studies is shown in Figure 4. The time basis was variable. Most measurements were made at a moderately slow sweep rate of about 18.5 mv/sec, although at the end of most experiments faster and slower sweep rates were also used. This experimental procedure is explained in greater detail in Table 2.

Cycling of Anodized Polycrystalline Nickel Foils. Current-voltage curves such as those of Figure 4 give both qualitative and quantitative results. The latter are obtained by direct observation and graphical integration of the oscilloscope traces. Table 3 gives the anodic and cathodic parameters for plana nickel foils at three different KOH concentrations. The magnitude of the anodic charge is in agreement with previous work (Ref. 33) on nickel anodization. It was surprising, however, that treatment in 6N KOH compared with that in 0.2N or 2N KOH did not increase the extent of surface oxidation beyond the two or three indicated monolayers of $Ni(OH)_2$. It was expected that 15 to 20 such layers could be formed on a planar electrode (as seen in Table 2), which would have been equivalent to the surface oxides on a battery plate. Such heavy anodization corresponds to severe corrosion in alkali. Since this would have been obtained at the cost of losing the identity of the surface, it was decided to proceed to cathodic precipitation of the active hydroxide mass.

A positive aspect of the thin-film experiments was the qualitative interpretation of the electrochemical reaction. For example, the following observations were made in experiments involving 0.2N KOH electrolyte:

1. In the first 100 cycles, the peak corresponding to the oxidation of Ni(II) shifted steadily to more positive values. This was not observed in 2N or 6N KOH.
2. Visible oxygen gassing occurred at about 560 mv (versus Hg/HgO) regardless of experimental conditions, and it did not change with cycling.
3. The extent of oxygen gassing affected subsequent cathodic discharge, which reached a maximum at 400 to 430 mv.
4. With cycle life, the separation between the two oxidation processes is reduced on the voltage scale. Thus, the process $Ni(II) \rightarrow Ni(III)$ becomes more passivated and finally merges into the oxygen evolution process, which still begins with substantial current density at about 560 mv.

Table 2

FUNCTION, OPERATIONS, AND VARIABLES IN INDIVIDUAL STEPS OF VOLTAMETRIC PROCEDURE

Step	Method	Function	Operation	Variables
1	Exposure to KOH at negative-controlled potential	Remove oxide scale	Hydrogen evolution and cathodic reduction of oxide	i, E, and t. Electrode reaction as function of constant potential, $i = f(E,t)$ where t = time of exposure
2	Decrease of hydrogen evolution current at clean metal surface	Reaching quiescent stage. This step is sensitive to impurities and indicates their presence	Time at rest without stirring. Cathodic and/or anodic pulses if necessary	Large, very short current pulses, if is presence of impurities indicated by E
3	Formation of hydroxide in [+2] state	Prepare $Ni(OH)_2$ to the extent of 15 - 20 monolayers equivalent to discharged battery plate	Time of anodization at constant potential	Constant (at 0.1 to 0.9 v versus NHE)
4	Potentiodynamic sweep (as indicated in Figure 3)	Oxidation of $Ni(OH)_2$ and reduction of the [+3]-oxide, simulating positive plate operation	Potentiodynamics, triangular sweeps	$i = f(E, dE/dt)$. In either case determine $Q = i,t$
5			Cycle and observe rechargeability and reproducibility	

Table 3

CYCLING NICKEL FOIL ELECTRODE AT ROOM TEMPERATURE

Cycle No.	Sweep Rate (mv/sec)	Scanned Range (mv)*	Anodization			Cathodization			Efficiency (QC/QA)
			Peak Current (ma/cm²)	At Voltage (mv)	Anodic Charge (mC/cm²)	Peak Current (ma/cm²)	At Voltage (mv)	Cathodic Charge (mC/cm²)	
			Electrolyte -- 0.2N KOH						
1	18.5	--	0.24	520	--	0.13	434	--	--
10	18.5	-194 to +558	0.30	495	1.01	0.35	430	0.84	0.84
117	18.5	-202 to +552	0.63	523	1.64	0.82	418	1.54	0.94
245	18.5	-194 to +586	0.72	525	1.66	0.75	415	1.50	0.90
940	18.5	-194 to +554	0.83	518	1.56	0.51	411	1.37	0.88
1003	2.96	-194 to +557	0.26	508	1.91	0.11	420	1.47	0.77
1020	100	-162 to +593	2.66	540	1.52	2.05	395	1.43	0.94
			Electrolyte -- 2N KOH						
1	18.7	-- to +562	0.18	538	--	--	--	--	--
5	18.7	-183 to +567	0.17	523	0.64	0.39	425	0.46	0.72
12	18.7	-183 to +566	0.23	525	0.73	0.51	423	0.63	0.86
25	18.7	-185 to +565	0.31	528	0.89	0.57	420	0.75	0.84
123	18.7	-176 to +572	0.72	532	1.28	0.62	420	0.89	0.70
1007	18.7	-179 to +574	0.95	508	1.21	0.35	398	0.96	0.79
1012	2.97	-224 to +537	0.21	498	1.52	0.076	398	1.07	0.70
1023	92.6	-174 to +567	3.17	514	1.02	1.46	391	0.98	0.95
			Electrolyte 6N KOH						
1	18.6	-- to +572	0.35	485	--	0.27	401	--	--
5	18.5	-18? to +572	0.41	480	1.29	0.40	402	0.98	0.76
10	18.6	-19? to +570	0.48	483	1.39	0.43	400	1.07	0.77
30	18.6	-182 to +574	0.76	507	1.67	0.44	410	1.11	0.66
105	18.6	-205 to +551	0.94	510	1.82	0.39	411	1.11	0.61
113	378.0	-194 to +562	8.43	516	1.06	4.86	400	1.01	0.95
212	18.6	-218 to +540	0.83	502	1.49	0.27	409	0.93	0.62
1005	18.6	-215 to +539	1.87	497	2.68	0.44	393	1.57	0.58
1013	2.92	-233 to +525	0.63	491	3.61	0.080	396	1.35	0.37
1039	100	-178 to +563	3.75	505	1.92	1.23	397	1.64	0.85

* All voltages measured versus Hg HgO reference electrode

Cycling of Anodized Electrolytically Deposited Nickel-cobalt Layers. The metals were codeposited on the same 99.91% pure nickel foil used in the thin film work described in previous paragraphs. The procedure of Vagramyan and Fatueva (Ref. 35) was modified so as to avoid appreciable hydrogen evolution. Electrolytic deposition was performed at -650 mv (versus NHE), with potentiostatic control from a solution of 1 M $NiSO_4$ and 0.25 M $CoSO_4$ at a pH of 1.9. An example of voltametric cycling of such an electrode is illustrated in Figure 5*. After completion of the preliminary stepping sequence, the electrode was cycled in 0.2N KOH with continuous argon purging at a potential sweep rate of 18.5 mv/sec, with a range of -180 to +560 mv (versus the Hg/HgO reference electrode**) and at room temperature. The test electrode area was 1 cm^2, with the counter electrode area being 4 cm^2. Figure 5a shows the current-voltage behavior for Cycle 42. The trace for Cycle 975 is in Figure 5b. After extensive cycling, the curves have the appearance of that of Cycle 4105 (Figure 5c), after which little further change occurred even beyond Cycle 7000.

The appearance of two anodic and cathodic peaks instead of one, which would be expected for a solid solution of $Ni(OH)_2$ and $Co(OH)_2$, led to the conclusion that the microstructure of the deposit was not homogeneous enough for the purpose of this study and that, in effect, separate surface patches of nickel and cobalt were dealt with. Electron microbeam scanning of the surfaces was inconclusive. However, since the behavior of these electrodes varied from one electrodeposited electrode to the next, this lack of reproducibility and the availability of a nickel-cobalt alloy led to the alloy study.

Cycling of Anodized Nickel-cobalt Alloy. Cobalt and nickel form a continuous series of solid solutions (Ref. 36). Thus, the thin film study was continued with experiments on metallurgically prepared alloys. Melted nickel and cobalt were forged, hot and cold rolled, and heated to 900°C in hydrogen. The resulting alloy was a solid solution of 89.8 weight % nickel and 10.2 % cobalt. Voltametric cycling did not show the double peaks of electrodeposited films. Therefore, it was confirmed that these double peaks were caused by isolated patches of $Ni(OH)_2$ and $Co(OH)_2$, and that those results with electrodeposited electrodes did not represent the behavior of a nickel electrode with cobalt additive.

The voltametric data on alloy cycling in Table 4 should be compared with those of pure nickel thin film electrodes in Table 3. Both sets of experiments

*In comparing the oscillograph traces with recorded and tabulated data, allowance must be made for a calibration correction factor for the oscilloscope voltage trace, which varied from 20 to 40 mv and was measured for each individual trace.

**The reference electrode Hg/HgO had a potential of +0.924 ±0.002 v versus a normal hydrogen electrode in the same solution.

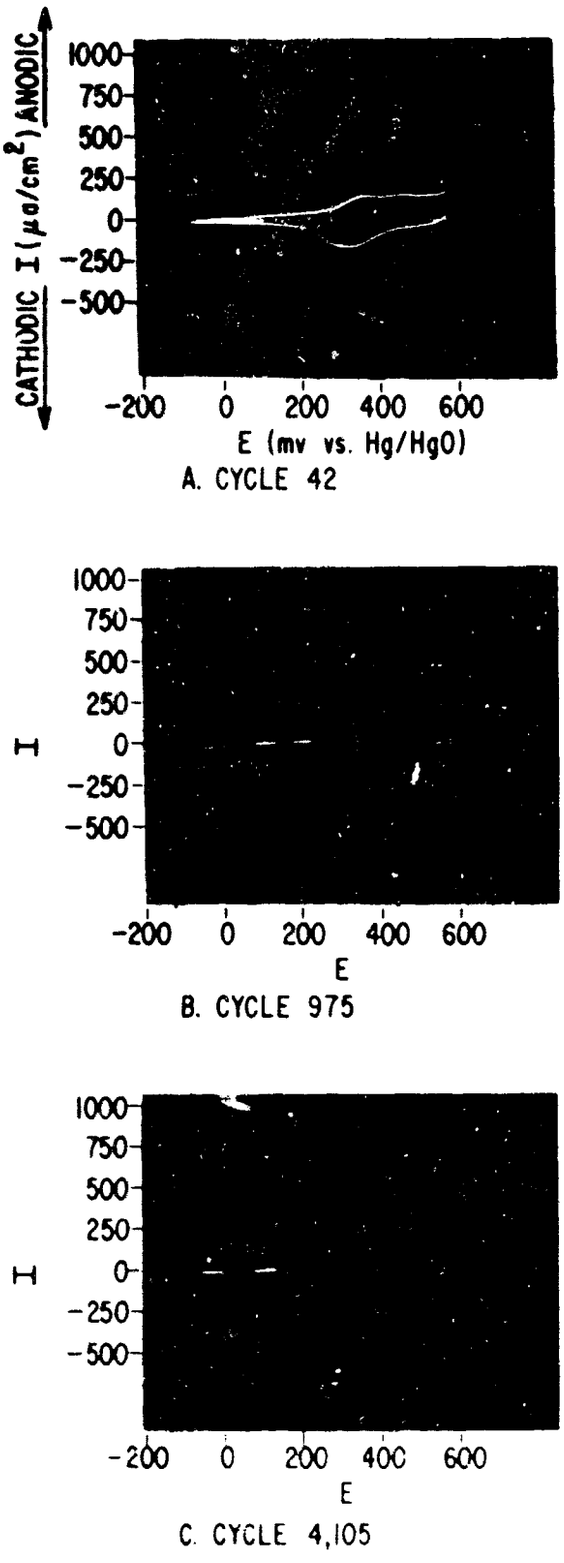

Figure 5. Voltametric Cycling of Anodized, Electrolytically Co-deposited Nickel-cobalt Electrode

Table 4

CYCLING OF 90% NICKEL -- 10% COBALT ALLOY FOIL AT ROOM TEMPERATURE

Cycle No.	Sweep Rate (mv/sec)	Scanned Range (mv)*	Anodization: Peak Current (ma/cm²)	Anodization: At Voltage (mv)	Anodization: Anodic Charge (mC/cm²)	Cathodization: Peak Current (ma/cm²)	Cathodization: At Voltage (mv)	Cathodization: Cathodic Charge (mC/cm²)	Efficiency (Q_C/Q_A)
			Electrolyte -- 0.3N KOH						
1	18.5	-202 to +542	0.24	480	--	0.04	397	--	--
10	18.5	-186 to +565	0.21	464	1.12	0.15	396	0.94	0.57
25	18.5	-204 to +544	0.28	487	1.06	0.22	411	9.82	0.78
200	18.5	-196 to +559	0.54	503	0.78	0.52	407	0.72	0.92
1032	18.5	-194 to +560	0.68	514	0.85	0.57	403	0.78	0.92
1040	2.91	-210 to +548	0.32	502	1.97	0.21	416	1.71	0.87
1055	98.3	-152 to +585	2.28	540	1.46	2.19	397	1.49	1.03
			Electrolyte -- 3N KOH						
1	--	--	--	--	--	--	--	--	--
30	18.5	-174 to +569	0.94	+508	2.87	0.60	409	1.63	0.57
200	18.5	-174 to 569	1.39	504	2.59	0.80	404	2.33	0.90
931	18.5	-182 to +570	2.35	504	2.85	0.88	395	2.29	0.80
1020	18.5	-185 to +566	2.50	508	2.88	0.88	398	2.52	0.87
10[illegible]	2.88	-201 to +554	0.82	495	5.68	0.21	396	3.05	0.55
1054**	98.3	-175 to +562	6.84	5.2	2.33	3.04	386	2.01	0.86
			Electrolyte -- 6N KOH						
1	--	--	--	--	--	--	--	--	--
7	18.7	-207 to +550	--	481	2.76	--	384	0.009	0.003
14	18.7	-207 to +549	--	481	2.51	--	381	0.30	0.12
25	18.7	-207 to +569	0.49	487	2.22	0.16	386	0.73	0.33
109	18.7	-220 to +537	0.68	489	1.37	0.19	397	1.10	0.80
200	18.7	-225 to +530	0.64	491	1.21	0.16	393	0.66	0.55
1005	18.7	-202 to +558	0.72	497	2.13	0.24	388	2.04	0.96
1009	2.95	-233 to +534	0.19	489	3.79	0.065	372	2.88	0.76
1016	100	-173 to +570	1.66	514	1.12	0.71	360	1.49	1.33

* All voltages measured vs Hg HgO reference electrodes

** See Figure 4

were performed at room temperature and with 0.2N, 2N, and 6N KOH electrolytes. The following observations were made of the oscillographs and the tabulated data:

1. Peak Voltages. For the alloy electrode in 0.2N KOH, the peak voltage of the anodic process, E_a, increases with cycling. This may reflect a preferential charge and discharge of $Ni(OH)_2$, which gradually displaces $Co(OH)_2$ at the electrode surface or an irreversible oxidation of cobalt (refer to paragraph 4 below). The effect is absent at higher electrolyte concentrations, but is also noted to a lesser degree for the nickel electrode in 0.2N KOH. Cathodic peaks remain unchanged in all cases.

2. Peak Currents. These were about the same except for the 2N KOH electrolyte, in which pure nickel had a small anodic current. In the same electrolyte, the alloy electrode had exceptionally high anodic and cathodic currents.

3. Capacities. The larger peak currents for the alloy in 2N KOH are also reflected in larger anodic capacity, Q_A. In Figure 6, Q_A values for nickel and alloy thin film electrodes are compared. These data indicate at least an initial, larger capacity for the alloy electrodes. But the effect of surface roughness must be considered. The chemical polishing before each experiment produced a very smooth electrode surface, with an approximate surface roughness of 1.1 for nickel. The polish is applicable to nickel, and its effect on the alloy was expected to be the same. It is possible that cobalt would be etched to a greater extent than nickel; but, since it was present in smaller proportion and was in solid solution with nickel, it was assumed that the alloy electrodes were nearly as smooth as the pure nickel electrodes. In any case, cycling produced more surface roughening which resulted in an increased apparent current density, at least in the case of 6N KOH electrolyte.

4. Oxygen Evolution. In Tables 3 and 4 it is seen that Q_A was consistently larger than Q_C. If these represented the oxidation and reduction of Ni(II) and Ni(III) hydroxides, respectively, then the difference between Q_A and Q_C was caused by the formation of oxygen. Because of the very limited amount of effective active mass in thin film electrodes, the relative effect of oxygen evolution on cycling thin film electrodes is larger than in experiments with thicker electrodes, to be described later. As a consequence, the efficiency, Q_C/Q_A, is substantially smaller than one. The experiments indicate that after early cycling, which may be taken as a conditioning period for the alloy, the efficiency achieved by the alloy electrode was greater in later cycles than that of pure nickel electrodes. With one exception, Table 5 shows that the values of the last column representing oxygen evolution are larger for nickel than for alloy thin film electrodes. A significant conclusion to be drawn from these data is that

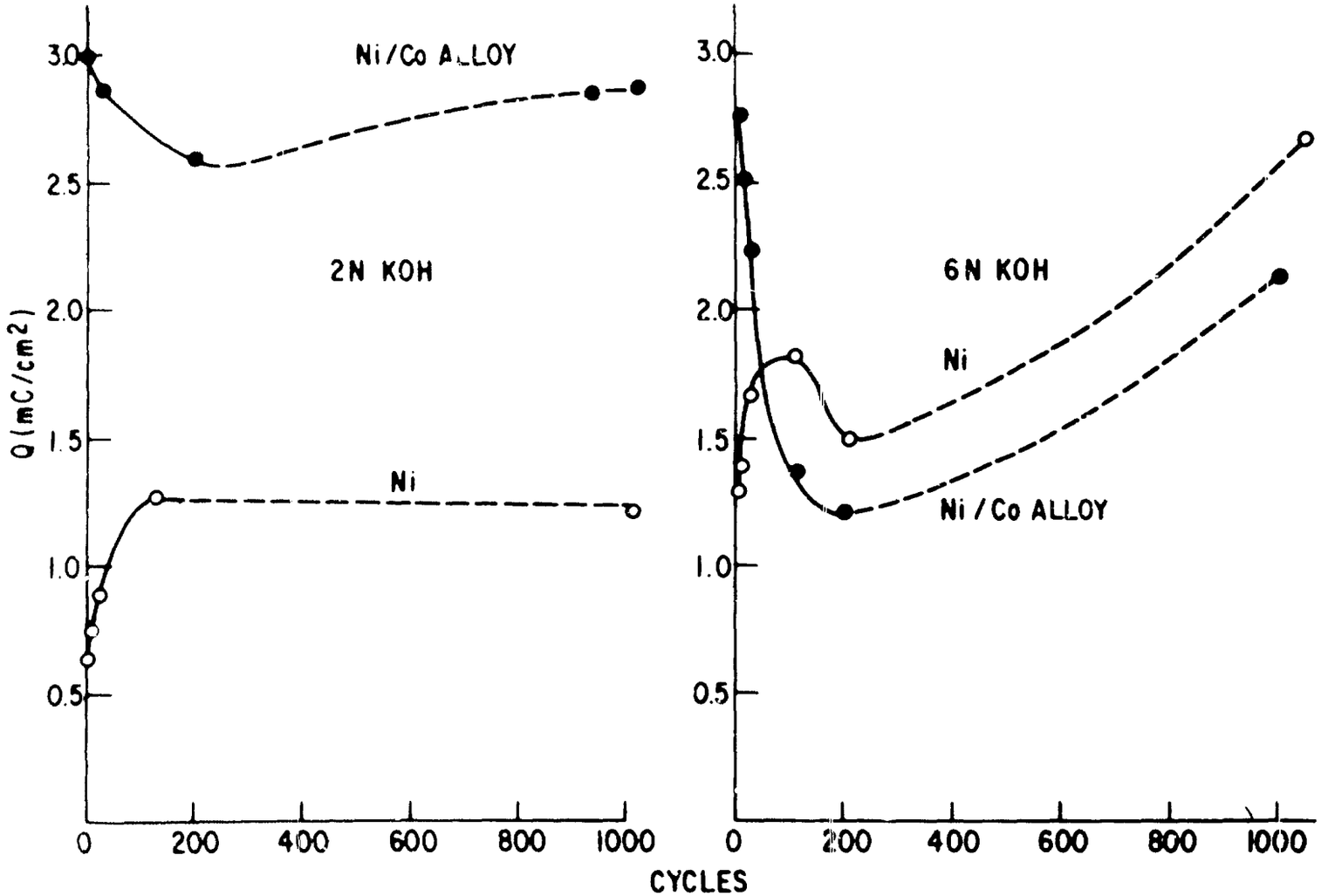

Figure 6. Anodic Charge of Thin-film 89.8% Nickel and 10.2% Cobalt Electrode in 2N KOH and 6N KOH

Table 5

OXYGEN EVOLUTION AS FUNCTION OF ELECTROLYTE CONCENTRATION, SWEEP RATE, AND ADDITION OF COBALT

Electrolyte	Electrode	Cycle No.	Sweep Rate (mv/sec)	Anodic Charge Not Discharged $[(Q_A-Q_C)/Q_A] \times 100$ (%)
0.2N KOH				
	Ni*	1003	2.96	30
		940	18.5	14
		1020	100.0	6.3
	Ni/Co**	1040	2.91	15
		1032	18.5	9.0
		1055	98.3	- 2.0***
2N KOH				
	Ni	1012	2.97	42
		1007	18.7	26
		1023	92.6	49
	Ni/Co	1026	2.88	86
		1020	18.5	14
		1054	98.32	16
6N KOH				
	Ni	1013	2.92	179
		1005	18.6	71
		1039	100.0	17
	Ni/Co	1009	2.95	31
		1005	18.7	4.4
		1016	100.0	-25

*99.91% Nickel

**89.8% Ni, 10.2% Co alloy

***Negative values indicate larger cathodic than anodic charge

the presence of cobalt reduces oxygen evolution. This effect is clear at about Cycle 1000. It may be masked by irreversible oxidation of cobalt at cycles below 200.

It should also be noted that oxygen evolution was an inverse function of sweep rate. This reflects the previously known fact that oxygen evolution is largely independent of the charging rate of the positive nickel electrode, being primarily dependent on the electrode potential or overpotential so that fast charging is more efficient than slow charging.

Voltametric Cycling of Cathodically Precipitated Hydroxide Electrodes. The bulk of the present work on additives to the $Ni(OH)_2$ electrode was performed with cathodically precipitated hydroxide. In this process, the active material is precipitated on a nickel matrix as cathodic polarization increases the pH in the immediate vicinity of the electrode. The process without additives is fully described by Häusler (Ref. 37), McHenry (Ref. 38), and by Bode and his co-workers (Ref. 7).

According to Bode's procedure, the hydroxides were precipitated from 0.1N nitrate solutions on cathodically polarized, sandblasted, pure nickel foil substrates. The surface area of the substrate was 8 cm^2. The deposition occurred at 1 ma/cm^2 for 30 minutes at room temperature. Electrodes with 0.5 to 0.6 cm^2 surface area were then prepared and cycled in 6N KOH*. Experimental conditions of the linear triangular voltage sweep experiments and their results (magnitudes of voltages, current density, and charge capacity of both anodic and cathodic processes) are given in Table 6. Table 6 is divided into the following six parts according to the active electrode material:

1. 100% $Ni(OH)_2$
2. Added $Co(OH)_2$ and 100% $Co(OH)_2$
3. $Zn(OH)_2$ added to the active mass and/or to the electrolyte
4. Added $Al(OH)_3$
5. Added $Cd(OH)_2$
6. 100% $Ni(OH)_2$ cycled in electrolyte containing LiOH as well as KOH

The following observations are pertinent to the additive study in the light of the voltametric results compiles in Table 6. As previously noted, the anodic capacity, Q_A, of linear sweep voltametric cycles can be identified with the charge acceptance of an electrode, and the cathodic capacity, Q_C, with the discharge of a nickel positive electrode. The charge efficiency or charge retention and the ability of the electrode to deliver charge are as important as the electrode capacities. Strictly speaking, charge retention should be examined as a function of the duration of the open circuit period prior to cell

*100% $Ni(OH)_2$ and 100% $Co(OH)_2$ electrodes were also cycled in 2N KOH.

Table 6

CYCLIC VOLTAMETRY OF CATHODICALLY PRECIPITATED $Ni(OH)_2$ ELECTRODES

Cycle No.	Sweep Rate (mv/sec)	Range Scanned (mv)	Anodization: Peak Current (ma/cm²)	Anodization: At Voltage (mv)	Anodization: Anodic Charge (mC/cm²)	Cathodization: Peak Current (ma/cm²)	Cathodization: At Voltage (mv)	Cathodization: Cathodic Charge (mC/cm²)	Efficiency (Q_C/Q_A)
			Electrode 1a -- 100% $Ni(OH)_2$, 0.537 cm², 6N KOH, 23°C						
1	18.2	-142 to +600	242.0	+521	1358	117.0	+267	704	0.52
2	18.2	-204 to +539	162.0	+472	739	117.0	+267	683	0.92
5	18.2	-220 to +523	160.0	+470	732	106.0	+270	620	0.85
10	18.2	-225 to +518	130.0	+456	601	93.1	+276	536	0.89
25	18.2	-210 to +532	101.0	+493	477	57.7	+304	480	1.01
55	18.2	-184 to +558	119.0	+522	438	50.3	+316	441	1.01
100	18.2	-185 to +560	114.0	+523	406	46.6	+320	434	1.07
208	18.2	-185 to +558	78.2	+520	272	31.7	+326	272	1.00
950	18.2	-192 to +549	42.8	+513	145	17.9	+338	143	0.99
1000	18.2	-192 to +549	42.8	+512	143	18.6	+340	142	0.99
1009	2.86	-230 to +514	14.0	+483	186	4.3	+349	147	0.79
			Electrode 1b -- 100% $Ni(OH)_2$, 0.488 cm², 6N KOH, 45°C						
1	18.0	-133 to +620	233.0	+577	1060	88.5	+304	488	0.46
2	18.0	-186 to +553	119.0	+524	541	78.2	+316	481	0.89
5	18.0	-177 to +561	115.0	+520	535	74.1	+309	510	0.95
10	18.0	-188 to +551	103.0	+524	420	65.8	+316	447	1.06
50	18.0	-196 to +541	59.7	+512	198	32.9	+333	208	1.05
100	18.0	-212 to +527	35.0	+499	92.6	20.6	+335	96.7	1.04
200	18.0	-219 to +519	24.7	+501	51.4	10.9	+346	55.6	1.08
1000	18.0	--	--	--	<10.2	--	--	<10.2	--
			Electrode 2a -- 90% $Ni(OH)_2$ + 10% $Co(OH)_2$, 0.631 cm², 6N KOH, 23°C						
1	18.8	-157 to +501	244.0	+517	1548	136.0	+208	916	0.59
2	18.8	-213 to +546	181.0	+447	976	111.0	+208	750	0.77
25	18.8	-234 to +524	146.0	+470	835	68.1	+260	719	0.86
110	18.8	-201 to +558	125.0	+524	670	33.3	+309	640	0.96
225	18.8	-194 to +564	101.0	+530	493	26.9	+328	491	1.00
600	18.8	-197 to +562	91.9	+526	422	31.7	+326	475	1.13
1000	18.8	-198 to +563	74.5	+535	319	28.5	+339	387	1.21
			Electrode 2b -- 90% $Ni(OH)_2$ + 10% $Co(OH)_2$, 0.570 cm², 6N KOH, 45°C						

1	18.2	-119 to +622	246.0	+580	1279	139.0	+240	874	0.68
2	18.2	-257 to +483	130.0*	+465	707	107.0	+254	723	1.02
5	18.2	-257 to +483	118.0**	+458	607	91.2	+255	584	0.96
10	18.2	-245 to +496	130.0	+466	561	78.9	+270	561	1.00
25	18.2	-214 to +526	149.0	+487	550	66.7	+288	470	0.84
60	18.2	-195 to +545	158.0	+514	607	52.6	+313	544	0.90
100	18.2	-195 to +545	151.0	+517	540	50.9	+316	581	1.08
200	18.2	-184 to +556	102.0	+516	418	35.1	+325	374	0.89
392	18.2	-201 to +538	70.2	+518	233	26.3	+332	274	1.18
521	18.2	-202 to +537	59.6	+517	205	24.6	+332	230	1.12
944	18.2	-214 to +529	--	--	<8.8	--	--	<8.8	--

*Second peak of 135 ma/cm² at +433 mv
**Second peak of 111 ma/cm² at +420 mv

Electrode 2c -- 100% $Co(OH)_2$, 0.586 cm², 2N KOH, 23°C

1	18.8	-- to +616	181.0	+381	1710	41.2	+ 68	462	0.27
5	18.8	-140 to +616	73.6	+207	530	41.6	+ 76	458	0.86
28	18.8	-194 to +560	67.4	+232	494	32.2	+ 76	460	0.93
101	18.8	-203 to +552	55.3	+320	458	17.4	+ 50	422	0.92
907	18.8	-197 to +560	43.7	+320*	422	13.3	+ 40†	374	0.89
920	2.92	-200 to +561	10.8	+237*	502	4.1	+ 95†	424	0.84
938	100	-121 to +619	100.0	+430**	288	‡	--	290	1.01

*Second small anodic peaks at +514 and +492 mv, respectively, for cycles 907 and 920.
**Larger peak of 109 ma/cm² at +524 mv.
†Second small cathodic peaks at +332 and +348 mv, respectively, for cycles 907 and 920.
‡A diffuse peak at +307 mv, no other distinct cathodic peaks.

Electrode 3a -- 95% $Ni(OH)_2$ + 5% $Zn(OH)_2$, 0.559 cm², 6N KOH, 23°C

1	18.4	-124 to +620	146.0	+520	782	43.1	+326	358	0.46
5	18.4	-171 to +569	81.0	+459	585	54.2	+321	435	0.74
10	18.4	-172 to +570	97.0	+460	476	60.5	+304	433	0.97
25	18.4	-205 to +539	83.0	+475	395	46.7	+314	360	0.91
50	18.4	-163 to +560	112.0	+524	428	41.0	+324	329	0.77
110	18.4	-175 to +568	111.0	+525	420	49.4	+319	401	0.95
200	18.4	-190 to +555	106.0	+525	370	47.6	+320	352	0.95
1025	18.4	-179 to +564	58.3	+505	200	24.5	+331	155	0.77
1034	2.91	-215 to +534	41.0	+479	530	14.1	+345	413	0.78
1040	98.0	-124 to +606	124.0	+526	140	68.3	+282	151	1.08

Table 6 (Cont'd)

CYCLIC VOLTAMETRY OF CATHODICALLY PRECIPITATED $Ni(OH)_2$ ELECTRODES

Cycle No.	Sweep Rate (mv/sec)	Range Scanned (mv)	Anodization: Peak Current (ma/cm^2)	Anodization: At Voltage (mv)	Anodization: Anodic Charge (mC/cm^2)	Cathodization: Peak Current (ma/cm^2)	Cathodization: At Voltage (mv)	Cathodization: Cathodic Charge (mC/cm^2)	Efficiency (Q_C/Q_A)
Electrode 3b -- 100% $Ni(OH)_2$, 0.518 cm^2, 6N KOH Containing 10 g/l ZnO, 23°C									
1	18.5	-122 to +620	251.0	+561	1618	145.0	+258	1166	0.72
2	18.5	-182 to +560	216.0	+524	1006	141.0	+270	1071	1.06
5	18.5	-182 to +560	222.0	+531	1087	139.0	+278	1098	1.01
10	18.5	-175 to +567	214.0	+528	1068	139.0	+281	1100	1.03
25	18.5	-178 to +564	207.0	+530	1048	135.0	+281	1062	1.01
60	18.5	-154 to +590	214.0	+556	1015	112.0	+310	1006	0.99
100	18.5	-153 to +588	207.0	+558	971	100.0	+318	1021	1.05
200	18.5	-149 to +593	201.0	+567	905	77.2	+337	969	1.07
295	18.5	-152 to +590	195.0	+568	846	75.3	+343	948	1.12
1000	18.5	-152 to +590	102.0	+560	483	44.4	+356	392	0.81
1115	18.5	-197 to +549	38.6	+501	604	15.8	+370	624	1.03
1144	18.5	- 23 to +704	151.0	+600	185	96.5	+337	226	1.22
Electrode 3c -- 95% $Ni(OH)_2$ + 5% $Zn(OH)_2$, 0.537 cm^2, 6N KOH Containing 10 g/l ZnO, 23°C									
1	18.0	-150 to +590	160.0	+602	823	26.1	+362	279	0.34
2	18.0	-184 to +556	108.0	+552	516	26.1	+362	289	0.56
5	18.0	-143 to +596	119.0	+554	573	35.4	+367	536	0.94
12	18.0	-148 to +592	130.0	+551	620	37.2	+366	646	1.04
30	18.0	-147 to +594	145.0	+552	665	44.7	+358	674	1.01
50	18.0	-154 to +586	149.0	+550	665	52.1	+356	691	1.04
100	18.0	-153 to +587	156.0	+547	698	57.7	+352	702	1.01
200	18.0	-154 to +587	160.0	+550	702	63.3	+346	749	1.07
1000	18.0	-151 to +587	108.0	+550	503	48.4	+347	514	1.02
1015	2.84	-211 to +536	42.3	+507	566	18.6	+371	521	0.92
1030	96.8	-126 to +601	182.0	+600	156	98.7	+319	251	1.60
Electrode 3d -- 95% $Ni(OH)_2$ + 5% $Zn(OH)_2$, 0.614 cm^2, 6N KOH Containing 10 g/l ZnO, 45°C									
1	18.1	-140 to +600	174.0	+541	650	74.9	+332	598	0.90
2	18.1	-199 to +541	127.0	+503	443	66.8	+388	508	1.15

5	18.1	-217 to +524	135.0	+503	482	76.5	+345	624	1.29
36	18.1	-181 to +560	163.0	diffuse	744	87.9	+333	761	1.02
50	18.1	-181 to +560	184.0	+540	730	87.9	+337	767	1.05
108	18.1	-181 to +560	179.0	+535	684	79.8	+337	691	1.01
200	18.1	-183 to +558	173.0	+536	612	65.1	+343	591	0.97
1000	18.1	-190 to +551	73.3	diffuse	296	30.9	+360	365	1.23

Electrode 4a -- 95% $Ni(OH)_2$ + 5% $Al(OH)_3$, 0.536 cm^2, 6N KOH, 23°C

1	18.3	-134 to +617	233.0	+547	1610	106.0	+304	849	0.53
2	18.3	-190 to +563	164.0	+506	953	106.0	+304	849	0.89
5	18.3	-189 to +563	149.0	+495	884	106.0	+302	871	0.98
10	18.3	-191 to +562	144.0	+498	856	103.0	+305	860	1.00
25	18.3	-192 to +561	138.0	+525	784	91.4	+316	748	0.95
55	18.3	-161 to +595	138.0	+542	672	69.0	+328	634	0.94
120	18.3	-174 to +583	119.0	+549	507	50.4	+340	571	1.13
200	18.3	-167 to +539	130.0	+547	468	44.8	+340	494	1.06
300	18.3	-178 to +575	85.8	+542	377	39.2	+337	384	1.02
424	18.3	-184 to +570	72.8	+541	308	33.6	+338	326	1.06
1000	18.3	-194 to +562	42.9*	+539	183	16.8**	+344	205	1.12
1050	2.88	-243 to +514	15.9	+493	237	5.6***	+353	194	0.82

*Second anodic peak of 37.3 ma/cm^2 at +540 mv

**Second cathodic peak of 20.5 ma/cm^2 at +372 mv

***Second cathodic peak of 6.0 ma/cm^2 at 374 mv

Electrode 4b -- 95% $Ni(OH)_2$ + 5% $Al(OH)_3$, 0.582 cm^2, 6N KOH, 45°C

1	18.7	-145 to +610	256.0	+555	1294	142.0	+288	665	0.51
2	18.7	-198 to +555	169.0	+526	907	132.0	+296	580	0.64
5	18.7	-198 to +556	165.0	+522	799	132.0	+297	733	0.92
10	18.7	-198 to +556	167.0	+523	728	128.0	+306	750	1.03
25	18.7	-205 to +550	175.0	+522	575	114.0	+313	590	1.02
65	18.7	-206 to +550	157.0	+521	489	89.0	+324	375	0.77
100	18.7	-207 to +548	142.0	+522	424	78.0	+332	372	0.88
200	18.7	-211 to +543	114.0	+522	343	64.0	+330	321	0.94
1000	18.7	-221 to +532	14.2	+509	38.4	7.1	+359	52.3	1.36

Table 6 (Cont'd)

CYCLIC VOLTAMETRY OF CATHODICALLY PRECIPITATED $Ni(OH)_2$ ELECTRODES

Cycle No.	Sweep Rate (mv/sec)	Range Scanned (mv)	Anodization: Peak Current (ma/cm²)	Anodization: At Voltage (mv)	Anodization: Anodic Charge (mC/cm²)	Cathodization: Peak Current (ma/cm²)	Cathodization: At Voltage (mv)	Cathodization: Cathodic Charge (mC/cm²)	Efficiency (Q_C/Q_A)
Electrode 5a -- 95% $Ni(OH)_2$ + 5% $Cd(OH)_2$, 0.541 cm², 6N KOH, 23°C									
1	18.3	-137 to +611	181.0	+513	865	87.0	+292	467	0.54
2	18.3	-209 to +539	139.0	+475	937	87.0	+292	439	0.47
5	18.3	-215 to +532	131.0	+477	502	74.0	+302	422	0.84
10	18.3	-222 to +525	126.0	+480	463	65.0	+307	375	0.81
25	18.3	-231 to +517	105.0	+489	372	41.0	+323	308	0.83
50	18.3	-200 to +550	100.0	+518	364	31.0	+336	340	0.93
100	18.3	-187 to +562	100.0	+531	331	26.0	+344	251	0.76
200	18.3	-184 to +572	94.0	+536	331	28.0	+346	276	0.83
275	18.3	-189 to +569	87.0	+535	310	28.0	+343	291	0.94
300	18.3	-186 to +572	87.0	+534	320	28.0	+344	242	0.75
1000	18.3	-196 to +567	59.0	+523	227	26.0	+358	169	0.74
1015	2.94	-246 to +519	17.6	+500	249	7.4	+382	192	0.77
1043	99	-109 to +634	130.0	+612	146	61.0	+364	113	0.78
Electrode 5b -- 95% $Ni(OH)_2$ + 5% $Cd(OH)_2$, 0.624 cm², 6N KOH, 45°C									
1	18.8	-166 to +592	176.0	+510	813	98.0	+275	556	0.68
3	18.8	-218 to +540	123.0	+498	476	80.0	+292	463	0.97
5	18.8	-218 to +520	125.0	+510	458	74.0	+305	446	0.97
10	18.8	-211 to +547	131.0	+522	451	59.0	+322	399	0.88
25	18.8	-208 to +551	122.0	+526	380	48.0	+331	291	0.76
50	18.8	-209 to +550	109.0	+526	311	45.0	+336	319	1.02
100	18.8	-202 to +557	98.0	+532	299	38.0	+341	259	0.86
200	18.8	-203 to +555	83.0	+533	265	38.0	+339	259	0.98
1000	18.8	-213 to +546	12.8	+523	37.2	4.8	+367	28.0	0.75
Electrode 6a -- 100% $Ni(OH)_2$, 0.630 cm², 1.3N KOH + 1N LiOH, 23°C									
1	18.9	-126 to +624	182.0	+586	971	63.0	+318	447	0.46
2	18.9	-187 to +563	102.0	+500	509	56.0	+327	445	0.88
5	18.9	[illegible]	[illegible]	[illegible]	[illegible]	[illegible]	[illegible]	[illegible]	[illegible]

5	18.9	-195 to +554	95.0	+490	457	49.0	+324	402	0.88
10	18.9	-205 to +543	89.0	+494	408	41.0	+324	373	0.91
25	18.9	-201 to + 547	92.0	+507	367	32.0	+336	331	0.90
50	18.9	-194 to +553	95.0	+522	326	27.0	?	317	0.97
115	18.9	-165 to +584	98.0	+538	394	27.0	?	350	0.89
200	18.9	-164 to +590	97.0	+542	395	27.0	+398	362	0.92
428	18.9	-163 to +596	86.0	+537	394	25.0	+396	317	0.80
475	18.9	-158 to +606	81.0	+544	379	25.0	+404	323	0.85
1000	18.9	-176 to +584	56.0	+530	235	22.0	+401	242	1.03
1015	2.90	-212 to +549	18.3	+496	288	4.8	+409	221	0.77
1025	98.7	-089 to +651	156.0	--	156	87.0	+390	265	0.70
1026	98.7	-026 to +714	--	--	229	87.0	+390	276	1.20

Electrode 6b -- 100% $Ni(OH)_2$, 0.636 cm^2, 4.3N KOH + 1N LiOH, 45°C

1	18.7	-131 to +621	226.0	+588	966	86.0	+290	673	0.70
2	18.7	-191 to +561	132.0	+508	605	69.0	+298	616	1.02
5	18.7	-200 to +555	124.0	+498	535	58.0	+292	529	0.99
10	18.7	-206 to +549	126.0	+500	498	47.2	+289	412	0.83
25	18.7	-206 to +549	123.0	+508	423	41.0	+297	407	0.96
50	18.7	-207 to +550	113.0	+511	379	36.0	+300	380	1.00
100	18.7	-209 to +547	99.0	+518	315	27.0	+307	293	0.93
220	18.7	-215 to +542	82.0	+524	218	19.0	--	239	1.09
309	18.7	-200 to +557	71.0	+529	243	19.0	--	213	0.88
1000	18.7	-161 to +593	47.0	+553	235	16.0	+538**	223	0.95
1256	18.7	-156 to +597	44.0	+555	226	16.0	+455	219	0.97
1467	18.7	-162 to +595	39.0	+557	196	14.2	+457	188	0.96
2000	18.7	-147 to +611	36.0	--	187	11.0	+471	157	0.84
2318	18.7	-151 to +603	35.0	--	166	13.0	+456*	183	1.04
2332	2.79	-184 to +573	8.5	+513	288	2.0	+433	190	0.66
2359	99.6	-138 to +604	5.8	--	60	22.0	+329	64	1.07
3348	18.7	-194 to +							
3348	18.7	-194 to +604	14.0	--	60	4.7	+414	65	1.09

*No distinct anodic peak

**Cathodic peaks after cycle 1000: ± 30 mv

discharge. In the voltametric procedure employed, however, the electrode is immediately discharged after charging. The charge and discharge processes under these conditions can be compared from the tabulated data. The column in Table 6 headed "Cathodization" refers to the cathodic discharge process where Q_C should be compared with the anodic charge capacity, Q_A, to determine the cycling efficiency of the electrode. Q_C/Q_A is a direct measure of this efficiency. Its value approaches 100% in these tests after the conditioning resulting from earlier cycles, i.e., Cycles 10 to 100, depending on the particular electrode.

Such aspects of the experimental results are treated separately below. In general terms, despite the increasing structural complexity of the active material in going from anodized single crystals of nickel and polycrystalline nickel foil to cathodically precipitated $Ni(OH)_2$, the main features of the i-E curves remained the same. This reflects the fact that cyclic voltametry is suitable for analyzing electrode reactions from a purely electrochemical point of view. While complications were anticipated as the electrode structure becomes more complex, it is remarkable that a nickel foil with approximately two monolayers of $Ni(OH)_2$ gave a result similar to that of a 2-μ thick, cathodically precipitated $Ni(OH)_2$ layer. Small but noticeable differences can be attributed to the structure of the precipitated $Ni(OH)_2$.

Figure 7 shows the initial cycles (1 and 2) for pure $Ni(OH)_2$ and for 90% $Ni(OH)_2$ + 10% $Co(OH)_2$ electrodes in 6N KOH at 45°C. In each case, the larger anodic peak is that of the first cycle, and the second peak for Cycle 2 is at a much lower potential and has only a fraction of the initial capacity. Cathodic peaks for Cycles 1 and 2 are identical for the co-additive electrode, but they are different for the pure $Ni(OH)_2$ electrode. In the latter case, a significant decrease in Q_C, or discharge capacity, is noted between the first and second discharge.

Figure 8 shows the first two cycles of the co-additive electrode in greater detail. Dashed lines indicate the approximate charge corresponding to the cathodic precipitation and the subsequent anodization of Cycles 1 and 2. Integrating under the curves gives the following:

1. Efficiency of cathodic precipitation =

$$\frac{\text{Equivalent of active material deposited}}{\text{Number coulombs used in cathodic precipitation}} = \frac{(Q)}{1.8}$$

2. Utilization = $\dfrac{\text{Charge used in oxidation of Ni(II)}}{\text{Equivalent of active material deposited}} = \dfrac{(Q_A)}{(Q)}$

3. Cycle efficiency = $\dfrac{(Q_C)}{(Q_A)}$

Typical values of about 92% for No. 1 can be explained by the loss of charge in cathodic impregnation (Ref. 39) during reduction of nitrate to lower-valent

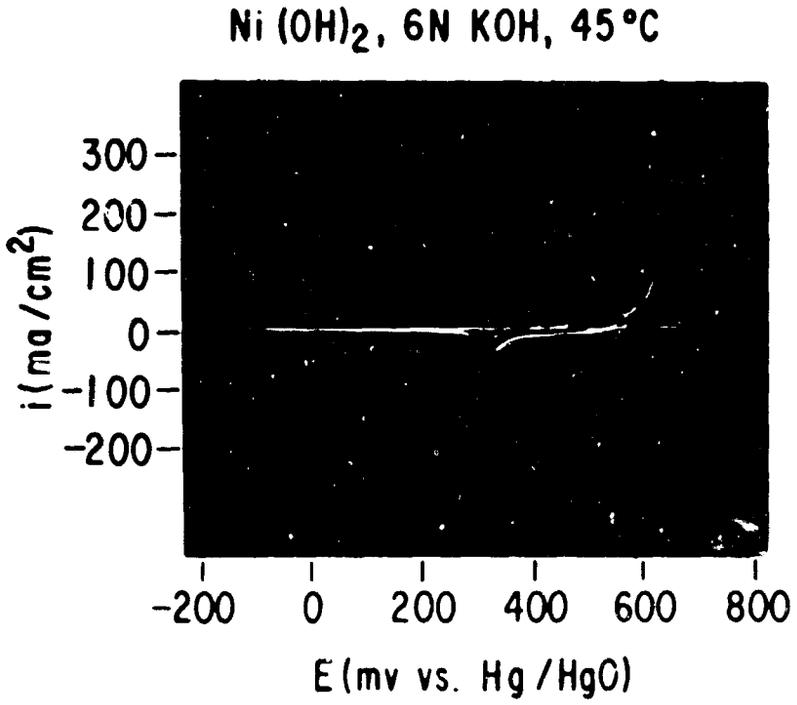

a.

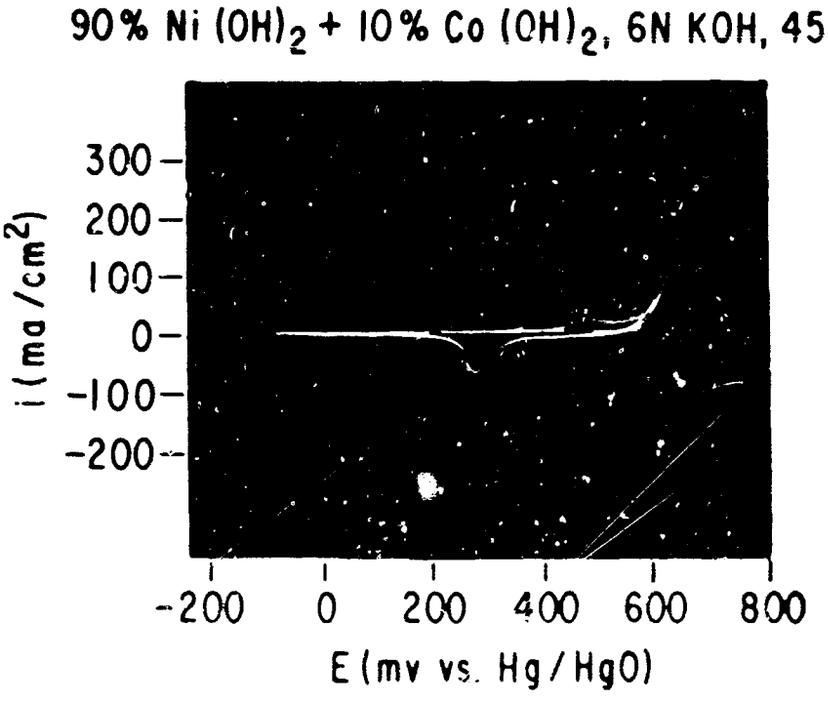

b.

Figure 7. Oscillograms of First (a) and Second (b) Cycle

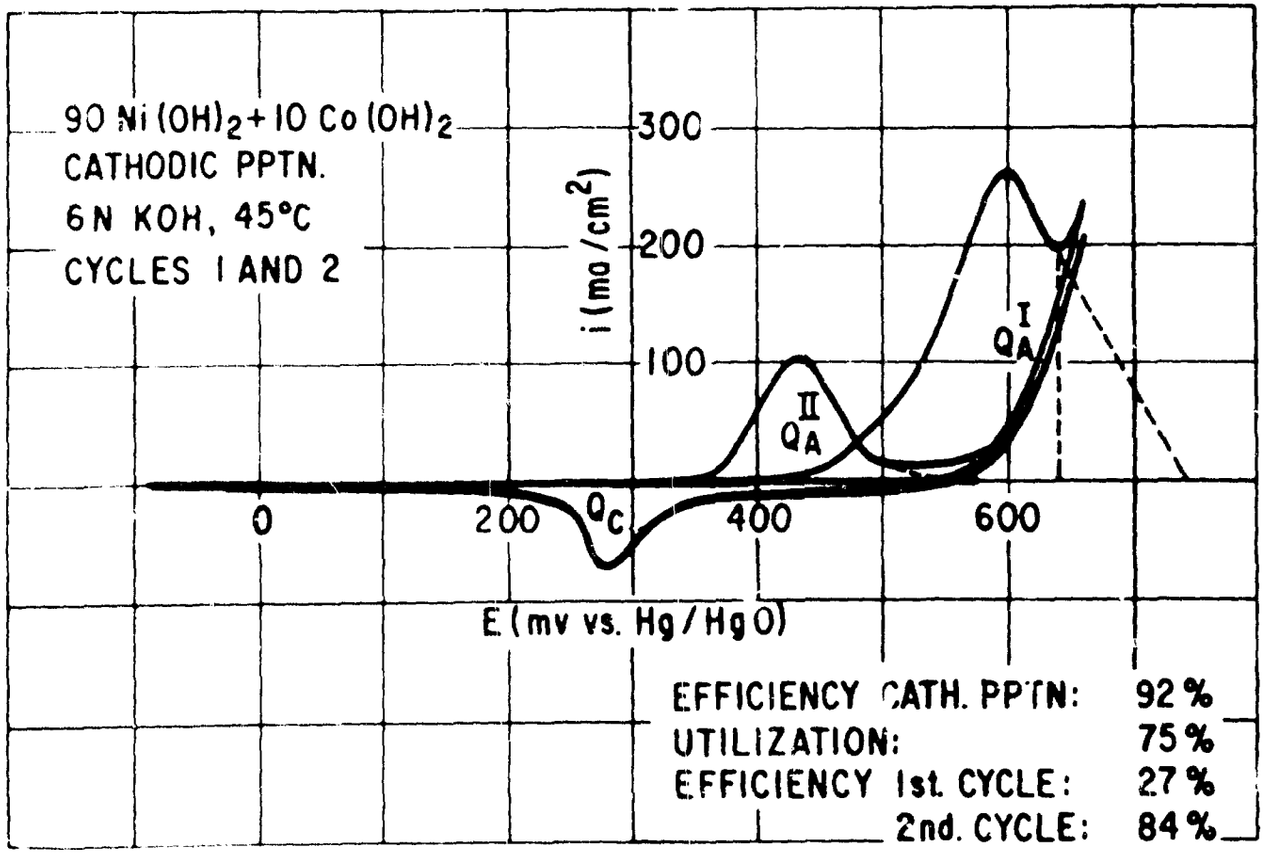

Figure 8. Oscillograms of First and Second Cycle (Drawing)

nitrogen species which, in turn, produces the necessary OH^- ions for cathodic precipitation, but not necessarily in equivalent amounts. The value of No. 2 is rather approximate because a possible 10% uncertainty exists in the estimate of Q. Values less than 100% were anticipated as a result of possible active material isolation or the lack of contact of certain deposited particles and the passivation of others. The very low efficiency of the first cycle Q_C/Q_A^1 is surprising and is related to the electrode structure and the insulating properties of $Ni(OH)_2$.

Bode (Ref. 7), Harivel (Ref. 32) and their co-workers have drawn attention to the structure of α - $Ni(OH)_2$ which is obtained by electrochemical cathodic deposition technique. Bode observed that the conversion to β or γ-$Ni(OH)_2$ is a function of temperature and alkali concentration. For example, in 6 to 9N KOH at 90°C a few hours are required for the conversion. In the pres nt experiment, this change occurs between Cycles 1 and 2, indicating that the α-phase is oxidized in Cycle 1 and is almost completely converted to β-phase before the start of Cycle 2. It may be concluded that the anodic oxidation greatly accelerates the conversion.

A chemical analog of this aspect of $Ni(OH)_2$ structure is found in the work of Klyukina (Ref. 40). Studying the surface and structure of $Ni(OH)_2$, she found that the primary structure of the active mass gradually crystallizes at various stages of the chemical preparation of $Ni(OH)_2$. Exposure of the precipitate to alkali at elevated temperature or precipitation at high temperature from concentrated KOH solutions were most effective in increasing crystallite size. Later work showed that initially formed $Ni(OH)_2$ contained molecular water, some adsorbed and some absorbed and incorporated into the structure by hydrogen bonds (Ref. 41). Compaction, crystallization, and elimination of molecular water are additional and concurrent changes to the phase transformation $\alpha \rightarrow \beta$- or $\alpha \rightarrow \gamma$-$Ni(OH)_2$, which are responsible for the decrease in electrode capacity shown in Figures 7 and 8.

The method used to prepare electrodes does not ensure that exactly equal amounts of active material are precipitated in experiments with and without added $Co(OH)_2$. Even the reported $Co(OH)_2$ content is based on the amount of $Co(NO_3)_2$ present in the solution from which the hydroxides are precipitated.

Nevertheless, electrodes with the addition of cobalt have shown consistently higher capacity at room temperature than pure $Ni(OH)_2$ electrodes. This effect is evident at 2N and 6N KOH and can be most clearly seen in four preliminary voltametric experiments. Figure 9 compares the charge acceptance (anodic charge Q_A) of electrodes with and without added 10% $Co(OH)_2$ in 2N and 6N KOH at room temperature.

While the charge efficiency Q_A/Q_C, was consistently at or above 90%, the absolute magnitude of Q_A and Q_C was larger for electrodes containing cobalt. This difference was particularly pronounced between Cycles 200 and 1000, as

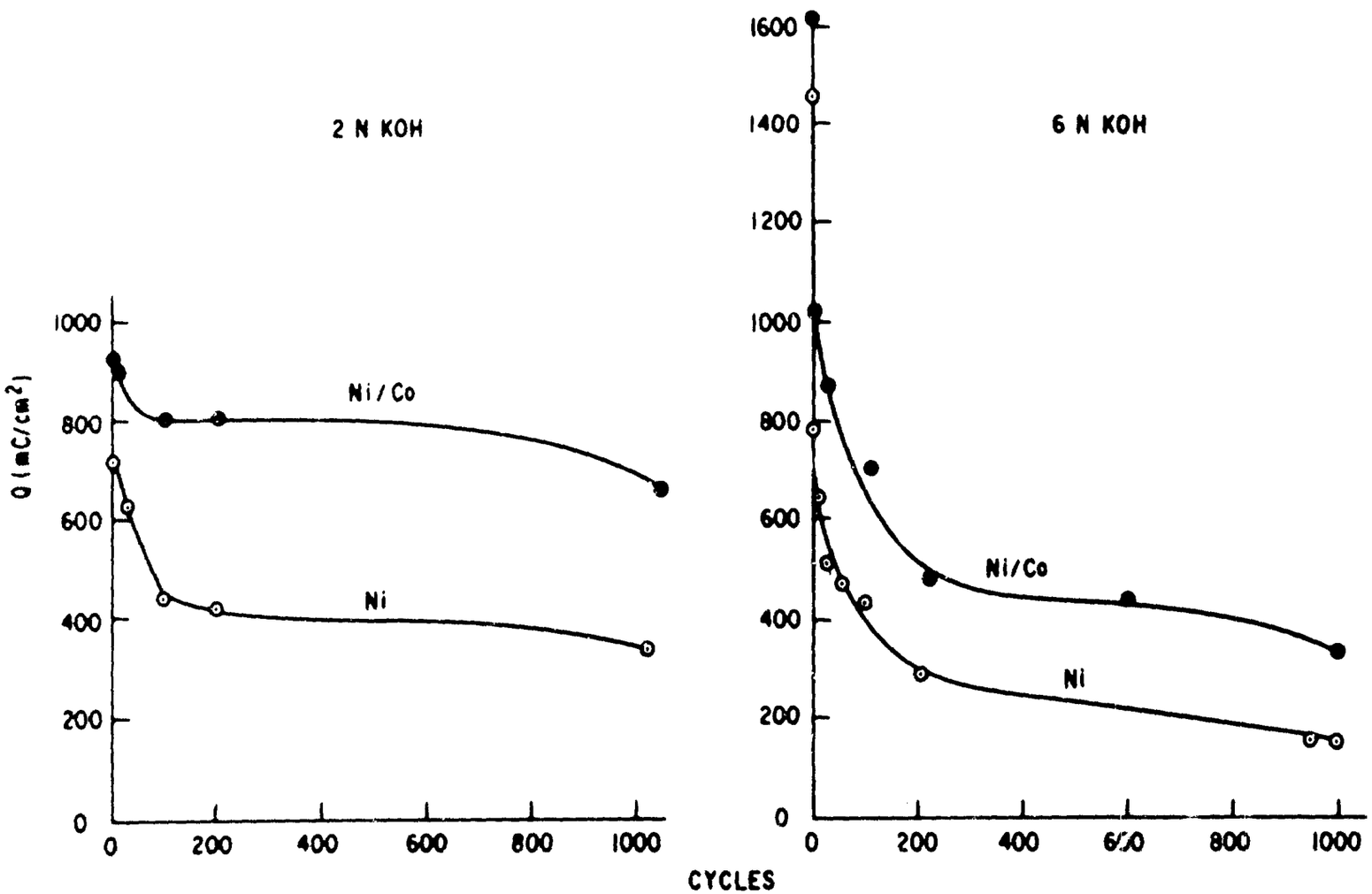

Figure 9. Anodic Charge in Voltametric Cycling at Room Temperature With and Without 10% Added Cobalt

can be seen in Figure 9. Comparison also showed a more rapid deterioration of both types of electrodes in the more concentrated 6N KOH electrolyte.

A similar behavior is shown by the temperature dependence of electrodes. At room temperature, cobalt-containing electrodes had about twice the capacity of equivalent pure nickel hydroxide electrodes after 1000 cycles. At 45°C, the pure nickel electrode lost capacity very rapidly with cycling up to about Cycle 200, at which point only about 10% of the original electrode capacity could be cycled. Under the same conditions, a cobalt-containing electrode could be cycled well beyond 1000 cycles before its reversible capacity was reduced to this extent. This is illustrated in Figure 10 and in Table 6 by comparison of Sections 1a and 1b (100% $Ni(OH)_2$) with Sections 2a and 2b (10% $Co(OH)_2$ added).

Thin-film electrodes showed lower anodic and cathodic peak voltages for electrodes containing $Co(OH)_2$ in 0.2N KOH. This distinction was no longer observed in cathodically precipitated electrodes. A more meaningful voltage-mark is the potential at the start of anodic oxidation of Ni(II) to Ni(III) or that of Ni(II) + Co(II) solid solutions. This value varied only slightly in each cycling experiment and was for pure $Ni(OH)_2$, 390 to 420 mv versus Hg/HgO^- and for added 10% $Co(OH)_2$, 280 to 310 mv.

The same general observation on sweep rates noted for the thin-film electrodes noted above is also valid for cathodically precipitated electrodes; i.e., charge efficiency improves with faster sweep rates. In addition, more charge is accepted during slow sweep rates than during faster ones.

Cathodically precipitated 100% $Co(OH)_2$ electrodes were also cycled voltametrically at room temperature in 2N KOH for the purpose of comparison with analogous $Ni(OH)_2$ electrodes. The following observations on the behavior of pure cobalt electrodes were made (refer to Table 6, Section 2c):

1. Lower anodic potentials for Co(II) going to Co(III)
2. The passivated state of the electrode extended over approximately 300 mv negative with respect to oxygen evolution
3. On cycling, the peak current of oxidation gradually shifted to more positive potentials, indicating a mixed potential with $Ni(OH)_2$
4. Although nickel is present only as a substrate below approximately 2 μm $Co(OH)_2$, there was evidence for Ni(II) to Ni(III) anodization after about 30 cycles
5. Q_A was no larger than that of equivalent electrodes containing $Ni(OH)_2$, but it remained more nearly constant with cycling. Also, the charge efficiency, Q_C/Q_A, was about the same as that of other precipitated electrodes

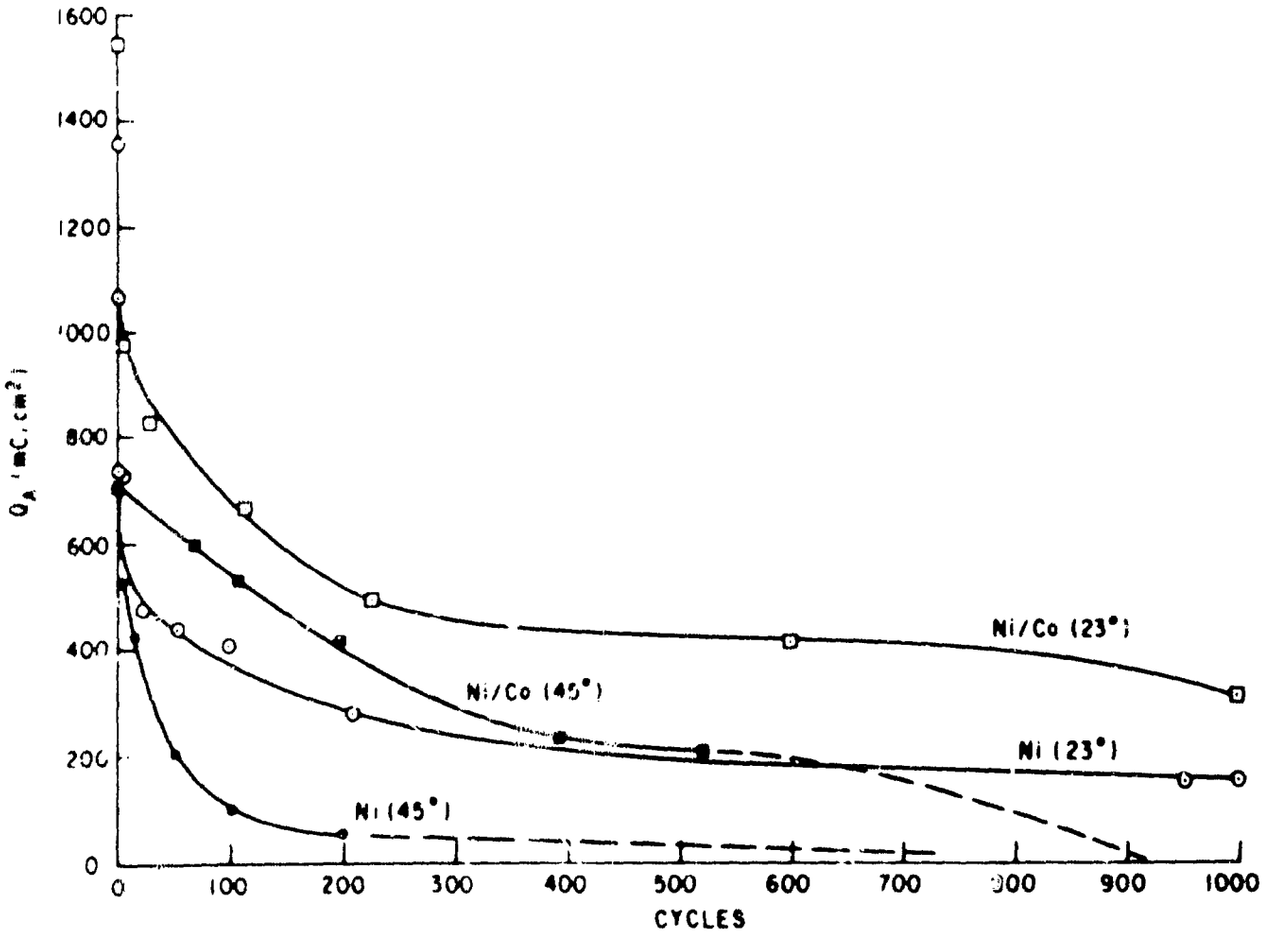

Figure 10. Charge Acceptance of Electrodes in 6N KOH as a Function of Temperature and Cycling

6. Fast sweep measurements showed that cobalt anodization has a higher degree of irreversibility than nickel

7. In Table 7, oxygen evolution potentials are compared at three different sweep rates. Voltages are measured on oscillograph traces which have precision of only about ± 10 mv. Within this precision, the overvoltage of oxygen evolution was the same for $Co(OH)_2$ and $Ni(OH)_2$ electrodes. The values are taken from the oscillograms where the trace crosses the zero-current line. Since there may be a small contribution of Ni(III) reduction to this trace, the overvoltage values represent a minimum. The actual values could be as much as 20 mv larger than those reported in Table 7.

Table 7

OXYGEN EVOLUTION POTENTIALS AT $Ni(OH)_2$ and $Co(OH)_2$ ELECTRODES IN KOH AT ROOM TEMPERATURE

	$Ni(OH)_2$			$Co(OH)_2$		
	Sweep Rate (mv/sec)	Cycle No	Voltage (mv*)	Sweep Rate (mv/sec)	Cycle No	Voltage (mv*)
Slow	2.90	1016	538	2.92	920	541
Medium	18.1	1010	564	18.8	907	558
Fast	99.1	1042	592	100.0	938	573

*Measured versus Hg/HgO to obtain oxygen overvoltage subtract 307 mv.

Quantitative analysis of cobalt in active material was difficult because it was present only in quantities of the order of 100 $\mu g/cm^2$. Atomic absorption and x-ray fluorescence were used as two separate methods for determining cobalt. First attempts at atomic absorption gave uncertain results because substrate nickel was digested with the solution, and cobalt impurities in the nickel substrate (0.055%) were of the same order of magnitude as the cobalt additive itself. Later on, a method devised by H.H. Krüger (Battery Business Section, General Electric Company, Gainesville, Florida) was used to remove active Ni(II) and Co(II) from the substrate without introducing the substrate into the sample to be analyzed.

The results are shown in Table 8. The weights are given in terms of the total weight for a 2-cm by 4-cm sample of nickel substrate foil, 0.0125 cm thick. The nominal values are based on the assumption that in a mixed solution of $Ni(NO_3)_2$ and $Co(NO_3)_2$ equivalent amounts of $Ni(OH)_2$ and $Co(OH)_2$ are precipitated. This need not be true, and it appears from the data of Table 8 that the process favors precipitation of cobalt. The starting material, $Ni(NO_3)_2$, was also tested for cobalt impurities and was found to contain no measurable quantity of cobalt.

Table 8

COBALT ANALYSIS BY ATOMIC ABSORPTION

Sample	Weight of Co (μg/sample)	Weight of Ni (μg/sample)	Total (corrected for blank)	Amount of Co (%) Nominal	Found
Blank Solution	0	45	45	--	--
Blank Solution + Nickel Substrate	0	258	258	--	--
2% $Co(OH)_2$ Nominal	60	2663	2465	1.1	2.4
5% $Co(OH)_2$ Nominal	150	2110	1992	2.7	7.5
10% $Co(OH)_2$ Nominal	320	2313	2375	5.4	13.5

X-ray fluorescence analysis (Table 9) was performed in an electron microprobe, which also yielded photographs of backscattered electron and x-ray scans showing a uniform distribution of nickel and cobalt in the active electrode material.

Table 9

COBALT ANALYSIS BY X-RAY FLUORESCENCE

Sample	X-ray Counts/100 Seconds Ni	Co	Amount of Cobalt (%) Nominal	Found
Standards				
Nickel metal	183,678	617	--	--
Cobalt metal	616	138,403	--	--
$Co(OH)_2$ on Nickel				
3μ	3138	126,483	--	--
8μ	703	129,494	--	--
$Ni(OH)_2$ on Cu(3μ)	99,800	403	--	--
Unknowns				
1% $Co(OH)_2$ nominal	111,625	2478	0.62	2.4
2% $Co(OH)_2$ nominal	117,049	3121	1.1	2.9
5% $Co(OH)_2$ nominal	112,772	8370	2.7	7.0
10% $Co(OH)_2$ nominal	81,055	10,233	5.4	8.5

These results show a considerable uncertainty in the total amount of cations found in the active mass of the electrode. Therefore, it was preferred to report the compositions in terms of the nitrate solutions from which the active mass was cathodically precipitated. However, the results in Tables 8 and 9 indicate that reported values may be minimum values of cobalt concentration and that actually a greater amount of cobalt may have been present.

Whereas the beneficial effect of cobalt on the $Ni(OH)_2$ electrode is fairly well documented, the literature on the effect of zinc addition is quite scant. One source indicates a detrimental effect. Flerov (Ref. 42) found that the presence of zinc in pocket-type $Ni(OH)_2$ electrodes (but not in sintered plates) led to a rapid and substantial decrease in electrode capacity. This was attributed to passivation which may have occurred on the larger $Ni(OH)_2$ particles of the pocket-type electrodes, whereas the distribution of active materials as thin layers prevented passivation in the sintered plate construction. Passivation is attributed to the insulating effect of zinc on the conductivity of $Ni(OH)_2$.

This reflects ideas previously expressed by Lukovtsev and Slaidin. They found only marginal differences in electrode potential with added zinc (Ref. 43), but observed increased oxygen overvoltage to a maximum of 20 mv in the microampere current range, when Li^+, Zn^{+2}, and Al^{+3} were added to $Ni(OH)_2$ (Ref. 44). It was postulated that these ions penetrate into the $Ni(OH)_2$ lattice, thereby hindering H^+ diffusion assumed to be essential for oxygen evolution. The concept of ion exchange in the $Ni(OH)_2$ lattice is now generally accepted. In the case of Zn^{+2}, there may be a connection with Flerov's observation that zinc poisoning was more effective on deep discharge and during prolonged open circuit stand in the discharged than in the charged state.

Cupp (Ref. 45) also tested sintered plates in KOH solutions saturated with LiOH or ZnO. The best cycling efficiency, corresponding to the Q_C/Q_A values obtained in this report, was found in cells with reduced KOH concentration and with ZnO additive. Battery tests were made at the C/4 rate, 25% depth of discharge, and at 60°C, but the reported data are quite sketchy.

In the present study, the effect of zinc additive was studied voltametrically in a manner similar to that employed in the cobalt additive analysis. All experiments were performed at room temperature and at 45°C in electrolytes of 6N KOH or of 6N KOH to which 10 g/l of ZnO had been added. Thus, two different methods were employed for introducing zinc into the $Ni(OH)_2$ electrode: 1) direct addition to the active mass by cathodic co-precipitation; and 2) cycling an electrode in the electrolyte containing ZnO. Sections 3a through 3d of Table 6 represent different combinations of these experimental conditions.

Figure 11 shows the charge acceptance of electrodes as a function of cycle life. For comparison with the electrodes containing zinc, curves for pure nickel and nickel plus cobalt additive are included in Figure 11. There is a beneficial effect of zinc on the maintenance of electrode capacity, par-

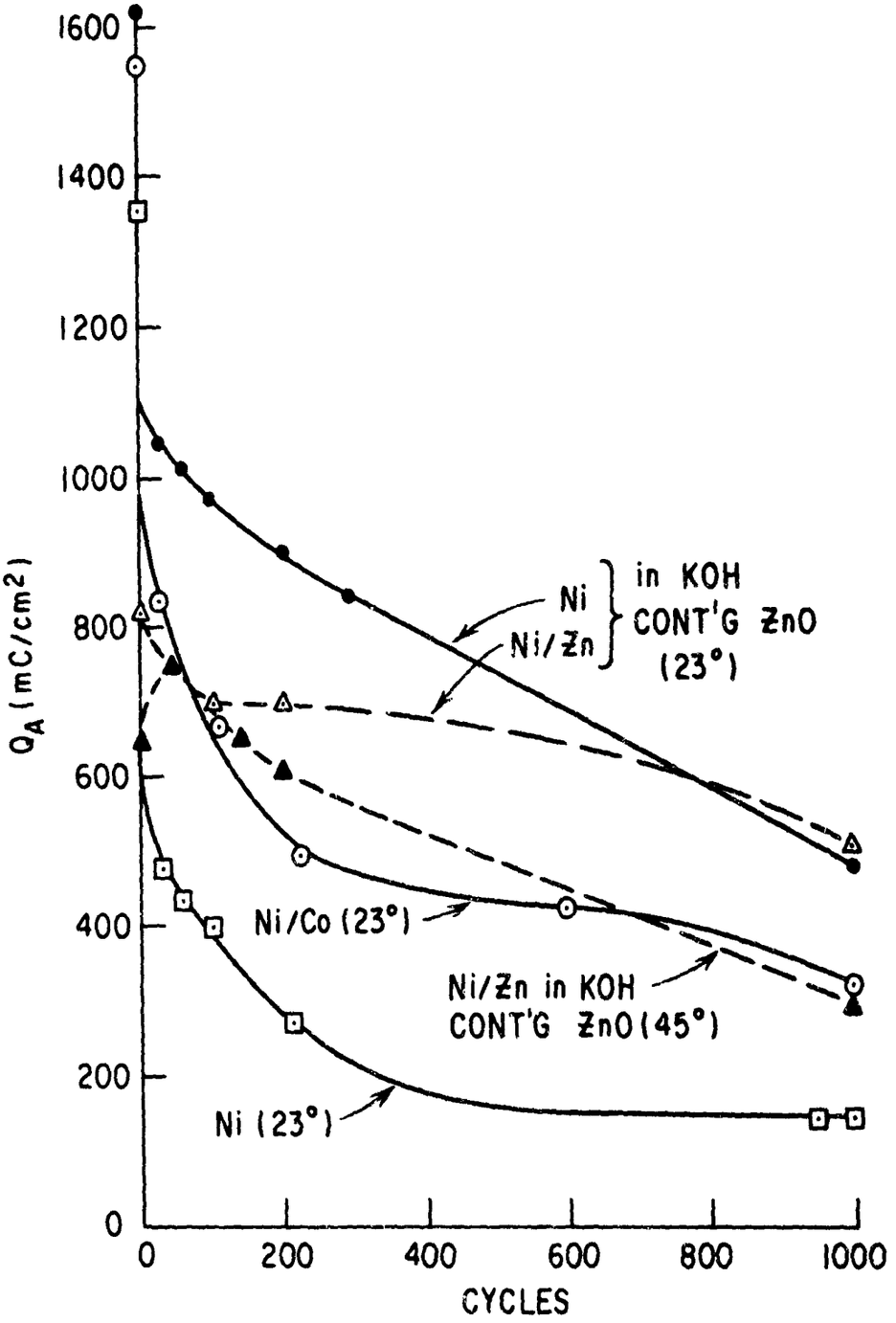

Figure 11. Charge Acceptance of Electrodes in 6N KOH as a Function of Additive, Electrolyte, and Temperature. (Nickel Zinc: Electrode Containing 5% Zinc. Nickel Cobalt: Electrode Containing 10% Cobalt.)

ticularly with ZnO in the electrolyte. For example, the performance of the nickel-zinc electrode in KOH/ZnO electrolyte at 45°C is comparable to that of the nickel-cobalt electrode at room temperature. The effect is most prominent at high temperature. Figure 12 shows the behavior on the 1000th cycle of the electrodes, with and without added zinc. A substantial electrode capacity still remained in the electrode with zinc additive, while the pure nickel electrode had essentially no remaining capacity (note the current density scales on the ordinates).

In the operation of a nickel-zinc cell, the addition of zinc to the nickel positive electrode occurs only as a result of the presence of dissolved ZnO in the electrolyte after some cycling. The above results show that this is a beneficial effect and later in this report it will be shown that appreciable absorption of zinc occurs in a commercial nickel electrode. The experiments pertaining to the effects of other additives aluminum, cadmium, and lithium, are listed in Sections 4, 5, and 6 of Table 6. Whereas 5% aluminum and 5% cadmium were added by cathodic co-precipitation, lithium was added by cycling in the electrolyte of 4.3N KOH + 1.0N LiOH, which was previously used by Tuomi (Ref. 9)

Figure 13 shows the charge acceptance of aluminum- and cadmium-containing electrodes at room temperature and at 45°C. An electrode with 100% $Ni(OH)_2$ as active mass at room temperature is added to Figure 13 to indicate that both aluminum and cadmium improve the performance of the electrode slightly, but not as effectively as cobalt or zinc (refer to Figures 10 and 11).

Figure 14 illustrates the case in which the additive, lithium is added from the electrolyte in the course of cycling. The inflection points in the lithium curves in Figure 14 reflect the incorporation of lithium ions in the active mass and show its beneficial effect. For comparison, points for the best additives (nickel in KOH containing ZnO and nickel plus 10% cobalt) have been added in Figure 14. With lithium as the additive, the $Ni(OH)_2$ electrode seems to suffer least deterioration over prolonged cycling. As an example, the high temperature curve nickel/lithium at 45°C of Figure 14 could have been extended to over 2000 cycles with only moderate further loss of capacity.

In Table 5, the efficiency of cycling thin film electrodes was examined. With the assumption that the difference in discharge and charge capacities is due to the evolution of oxygen, a measure was obtained for the efficacy of an experimental procedure or electrode composition to reduce oxygen evolution. With thin-film electrodes, additives were beneficial to capacity. Table 10 contains a similar tabulation of data extracted from Table 6 for cathodically precipitated electrodes.

In each case, changes in sweep rate were left to the end of the experiment (near Cycle 1000) so as not to interfere with repetitive cycling of the electrode. The data in Table 10 show the same general trend for cathodically precipitated electrodes as for thin-film electrodes (Table 6). Increasing the sweep rate

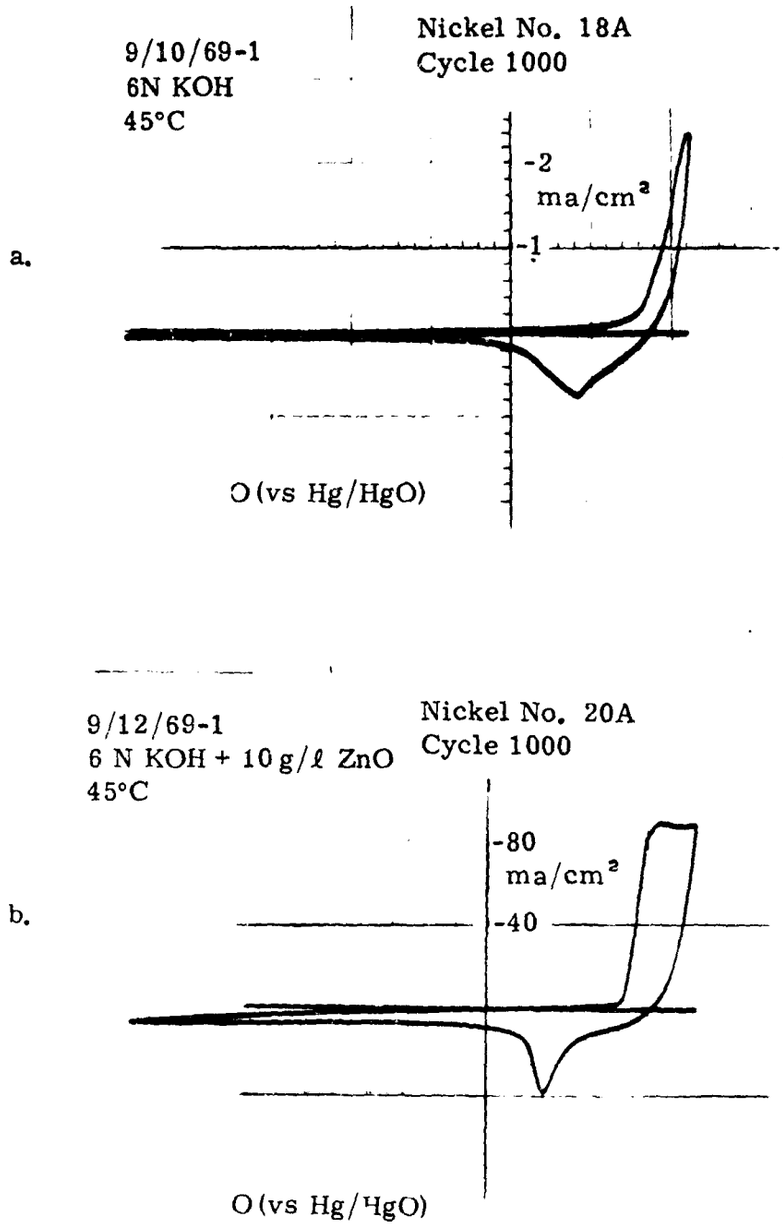

Figure 12. Behavior of Nickel Electrode with (a) and without (b) Zinc Additive in Cycle 1000

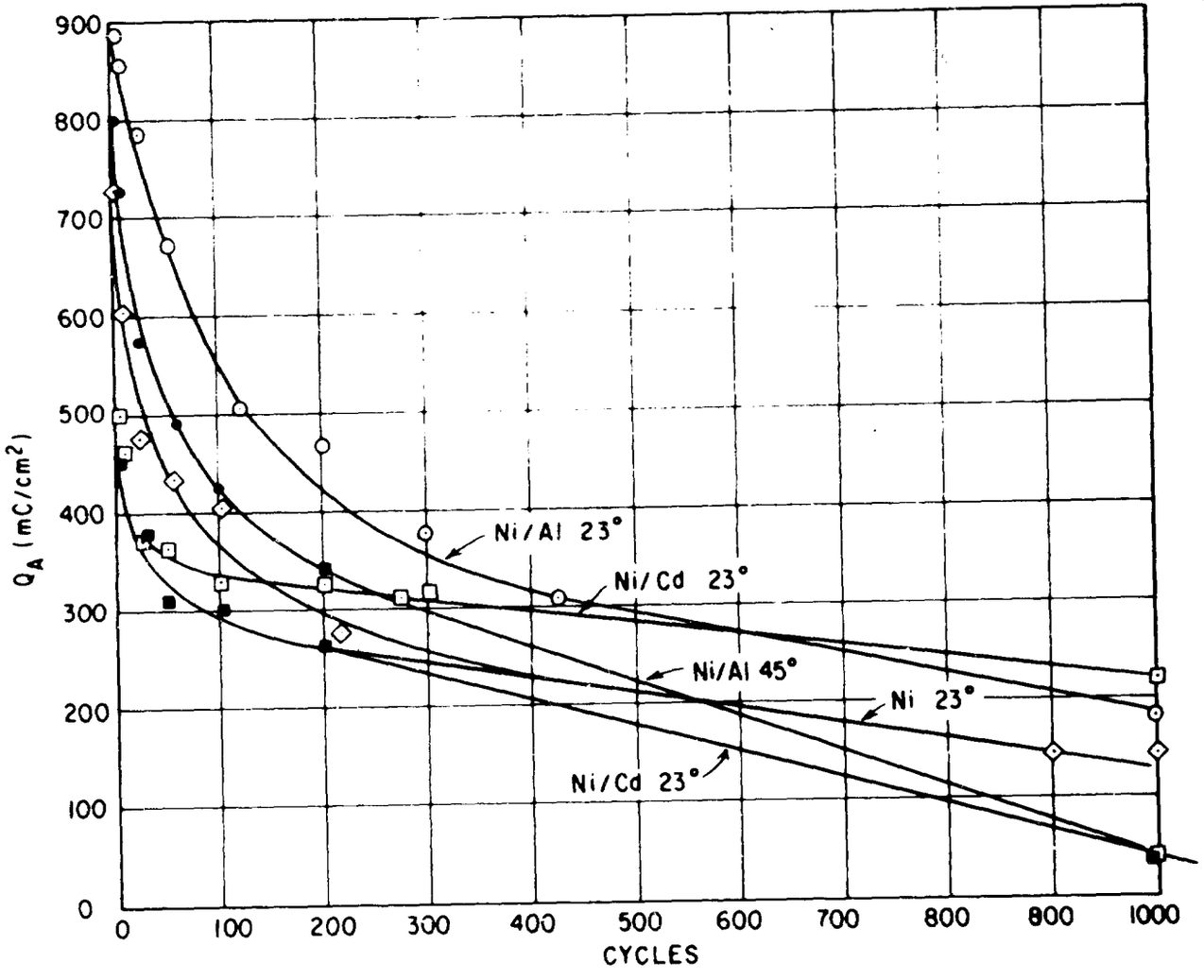

Figure 13. Charge Acceptance of $Ni(OH)_2$ Electrode in 6N KOH with 5% Cd and 5% Al Added (Compared with 100% $Ni(OH)_2$)

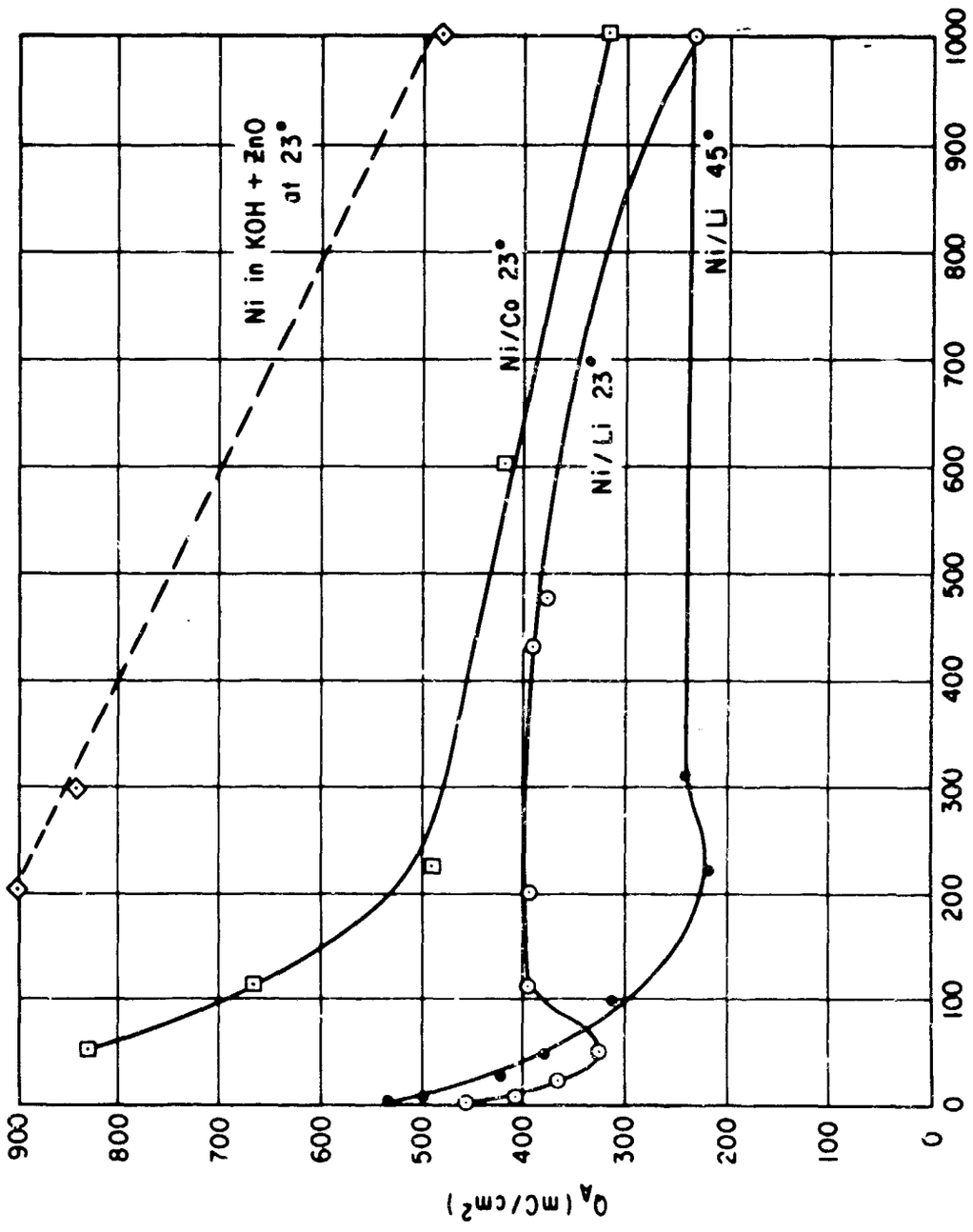

Figure 14. Charge Acceptance of $Ni(OH)_2$ Electrode with Added Lithium from an Electrolyte of 4.3N KOH + 1.0N LiOH

decreased the oxygen evolution and increased the efficiency of cycling. The data exhibit deviations due to experimental factors (such as the influence of the preceding experimental procedure on individual cycles at given sweep rates), but the general trend is that previously indicated. Additives described as most beneficial for electrode capacity by previous data tabulations and graphs show here the least excess of anodic charge over cathodic discharge, e.g., the cases of electrodes in 6N KOH + 10 g/l ZnO.

Table 10

ELECTRODE EFFICIENCY AS A FUNCTION OF ADDITIVE, TEMPERATURE, AND SWEEP RATE

Electrode	Electrolyte	Temperature (°C)	Cycle No.	Sweep Rate (mv/sec)	Anodic Charge Not Discharged $[(Q_A-Q_C)/Q_A] \times 100$ (%)
100% $Ni(OH)_2$	6N KOH	23	1009	2.86	26.0
			1000	18.2	0.7
95% $Ni(OH)_2$ + 5% $Zn(OH)_2$	6N KOH	23	1034	2.90	28.0
			1025	18.4	29.0
			1040	98.0	- 7.9*
100% $Ni(OH)_2$	6N KOH + 10 g/l ZnO	23	1115	2.86	- 3.2
			1000	18.5	23.3
			1144	96.9	-18.0
95% $Ni(OH)_2$ + 5% $Zn(OH)_2$	6N KOH + 10 g/l ZnO	23	1015	2.84	8.6
			1000	18.0	- 2.1
			1030	96.8	-38.0
95% $Ni(OH)_2$ + 5% $Al(OH)_3$	6N KOH	23	1050	2.88	41.0
			1000	18.3	-11.0
95% $Ni(OH)_2$ + 5% $Cd(OH)_2$	6N KOH	23	1015	2.94	31.0
			1000	18.3	34.0
			1013	99.0	29.0
100% $Ni(OH)_2$	4.3N KOH + 1N LiOH	23	1015	2.90	19.0
			1000	18.9	6.3
			1025	98.7	-41.0
100% $Ni(OH)_2$	4.3N KOH + 1N LiOH	45	2332	2.79	52.0
			2318	18.7	- 9.3
			2359	99.6	- 6.7

*Minus value indicates larger discharge than charge.

ABSORPTION OF ZINC IN NICKEL POSITIVE ELECTRODE

The above results showed that $Ni(OH)_2$ electrodes cycled in an electrolyte containing ZnO should have good rechargeability and electrode capacity. That no negative effect (i. e., zinc poisoning) was involved, was corroborated by the analysis of a commercial positive plate which had been used in a nickel-zinc cell. A large nickel electrode was taken from a nickel-zinc cell which had been operated at the C/5 rate for about 40 cycles to a 100% depth of discharge (negative limiting). Reference electrode measurements in conjunction with the nickel-zinc cell cycling test showed that the performance of the positive electrode was unaffected by zinc absorption which took place over the test period (40 cycles to 100% depth of discharge at C/5 = a minimum exposure time of 400 hours). Two samples (A and B) were taken from widely separated areas of the plate and were chemically analyzed.

These areas were noticeably different with regard to color. Sample A came from a lightly colored area which resembled the color of a new plate. Sample B came from a very dark, almost black, region of the electrode. The "active" materials of these samples (hydroxides or oxides of nickel, cobalt or zinc) were dissolved from the sinter and the resulting solution was analyzed by atomic absorption methods to determine the relative amounts of cations present. These results are shown in the first two columns of Table 11. Normalized weight percentages computed from these results (Columns 3 and 4) are in good agreement with actual weights based on the acetates of nickel, cobalt and zinc present in the solution (Columns 5 and 6). This close agreement confirms the assumption that the values obtained correspond to the actual amounts of cations present in the "active" material of the electrode. The difference between Samples A and B is not significant. The major conclusion to be drawn from the analysis is that zinc was absorbed into the positive plate to the extent of about 20% of its "active" cation content during the cycling tests performed on this particular nickel-zinc cell. These results also indicate that the nickel-positive electrode originally contained about 4% cobalt in the active mass.

Table 11

ANALYSIS OF POSITIVE PLATE FROM CYCLED NICKEL-ZINC CELL

Cation	Weight by Analysis (%)		Normalized Weight (%)		Weight Based on Acetates Present (%)	
	A	B	A	B	A	B
Nickel	26.2	28.2	77.5	79.8	79.0	84.8
Zinc	8.0	7.2	18.6	16.1	22.5	20.2
Cobalt	1.4	1.4	4.1	3.9	4.2	4.1
Total	35.6	36.8	100.2	99.8	105.7	109.1

VOLTAMETRIC CYCLING OF CATHODICALLY IMPREGNATED NICKEL PLAQUES AND OF A COMMERCIAL PLATE

In the final series of experiments, the planar nickel foil substrate was replaced by a commercial nickel plaque structure and by a commercially impregnated plate. Thus, the geometry of the electrode became more complex and the voltametric test method was put to the limit of its applicability. Experimental conditions remained the same as those used in conjunction with previous tests on foil electrodes, except that the sweep rates were lowered in order to obtain greater utilization of deeper-lying active materials resulting from heavier plate loading.

The greater depth of the active material in the commercial plate made it difficult to separate the Ni(II) → Ni(III) oxidation peak from the oxygen evolution peak. Attempts to accomplish this separation were only partially successful. Therefore, it was decided to base the quantitative determinations of capacity with respect to the number of cycles on the nickel reduction peak (electrode discharge capacity, Q_C) instead of on the previously used oxidation peak, Q_A.

Table 12 lists the electrodes studied in this series of experiments with respect to the extent of cobalt addition and loading (impregnation) of the sintered matrix. The bare sinter consisted of a 4-mil strip of perforated steel with 10.5 mils of nickel sinter on either side of the strip. This material was used as a blank without any impregnation to judge the effect of the corrosive alkali attack on the sinter during cycling. In four other cases, the sinter was impregnated to a different extent by cathodic precipitation with $Ni(OH)_2$ plus 0, 2, 10, and 20% $Co(OH)_2$. Finally, an electrode prepared commercially by decomposition of the nitrates in an alkaline solution was evaluated as another boundary case of a commercially successful plate.

Table 12

PREPARATION AND COMPOSITION OF ELECTRODES WITH SINTERED NICKEL MATRIX

Electrode No.	Structure	Composition (%) Ni	Co	Impregnation (ma/cm², minutes, mC cm²)			Thickness (inches)	Theoretical Capacity (amp-hrs in.³)
1	Sinter only			no impregnation				
2	Cathodic precipitate in plaque	100	0	0.911	30	1640	10.5	0.28
3	Cathodic precipitate in plaque	98	2	1.85	75	8328	10.5	1.42
4	Cathodic precipitate in plaque	90	10	2.12	150	19,068	10.5	3.25
5	Cathodic precipitate in plaque	80	20	2.05	75	9211	10.5	1.57
6	Commercial plate	95	5 *	(3.2 amp-hrs in.⁻³)			25.0	8.26

* Experience

Electrode 1 had an initial capacity of 130 mC/cm^2 (Cycle 1) which at Cycles 50 and 100 went through a minimum of 115 mC/cm^2 and then increased approximately linearly to 345 mC/cm^2 at Cycle 2000. At this time, it was comparable to an electrode capacity of 0.03 ampere-hour/$inch^2$. Although not negligible, this represents only a small percentage of the capacity of the impregnated electrodes (note the last column of Table 12). Furthermore, the initial capacity of the sinter indicates a ratio of effective-surface to apparent-surface (or roughness factor) of about 100, based on the presence of approximately two monolayers of the hydroxide on the sinter.

The experimental data and the results for the remaining electrodes (2 through 6) are given in Table 13. All experiments were performed at 45°C in order to accelerate the cycle-life test.

The discharge capacity, Q_C, for all of these electrodes is shown as a function of cycle life in Figure 15. After an increase in capacity, the commercial plate had a loss from 3.83 to 1.81 ampere-hours/$inch^3$ (refer to Table 13), whereas cathodically impregnated plaques experienced less deterioration. This may be traced to the greater extent of loading in the commercial plate.

Different plate loadings and sweep rates influence the relative rating of the electrodes, as seen in Figure 15. The effect of loading is illustrated in Figure 16, in which the utilization (i.e., the ratio of actual discharge over the theoretical capacity) is plotted against cycle life rather than the discharge capacity itself. A different ranking, favoring the lightest-loaded electrode, is obtained.

Obviously, both loading and discharge capacity must be taken into account in determining the optimum amount of cobalt additive. Regarding the sweep rate, it is noted in Table 13 that Electrode 6 was cycled more slowly at first, then after Cycle 274 more rapidly than Electrodes 3, 4, and 5. This could only account to a small extent for the more rapid decrease in utilization of this electrode (refer to Figure 16). A greater variation of sweep rate, from 10 mv/sec for Electrode 2 versus 2.8 mv/sec for others, could increase the value of Q_C for the cobalt-free Electrode 2 by as much as 30% (refer to Figure 15).

CONCLUSIONS

The mechanism of the $Ni(OH)_2$ electrode reactions is discussed at some length in the introduction to this section. Two main factors to be considered are the electrochemical parameters and the physical structure of the electrode. The former can be isolated and uniquely studied in idealized electrode configurations; the latter may be decisive in determining the battery performance of commercial cells. Also important is the intimacy with which the experimental methods are tied to the materials and processes. Thus, the results of the present study have to be considered in view of the different

Table 13

CYCLIC VOLTAMETRY OF IMPREGNATED NICKEL PLATE ELECTRODES

Cycle No.	Sweep Rate (mv/sec)	Scanned Range (mv)	Anodization			Cathodization				Efficiency (Q_C/Q_A)	Utilization (%)
			Peak Current (ma/cm^2)	At Voltage (mv)	Anodic Charge (mC/cm^2)	Peak Current (ma/cm^2)	At Voltage (mv)	Cathodic Charge (mC/cm^2)	($amp\text{-}hrs/in^3$)		
			Electrode 2 -- 100% $Ni(OH)_2$, 2.195 cm^2, 6N KOH, 45°C								
1	10	-211 to +611	98	545	1149	76	271	1109	0.19	0.97	68
2	10	-211 to +611	87	517	1113	76	271	1109	0.19	0.99	68
10	10	-173 to +648	63	561	870	69	293	939	0.16	1.07	57
25	10	-178 to +640	64	576	831	60	292	847	0.14	1.02	51
50	10	-116 to +703	66	581	816	63	300	843	0.14	1.03	51
100	10	-157 to +633	68	571	807	62	285	866	0.15	1.07	53
125	10	-173 to +643	66	563	767	61	290	805	0.14	1.05	49
460	10	-180 to +645	66	565	701	52	295	715	0.12	1.05	44
600	10	-172 to +652	68	548	724	52	290	710	0.12	0.98	43
			Electrode 3 -- 98% $Ni(OH)_2$ + 2% $Co(OH)_2$, 2.162 cm^2, 6N KOH, 45°C								
5	2.86	-121 to +608	93	583	3375	91	303	3869	0.65	1.13	46
140	2.86	-108 to +621	103	583	3461	78	303	3478	0.59	1.00	42
190	2.86	-113 to +619	103	589	3266	78	299	3487	0.60	1.07	42
319	2.86	-116 to +616	105	593	3357	84	299	3776	0.64	1.12	45
476	2.86	-115 to +615	100	590	3212	79	303	3519	0.60	1.09	42
657	2.86	-119 to +614	96	590	2923	69	314	3093	0.53	1.06	37
794	2.86	-116 to +616	99	595	2987	60	324	3257	0.56	1.09	39
854	2.86	-116 to +616	94	590	2878	53	332	3089	0.53	1.07	37
964	2.86	-116 to +616	101	600	2872	62	372	3096	0.53	1.08	37
			Electrode 4 -- 90% $Ni(OH)_2$ + 10% $Co(OH)_2$, 1.888 cm^2, 6N KOH, 45°C								
3	2.81	-127 to +598	180	593	10,000	185	108	11,030	2.39	1.40	74
9	2.81	- 99 to +629	121	595	7850	121	169	9625	1.64	1.23	50
11	2.81	- 99 to +629	122	603	8970	127	165	9676	1.65	1.39	51
129	2.81	- 63 to +660	119	632	4810	91	260	6724	1.15	1.40	35

320	2.81	- 56 to +669	127	639	5470	99	266	6115	1.04	1.11	32
471	2.81	- 58 to +657	130	629	5710	108	257	7218	1.23	1.26	34
638	2.81	- 58 to +667	125	668	5450	102	255	6272	1.07	1.15	33
799	2.81	- 58 to +668	125	633	5340	93	273	5661	0.97	1.01	30

Electrode 5 -- 80% $Ni(OH)_2$ + 20% $Co(OH)_2$, 1.954 cm^2, 6N KOH, 45°C

1	2.93	-116 to +616	143	550	7212	117	217	5876	1.00	0.82	64
2	2.93	-116 to +616	107	494	5290	110	192	5436	0.98	1.08	62
7	2.83	-171 to +560	104* (89)	466 (513)	5180	104	196	4998	0.85	0.96	54
13	2.83	-171 to +561	92 (90)	470 (522)	4715	93	218	5100	0.87	1.08	55
187	2.83	-121 to +612	105	578	3546	69	224	3571	0.61	1.01	39

* Parentheses indicate 2nd peaks

Electrode 5 -- 80% $Ni(OH)_2$ + 20% $Co(OH)_2$, 1.954 cm^2, 6N KOH, 45°C (cont'd)

238	2.83	-121 to +610	116	582	3524	72	325	3595	0.61	1.02	39
395	2.83	-101 to +630	103	602	3417	67	324	3032	0.52	0.39	33
570	2.83	-102 to +629	103	608	3640	70	310	3182	0.54	0.87	35
715	2.83	-102 to +629	99	608	3168	71	321	3438	0.59	1.09	37
927	2.83	-102 to +629	99	612	3114	58 (56)	328 (375)	3582	0.61	1.15	39
1037	2.83	-103 to +628	100	613	2971	54 (59)	334 (364)	3264	0.56	1.10	35
1040	1.57	-127 to +604	46	581	3991	37 (42)	352 (370)	3377	0.58	0.85	37
1045	7.47	- 55 to +675	--	--	2199	105	326	3223	0.55	1.47	35

Electrode 6 -- Commercial Nickel Plate, 0.301 cm^2, 6N KOH, 45°C

26	1.50	03 to +691	158	625	12,770	160	277	20,600	2.95	1.61	36
101	1.50	- 81 to +654	185	586	14,170	150	284	20,380	2.92	1.44	35
199	1.50	- 33 to +674	226	592	19,270	204	252	26,740	3.83	1.38	46
274	1.50	- 62 to +648	240	594	22,330	199	270	25,470	3.65	1.14	44
595	4.24	- 10 to +706	445	656	6606	385	222	14,150	2.02	2.14	24
825	4.24	- 16 to +699	459	655	9704	356	219	12,600	1.81	1.28	22

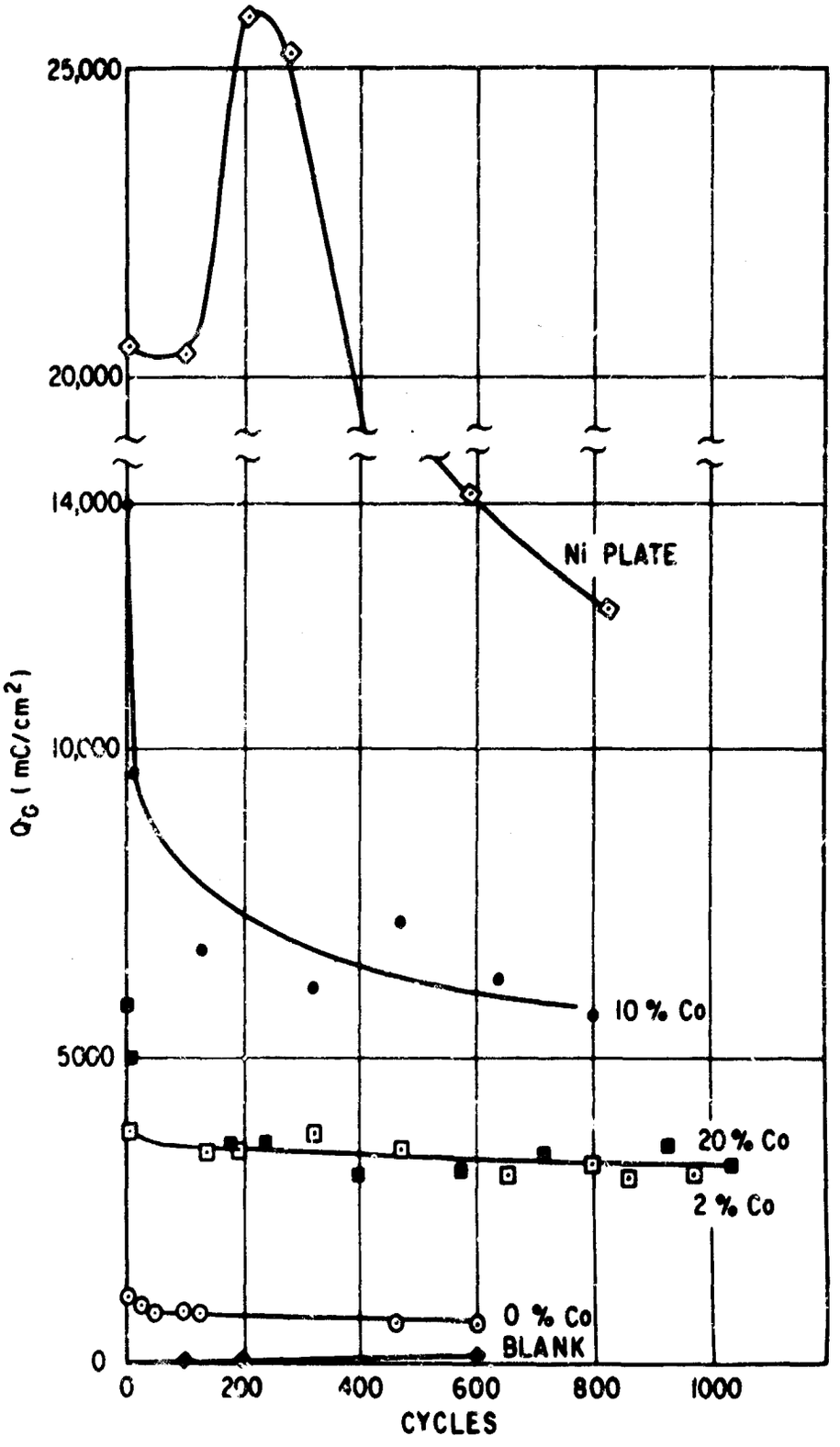

Figure 15. Discharge Capacity of Impregnated Nickel Plate Electrodes at 45°C

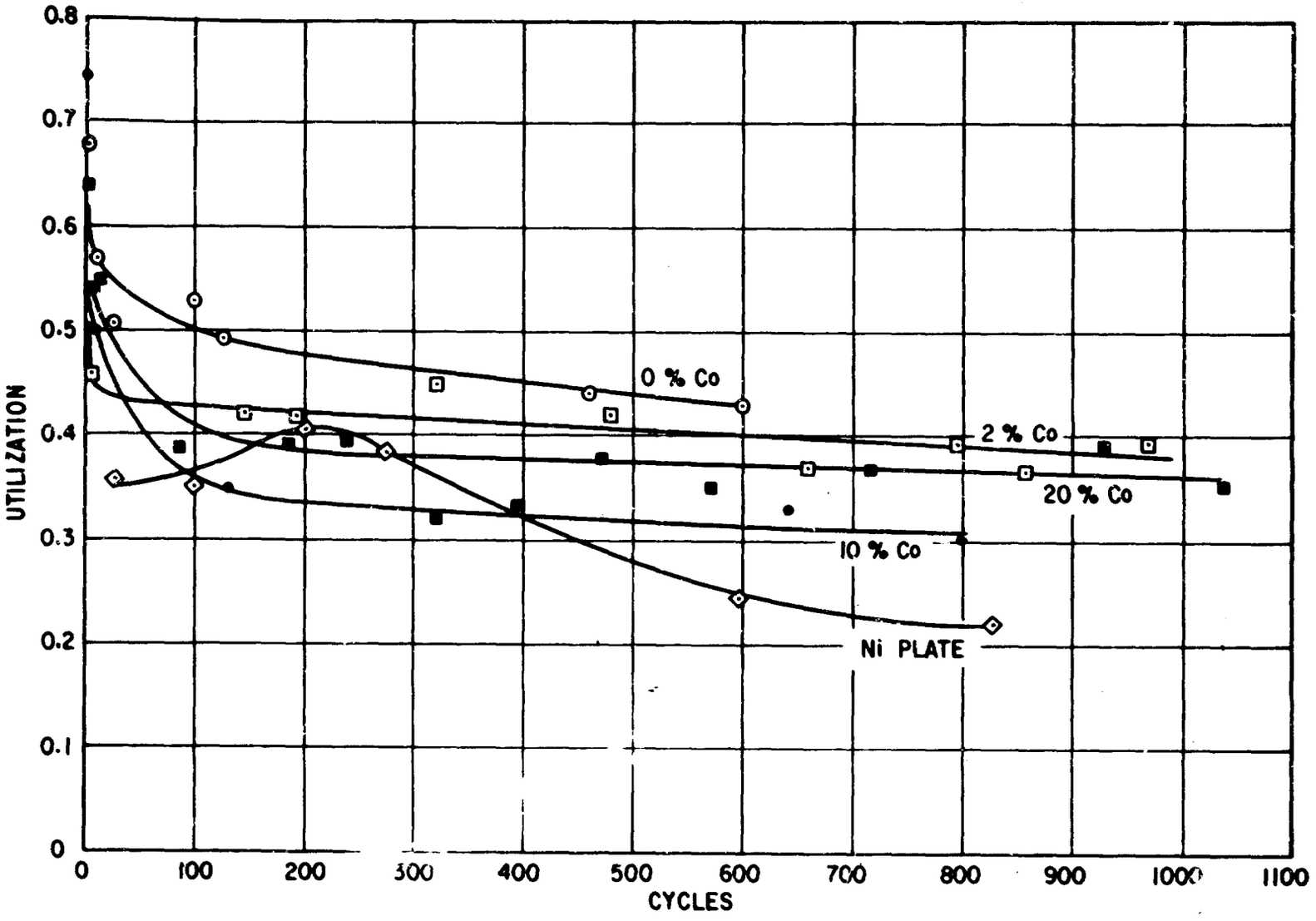

Figure 16. Utilization of Active Material in Impregnated Nickel Plate Electrodes as a Function of Cycle Life at 45°C

electrode structures examined and also with respect to the specific testing program used.

A spectrum of electrode structures, from thin monolayers of active material to commercial plates, was studied. This comprehensive selection was made possible by severely restricting the additive study to essentially one approach -- voltametric cycling. This technique is commonly used in basic electrode studies, but only recently has it been applied to battery studies (Ref. 46).

The following are the central conclusions of the work on additives:

1. Cobalt and zinc are effective cation additives to the $Ni(OH)_2$ active mass. They increase charge acceptance and maintain discharge capacity as a function of cycle life, particularly at high temperature (45°C).

2. Addition of the foreign ion to the $Ni(OH)_2$ lattice from the electrolyte solution is more effective than direct incorporation of the cation by co-precipitation, co-deposition, or alloy oxidation.

3. Other additives, cadmium and aluminum, had a lesser effect on improving capacity at cycle life and high temperature. However, all deliberately added cations, Li^+, Co^{+2}, Zn^{+2}, Cd^{+2}, and Al^{+3}, had some positive effect, and none were deleterious.

4. Although an optimum cobalt content was not established, cycling of cathodically precipitated material in nickel plaques indicated improved capacity with 2 to 20% cobalt added. The largest capacity was that of an electrode with 10% cobalt, however, that electrode was also the most heavily loaded one.

Lack of time permitted only a limited number of experiments in the final series with nickel plaques containing cathodically precipitated hydroxides and with the impregnated commercial plate (Table 13 and Figure 15 and 16). Two factors influencing electrode performance, loading (indicated by discharge capacity), and utilization have already been singled out. They are depicted in Figures 17 and 18. In Figure 17, the electrode containing 10% cobalt has the largest discharge capacity. However, as pointed out previously, it also had the greatest amount of active material. This loading was the same for the 2 and 20% cobalt samples, of which the latter had the higher capacity. The advantage of adding cobalt is clear when compared with the cobalt-free electrode in Figure 17. Conversely, the cobalt-free electrode has highest utilization in Figure 18. This reflects the more irreversible oxidation of Co(II) → Co(III) than the analogous Ni(II) oxidation. Otherwise, utilization remained the same for all of the cobalt-containing electrodes during cycling. Taking into account that higher loading should be detrimental to high utilization, 10% cobalt is still the choice in spite of the reservation mentioned above. This choice is also in agreement with the findings of Januszkiewicz (Ref. 47), who finds a plateau at 10 to 30% cobalt for the beneficial effect of cobalt on electrode capacity.

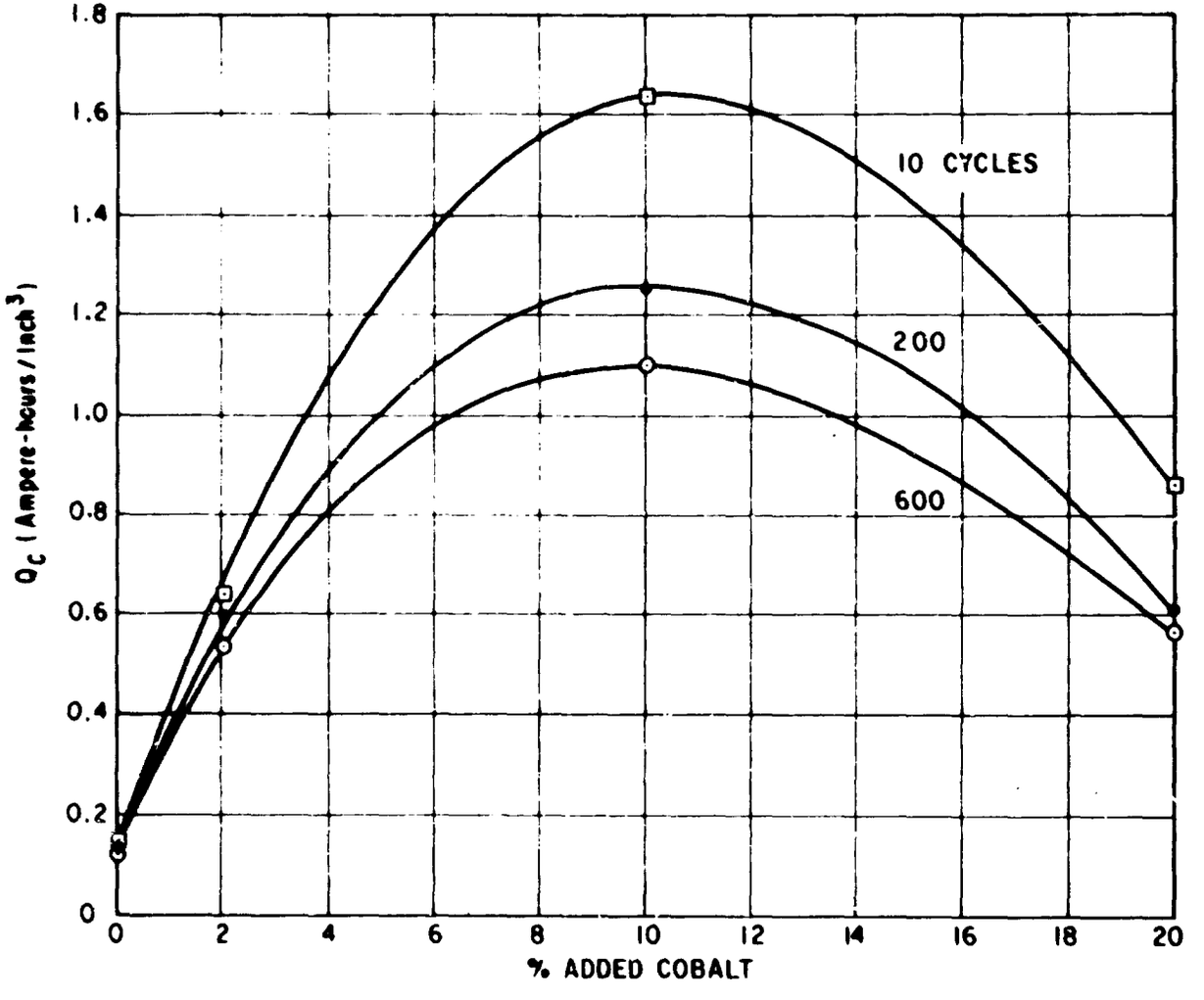

Figure 17. Discharge Capacity as a Function of Cobalt Content and Cycle Life at 45°C

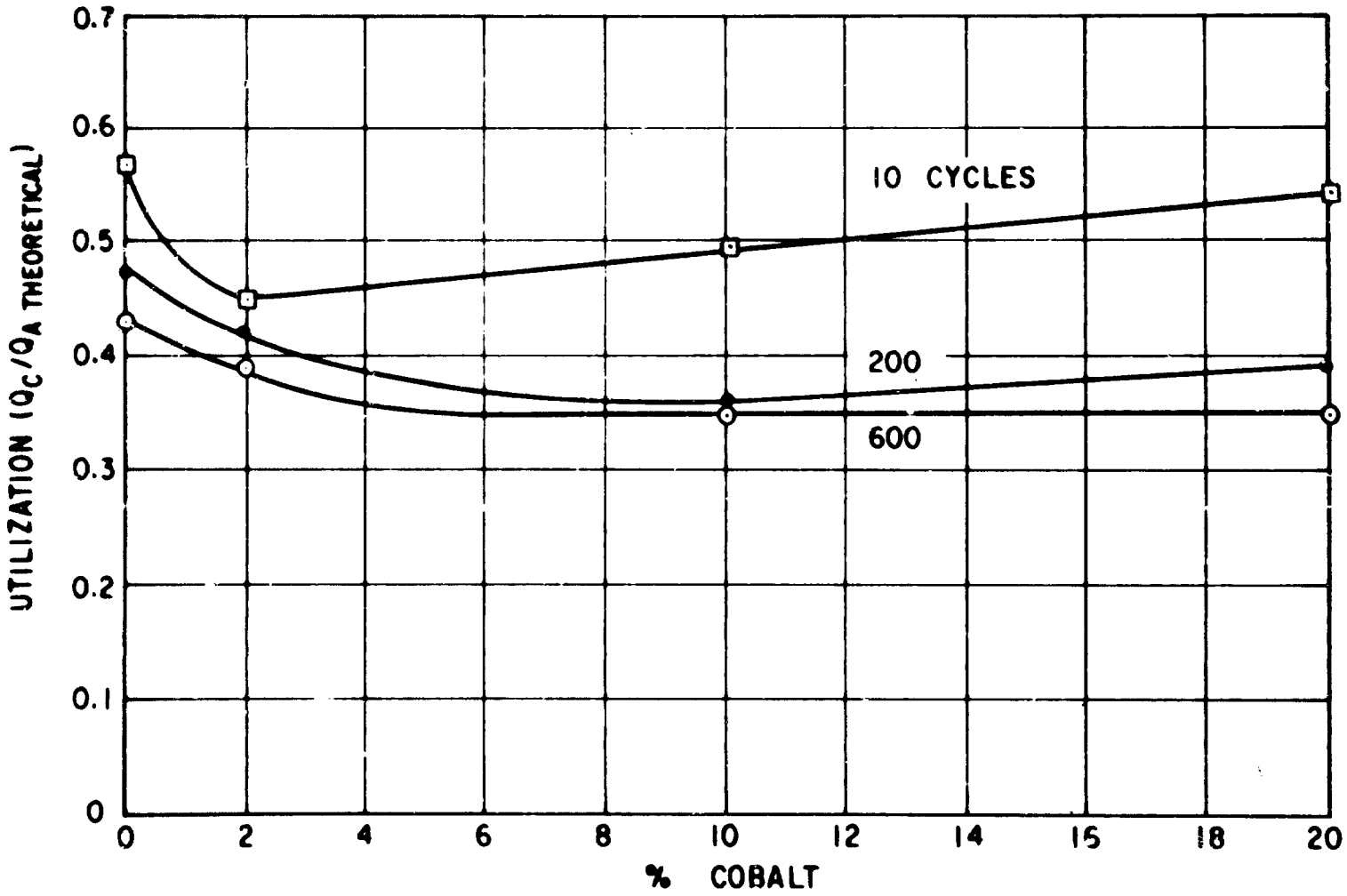

Figure 18. Utilization of Active Material as a Function of Cobalt Content and Cycle Life at 45°C

The effect of cobalt on the $Ni(OH)_2$ lattice structure is characterized by increased electrode charge acceptance, lower cathodic potential (higher overvoltage), and incomplete reduction of active material at higher potentials. These factors suggest a possible retarding influence by cobalt on the electrode reactions. In thin-film electrodes, the presence of cobalt also reduces oxygen evolution. In battery practice, these phenomena may lead to better charge retention. Such an interpretation of the data fits into the recognized mechanism of the $Ni(OH)_2$ electrode reaction described in terms of the work of Wynne-Jones, Casey, Harivel, and others. Cobalt ions penetrate into the $Ni(OH)_2$ lattice together with protons, OH^- ions, and other species related to the water molecule. Thus, the disordered structure of the lattice is increased, thereby preventing the greater order and compaction of crystallites resulting from grain growth and phase change.

The open α-phase structure, described by Bode (Ref. 7), was encountered in the present study in the first electrode cycles only. The much greater first-cycle capacity of the electrodes can be directly traced to crystal structure. In the cited work of Bode, it is also pointed out that $Zn(OH)_2$ (forming a mixed $Ni(OH)_2$-$Zn(OH)_2$) stablizes the α-phase. This explains the beneficial effect of the zinc additive.

The observation that additives are best added from the liquid phase during the formation of electrodes also fits into this picture. They are introduced onto the surface of the active material and change the crystal lattice in the surface layers of the active mass where needed most for later electrode reactions.

Finally, it must be reiterated that these results were obtained with a specific test procedure. Linear sweep voltametry discharges active materials in seconds or minutes, whereas conventional battery testing techniques range into hours. The voltametric procedure applied to commercial plates is analogous to constant potential charging, in that the maximum electrode potential is limited. The controlled, gradual rise in charging voltage up to this maximum value in the voltametric procedure protects the electrode from exposure to the high initial current surges and correspondingly high operating stresses which occur in conventional constant potential charging regimes.

Nevertheless, the method essentially involves fast charging and discharging, conventionally viewed in battery technology as high C rates. Further work and experimental improvements of the voltametric test method are recommended. If it can be reconciled and correlated with more common battery tests, a new method of accelerated battery life testing based on the observation of electrode reactions would become available. Transient and uncertain phenomena, such as the memory effect, may become amenable to systematic study.

The following information was added during the final review of this report.

A study of ionic transport during the anodic oxidation of $Ni(OH)_2$ has been published (Ref. 48) in which a mechanism of OH^- exchange at the electrode

electrolyte interface and both H^+ and OH^- ion transport in the hydroxide are postulated. Substantial isotopic exchange of O^{18} with O^{16} occurred when thin films of cathodically precipitated hydroxide were anodized in H_2O^{18}. Coulometric and thermogravimetric experiments were also performed. As a result, the self-diffusion coefficient for OH^- ions in $Ni(OH)_2$ of 2.5×10^{-16} cm^2/sec was determined.

Contrary to the large mobility of protons in $Ni^{II}(OH)_2$ (refer to MacArthur's work, unpublished result), radiometric measurements indicated that participation of H^+ ions in the charge process is very limited. This passivation of protonic transport is attributed to trapping of H^+ in the oxidized structure, that is, in the form of $Ni(OH)_3$.

The perturbation of the crystalline structure by incorporation of cations (Li^+) and anions is also mentioned. Only chromate anions had a detrimental, passivating effect on the discharge of the oxidized hydroxide.

Section 3

SUBSTRATE ANALYSIS

INTRODUCTION AND OBJECTIVE

This task has been directed toward finding a practical, stable substrate material as one means for achieving the ± 1% electrode capacity reproducibility goal of this program. It is a well known fact that pure nickel substrates corrode to some extent during cycling of the nickel hydroxide electrode. This phenomenon leads to alteration of the active mass and, under severe conditions, to the eventual loss of mechanical integrity of the structure. In the case of sintered nickel substrates, corrosion may be so extensive as to place the capacity reproducibility tolerance completely out of range.

Popat et al (Ref. 49) have shown that from 30 to 40% of the initially formed plate capacity can be attributed to nickel substrate corrosion during conventional impregnation and forming processes. Briggs (Ref. 50) "induced" capacities up to 1 ma hour/cm^2 on planar nickel foils by anodically oxidizing the foils under conditions similar to those encountered during the charging of conventional nickel hydroxide electrodes. It was anticipated that these corrosion phenomena would occur with any nickel substrate configuration whether it be sintered, foam, fiber, filamentary,or flake material. It was also anticipated that it might, therefore, be extremely difficult to specify or control the final plate capacity of electrodes employing nickel as the substrate material.

As a result, it was decided that materials other than pure nickel should be examined for suitability in providing the required electronic conductivity and mechanical support for the active material of the electrode. The objective of this task was, therefore, aimed at finding electronically conductive substrate materials which would satisfy the following basic criteria:

1. Compatibility. The substrate must be completely compatible with the charged and discharged forms of the active material i.e., NiOOH and $Ni(OH)_2$ respectively.
2. Stability. The substrate must be stable with respect to corrosion or attack by the alkali electrolyte or the cell impurities over the entire range of potentials normally encountered by the operating electrode.
3. Overvoltage. The substrate must have sufficiently high oxygen overvoltage to permit efficient and complete charging of the active material prior to the onset of oxygen evolution.
4. Fabrication. The selected material must be suitable with regard to economic methods for fabricating the appropriate configuration.

SELECTION OF SUBSTRATE MATERIALS

In this task, candidate substrate materials, or alloys, were chosen for evaluation on the basis of their corrosion-resistant rating in aqueous alkali, nitrate, and carbonate solutions, as reported in Reference 51. This reference lists over 100 metals and alloys which are rated "good" for chemical resistance to aqueous NaOH. About 40 of these materials are rated "good" with respect to $NaNO_3$ and Na_2CO_3 solutions at various concentrations and temperatures. From the latter list and with consideration of the four substrate criteria discussed above, the following candidate materials were selected for study:

- Carbon
- Nickel porous plaque*
- Stainless steel
- Pure nickel
- Pure platinum
- Hastelloy** nickel-base alloy
- Platinum alloys
- Nickel-copper alloy (Monel**)
- Lithiated nickel oxide

The decision to include lithiated nickel oxide in the above list of materials was based on the fact that semiconducting lithium-nickel oxide surfaces were reported to offer good corrosion protection for high temperature nickel, fuel cell electrodes and auxiliary charging electrodes for rechargeable zinc-air cells. In addition, it appeared that a conventional nickel battery plaque could be used as the starting material to prepare porous "lithiated" plaque samples for immediate evaluation.

Bacon and Jones (Ref. 52) were the first to disclose the practical use of "lithiation" for corrosion protection in electrochemical systems. They applied lithium salts in aqueous solution to porous nickel plaques prior to high temperature air oxidation of the sinter. The lithium ions, which become incorporated in the oxide, convert the usual nonconductive green nickel oxide to a black, semiconducting, adherent surface oxide. This has been shown to decrease the oxidation rate of the underlying nickel in alkaline liquids under strongly oxidising conditions, such as those that occur when oxygen is present at higher pressure.

Garfinkel and Weininger (Ref. 53) have obtained improved results from the standpoint of a more uniform and impervious thin oxide film on nickel substrates. They accomplished this by introducing lithium via a vapor-phase transport from a large excess of Li_2O present with the sample during the heat treatment process. This improvement is thought to be caused by the relatively high vapor pressure of Li_2O at temperatures above 600° C.

*Conventional battery plaque from the General Electric Company's Battery Business Section.

**Trademark

After examining several alternative lithiation processes, the following procedure was selected for preparing the lithiated nickel foil and plaque samples for this study:

1. Anneal -- at 1000°C for 30 minutes in a hydrogen atmosphere (stainless steel retort).
2. Degas -- at 1000°C for 10 minutes in a vacuum (vacuum induction furnace).
3. Oxidize -- at 680°C for 10 minutes in air (box furnace).
4. Lithiate -- at 680°C for one hour in air by introducing a stainless steel boat containing a premixed Li_2O-Ni p wder under the samples to be treated (box furnace).

Initial attempts to determine the amount of lithium incorporated in the oxide surface of the treated samples, using either x-ray analysis or flame photometry, were unsuccessful because of the extremely thin (~500Å) oxide layer thickness. Since the surface conductivity of the treated samples, as determined by means of a simple ohmmeter (two point method), was found to be comparable to that of the same but untreated nickel material, no further effort was made to analyze the composition of the surface oxides obtained. In all cases, the latter was a thin, dark green, almost black, adherent coating with a metallic luster (when prepared as above).

Evaluation Tests

Corrosion tests on the candidate substrate materials were conducted in a hydrolysis cell shown schematically in Figure 19. Figure 20 shows the six-station test stand used in conjunction with this task. In these screening tests, oxygen was generated at the test sample by means of a constant-current power supply to simulate the conditions of the nickel hydroxide electrode during overcharging. The potential of each test electrode (versus a Hg/HgO reference electrode) was continuously recorded throughout these tests. The cells were sealed by means of a rubber stopper and purged with oxygen to prevent CO_2 contamination from the ambient.

The first screening test was conducted in a pure 31% KOH electrolyte for a total exposure of about 7 ampere-hours/cm² at a current density of approximately 15 ma/cm², based on the geometric area of the samples. At the end of this test, a quantitative analysis of the electrolyte in each cell was made. The results of this initial test are summarized in Table 14. The purpose of this test was to eliminate from further testing those materials which showed evidence of gross physical attack or an unusually low oxygen overvoltage. With regard to the latter condition, all of the samples demonstrated sufficiently high operating potentials under the test conditions that this criteria could not be used as a significant factor in ranking the alloy samples. The platinum

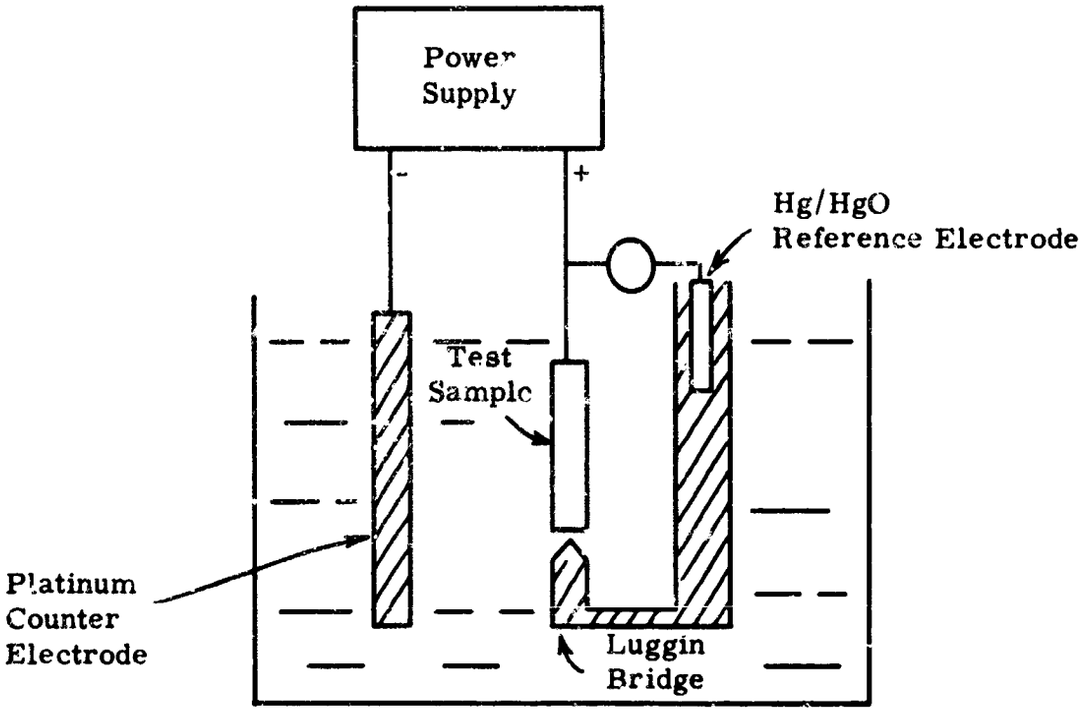

Figure 19. Schematic Diagram of Hydrolysis Cell

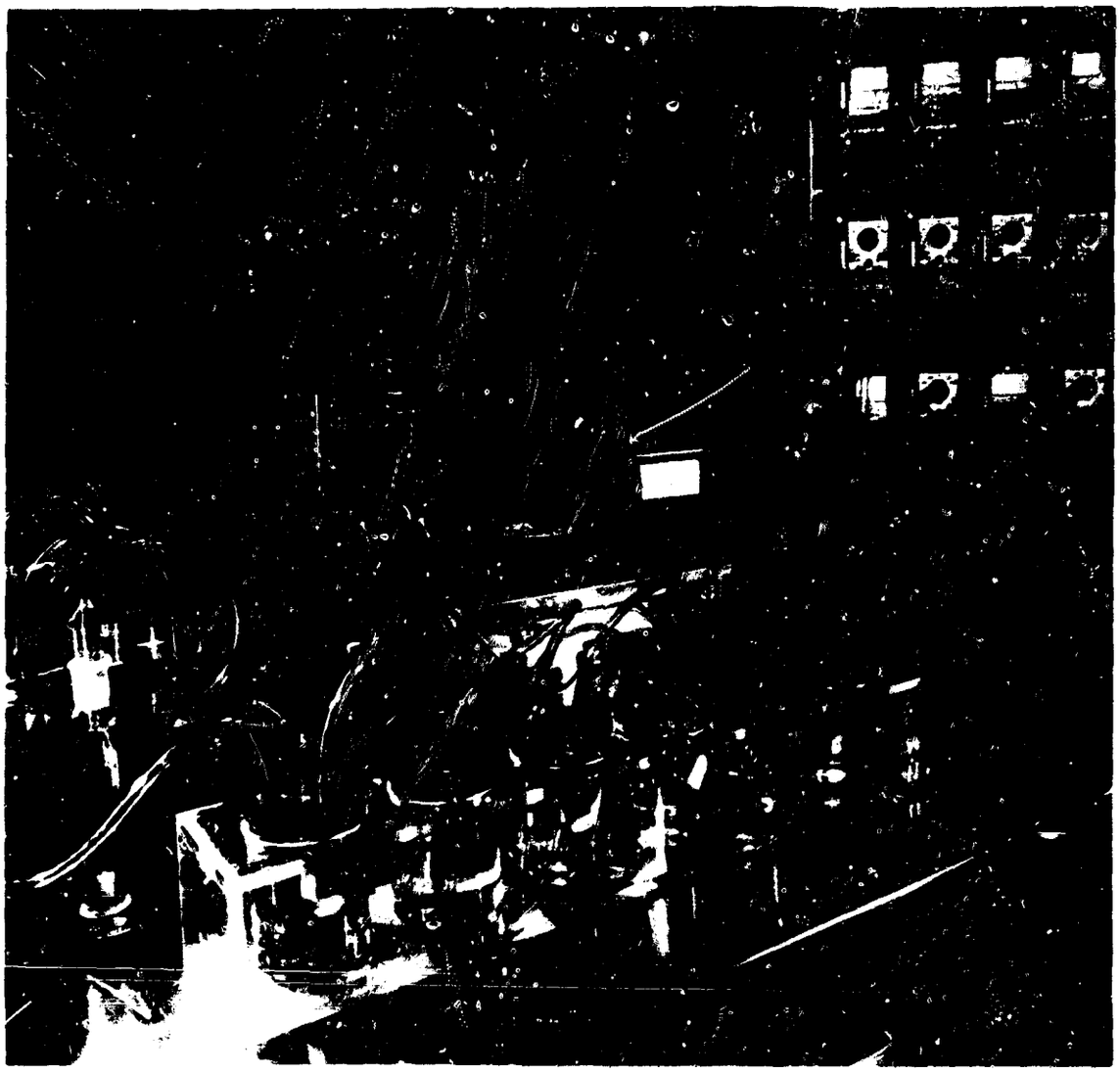

Figure 20. Six-station Corrosion Test Stand

Table 14

RESULTS OF PRELIMINARY SUBSTRATE CORROSION TEST

Sample Identity	Anodic Exposure (amp-hrs/cm²)	Polarization			Quantitative Analysis of Electrolyte			
		Initial (volts)	Terminal (volts)	Change (volts)	CO_3 (%)	Fe (ppm)	Cr (ppm)	Ni (ppm)
Pure Platinum	6.7	0.723	0.975	0.252	0.35 ± 0.06	--	--	--
Nickel(1 Plaque	6.7	0.507	0.534	0.027	0.41 ± 0.06	--	--	<
Nickel(2 Strip (Pure)	6.7	0.554	0.635	0.071	0.41 ± 0.06	--	--	<1
Graphite(3	8.6	0.577	0.637	0.060	0.36 ± 0.06	--	--	--
Stainless Steel 30%	6.7	0.535	0.581	0.046	0.29 ± 0.06	<0.4	<0.4	--
Hastelloy	6.9	0.556	0.632	0.076	0.35 ± 0.06	--	--	<1
Blank (31% KOH)	--	--	--	--	0.46 ± 0.06	--	--	--

1) Battery Business Section commercial plaque

2) 99.9% nickel

3) Graphite tape, "Grafoil"; from Union Carbide Corp., high purity grade

foil sample did, however, exhibit the highest overvoltage value (refer to Table 14), as expected. During the course of this test, the following qualitative observations were made:

1. The nickel plaque became black in color after two or three days of exposure, indicating possible oxidation of the sample.
2. The graphite did not liberate oxygen gas a rapidly as the metallic test samples, but became covered with large, clinging bubbles.
3. Physical degradation of the graphite was evident from the fact that a large quantity of black sediment was found in the test cell containing this specimen.
4. A light brown deposit formed on the platinum counter electrodes for the graphite, stainless steel, and Hastelloy samples during an open circuit stand after the exposure test. These deposits were qualitatively analyzed to determine the composition of the deposit. The results are shown in Table 15.

Table 15

QUALITATIVE ANALYSIS OF PLATINUM COUNTER ELECTRODE DEPOSIT

Sample Material	Major	Minor	Trace	Faint Trace
Graphite*	Cu	Zn	Mg, Ca, Pt	Pb, Ag, Al
302-SS	Fe	Mn	Mg, Cu, Ca, Al, Pt, Cr	--
	Fe	--	Mg, Cu, Ca, Pt, Al, Mn	--

*This analysis shows that the brass rivet connection to the test specimen was not adequately protected by the applied epoxy coating. Metallic test electrodes were spot-welded directly to platinum-lead wires.

On the basis of the above results, it was decided that graphite, stainless steel, and Hastelloy nickel-base alloy should be eliminated from further consideration and that the remaining samples (platinum, nickel foil and nickel plaque) should be compared to other materials in subsequent tests.

The second corrosion screening test was performed in the same general manner as above, but with the following additional test features:

1. Double-layer capacitance (surface area) measurements were made on the specimens before and after the exposure test by Brodd and Hackerman's (Ref. 54) method in an effort to determine the degree of pitting or attack on the sample. Figure 21 is a circuit diagram of

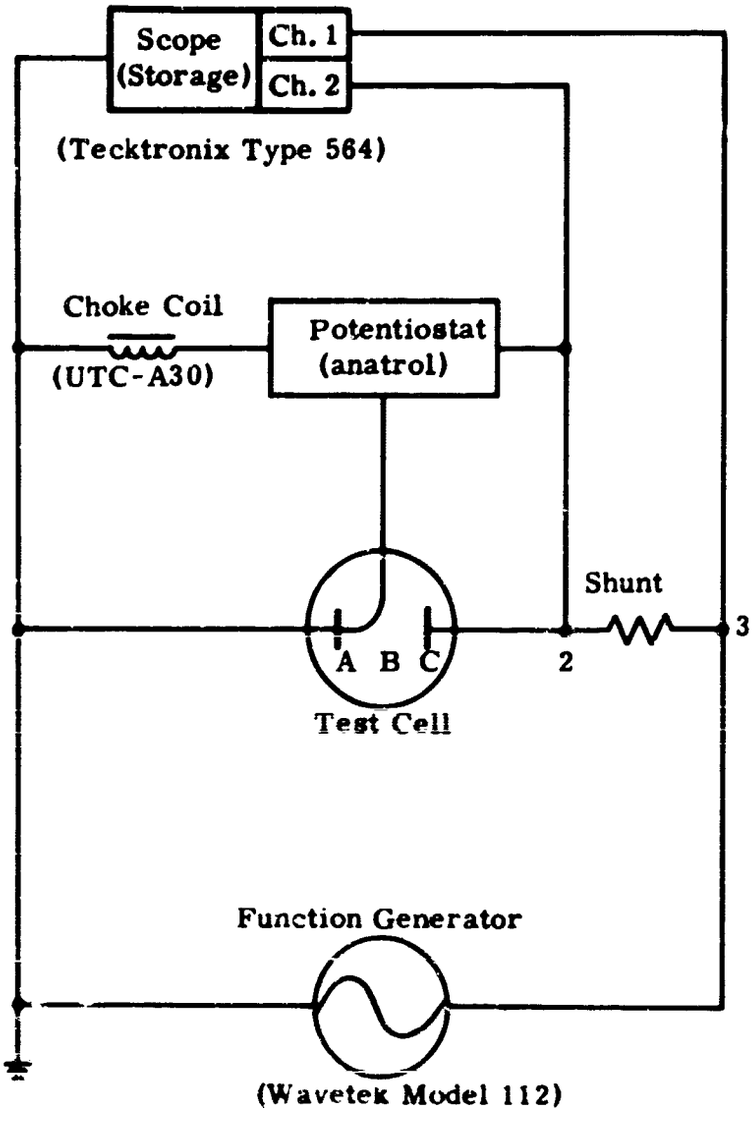

Scope Connections: 1-2 Cell Volts
2-3 Cell Current

Electrodes:
A -- Test Specimen
B -- Hg/HgO Reference Electrode
C -- Large Platinum Counter Electrode

Figure 21. Circuit Diagram for Determination ble Layer Capacity

the apparatus employed in this test. Figure 22 is an oscillogram showing the charging curve obtained from a platinum foil test sample.

2. Oxygen evolution polarization data were recorded for current densities up to 50 ma/cm^2 apparent surface area at the outset of this test.

3. The test electrodes were weighed before and after the anodic exposure as an additional means for determining the extent of attack.

A 15 ma/cm^2 constant-current anodic exposure test on two lithiated nickel foils, a lithiated porous nickel battery plaque, a Monel nickel-copper alloy foil, and a platinum-5% ruthenium alloy was conducted for 38 days. This corresponded to a total exposure of about 12 ampere-hours/cm^2 on these samples. Pertinent data from this test are summarized in Table 16.

Table 16

RESULTS OF ADVANCED CORROSION SCREENING TEST
(12 Ampere-hours/cm^2 Anodic Exposure in 31% KOH)

Identify	Double Layer Capacity: Initial Value (mf/cm^2)	Double Layer Capacity: Relative Change (%)	Weight Loss (mg/cm^2)	O_2 Overvoltage at 30 ma/cm^2 (Versus Hg/HgO): Initial	O_2 Overvoltage at 30 ma/cm^2 (Versus Hg/HgO): Final	Electrolyte Analysis: CO_3 (%)	Electrolyte Analysis: Cations (ppm)
Monel (70% Ni, 30% Cu)	941	+112	4.51	580	590	0.35	Cu (Faint)
Pt-5% Ru	775	- 10	0.62	1175	740	0.46	--
Li/Ni Foil	11,800	- 31	25.5	600	540	0.46	--
Li/Ni Foil	57,200	- 15	19.8	600	610	0.46	--
Li/Ni Plaque	21,900	-446	1.24	600	570	0.52	--
Blank (31% KOH)	--	--	--	--	--	0.46 ±0.06	--

The relative double-layer capacitance values obtained are in agreement with expected results. The Monel and platinum-5% ruthenium electrodes were foils polished by mild sandblasting, and they presented a smoother surface than the rougher and somewhat more porous surface of the treated nickel samples. Except for the Monel sample, all electrodes showed a loss in double-layer capacitance as a result of the corrosion test. This reduction in double-layer capacity could be caused by the formation of an oxide layer on these samples, but the fact that all samples lost weight during the anodic exposure militates against this as a firm conclusion. It is possible that the initial surface roughness was reduced as a result of anodization, while the Monel sample corroded via surface "pitting."

In terms of technical considerations alone, the platinum and platinum alloy samples examined in this screening test appear to be the best possible substrate materials for the nickel hydroxide electrode. The high oxygen evolution o'er-

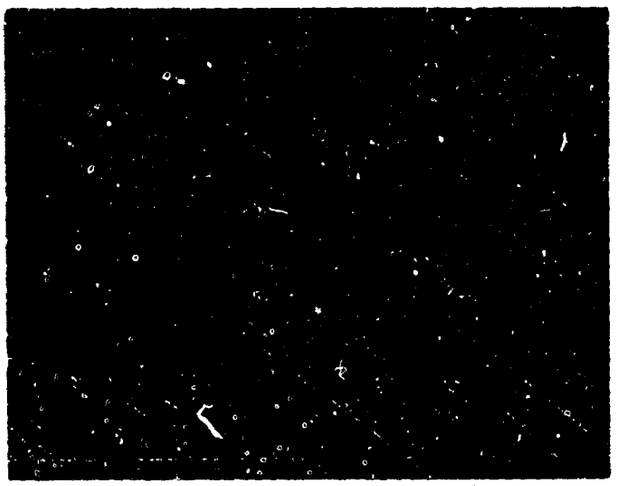

Current: 0.10 ma/div.

Voltage: 10 mv/div.

Sweep Rate: 0.10 sec/div.

Capacity, $C = I/(dv/dt) \propto$ Surface Area

Figure 22. Determination of Surface Area by Charging Curve Method (Oscillogram of Platinum Foil Sample)

potential and low rate of "attack" are consistent with the desired goals of this program. However, the use of platinum substrates in nickel hydroxide electrodes is totally impractical on the basis of economic considerations. For this reason, a choice had to be made between Monel and the lithiated nickel oxide surface treatment. The double-layer capacitance and gravimetric measurements indicate that Monel is attacked to a greater degree during anodic exposure than the lithiated nickel plaque material, but not to the extent of attack indicated for the lithiated nickel foil samples. This discrepancy can be attributed to differences in the surface oxide, since the foils appeared to be more severely oxidized by the lithiation process as evidenced by their scale-like, blistered surface. The oxidized surface of the plaque material was quite adherent and appeared to have a uniform, blue-black color. Therefore, spalling of the oxide scale from the foil samples could account for the high weight loss of these samples.

A third corrosion screening test was devised to determine the extent of "induced" electrode capacity resulting from the oxidation of these materials. In this test, foils of Monel, pure nickel, lithiated nickel, and samples of plain and lithiated porous nickel plaque were exposed to about 250 charge-discharge cycles in 31% KOH electrolyte. The test electrodes were all of the same size (1 inch by 1 inch) and were cycled in series at a constant anodic current value that produced gaseous oxygen on all of the samples (~3 ma/cm^2). The cathodic discharge rate employed was equal to the above charge rate, and each test electrode was individually protected from exposure to hydrogen evolution by means of a voltage cutoff relay set at -0.75 volt with respect to the Hg/HgO reference electrode system. Table 17 shows the gravimetric and oxygen overvoltage data which was obtained in the course of this screening test.

Table 17

RESULTS OF CORROSION CYCLING TEST

Sample	Weight Change (mg/cm^2)	O_2 Evolution Overpotential mv (ma/cm^2) 1.0	3.0	10
Monel	+0.052	--	--	--
Nickel Foil (pure)	-0.011	555	576	600
Nickel Foil (lithium-treated)	-0.055	615	635	720
Nickel Plaque (standard)	+0.228	515	530	545
Nickel Plaque (lithium-treated)	-0.101	532	554	578

The standard nickel plaque was the only sample which developed a measurable discharge capacity in this test (~0.17 ma hours/cm^2). This result is consistent with the fact that it also showed the greatest weight gain.

While these screening tests indicate that monel may satisfy the chemical stability criteria, time did not permit the subsequent evaluation of this alloy in any practical electrode configuration. However, in view of the encouraging results obtained in the preceding corrosion tests with the lithium-treated nickel plaque (relative to untreated, standard battery plaque) and the fact that such samples could be readily produced for this task at reasonable cost, it was decided that an evaluation of impregnated, lithiated plaque would be the next step in determining the suitability of this material as an electrode substrate.

To this end, four nickel hydroxide electrodes were prepared by the multi-step, cathodic deposition technique described in Section 4 of this report. Two of the electrodes were made from a nickel battery plaque which had been subjected to the lithiation treatment, while the two control electrodes were made from untreated plaque material. The four electrodes were mounted in flooded test cells, designed with a large excess of cadmium (negative) capacity and subjected to ten 100% depth-of-discharge cycles at 3.0 ma/cm^2 per side.

When the test electrodes were removed from the cells after cycling, the lithium-treated samples were very brittle and crumbled readily on handling. This phenomenon was not observed with the control electrodes, suggesting that the lithiation treatment severely weakens the sintered nickel structure. Apparently, the swelling of the active material in the heavily loaded plates, previously observed in this program (refer to Section 4) and by others (Ref. 37), is sufficient to cause the mechanical failure of the lithiated nickel sinter.

RECOMMENDATIONS

In view of the results discussed, it is recommended that the lithiated nickel oxide surface treatment be eliminated from further consideration in this program.

From an economic point of view, future experimental electrode evaluations should continue, using commercially available nickel plaque as the electrode substrate material until the primary fabrication techniques, design parameters, and performance limitations have been more fully established. In the light of the objectives of the other work areas of this program, the substrate evaluation task should be assigned the lowest priority.

Major emphasis should continue to be placed on electrode preparation techniques aimed at achieving higher electrode energy densities and charge efficiencies. If in the next phase of this program it is concluded that substrate corrosion represents a major obstacle for achieving "an improved nickel hydroxide electrode," the proposed assignment of task priorities could be modified accordingly. Meanwhile, the cost associated with the continued search for alternative substrate materials and the ultimate use of such materials in electrodes for practical cell applications discourage further efforts in this direction.

Section 4

IDEAL STRUCTURE ANALYSIS

INTRODUCTION AND OBJECTIVE

Many electrode fabrication processes have been developed and adopted for battery systems by a cut-and-try approach, lacking any real knowledge of the resulting electrode structural properties. In this study, a preliminary mathematical analysis of the $Ni(OH)_2$ electrode was undertaken with appropriate experimental work to help identify the key electrode design parameters. The purpose of this analysis was to provide a rational basis for selecting suitable fabrication techniques and experimental approaches. Primary concern was focused on achieving an improved electrode energy density relative to that of the presently available commercial plates. Accordingly, the ideal structure analysis was aimed at determining the effects of pore size, porosity, plate thickness, and the general configuration of the substrate and the active mass on the available energy density of the electrode. Such efforts were not intended to take the place of experimental work, but rather to provide proper direction in the electrode fabrication and evaluation tasks and in evaluating or correlating the experimental results of this program.

DEVELOPMENT OF THE MATHEMATICAL MODEL

Essentially three different electrode configurations can be considered from an "ideal" point of view:

1. Planar or foil electrodes upon which a thin layer of active material is formed or deposited
2. Sintered electrodes in which active material is deposited within the pores of a rigid conductive substrate
3. Pasted or bonded structures in which the active material, the binder, and the conductive particles are intimately blended and applied to a conductive grid support or current collector

Before attempting an analysis of these structures, some of the more general features of the nickel hydroxide electrode were considered.

An estimate of the ultimate energy density or volumetric capacity of the active material was made on the basis of the assumed electrode reaction

$$Ni(OH)_2 + OH^- \underset{\text{discharge}}{\overset{\text{charge}}{\rightleftharpoons}} NiOOH + H_2O + e^- \qquad (1)$$

and the effective density of the hydroxide or active material, ρ_a, as follows:

$$(Q_v^o \text{ ampere-hours inch}^3) =$$

$$\left(\frac{26.8 \text{ ampere-hours}}{\text{equivalent}}\right)\left(\frac{1 \text{ equivalent}}{92.7\text{g Ni(OH)}_2}\right)\left(\rho_a \frac{\text{g}}{\text{cm}^3}\right)\left(\frac{16.39 \text{ cm}^3}{\text{inch}^3}\right) \qquad (2)$$

Bode (Ref. 7) has reported the density of β-$Ni(OH)_2$ to be 3.85 g/cm³. The density of freshly prepared $Ni(OH)_2$ measured with a picnometer (using water displacement) was found to be 3.44 g/cm³. The discrepancy between this and Bode's value may be caused by possible hydration of the $Ni(OH)_2$ in the latter evaluation.

The density of the oxidized active material has not been reported in the literature; but, for this analysis it was assumed to be the same as that of the discharged material. Using Bode's value of 3.85 g/cm³, Equation 2 gives a maximum volumetric energy density value for the active material of 18.2 ampere-hours/inch³. Since a portion of any electrode must be allocated to "inert" substrate material and to voids or residual porosity for electrolyte access, a direct reduction in Bode's value must be implemented for practical electrode structures. Also, not all of the active material is electrochemically available for the desired electrode reaction (Equation 1). Therefore, this "utilization factor" reduces the electrode energy density to an even greater extent. A useful expression for the energy density of the nickel hydroxide electrode in terms of the above considerations is:

$$(Q_v \text{ ampere-hours/inch}^3) = \eta Q_v (1 - V_c - \theta) \qquad (3)$$

where:

η = Fraction of the active material electrochemically active in the electrode

V_c = Volume fraction of all of the "inert" material in the electrode (grid, binder, conductor, etc.)

θ = Residual porosity of the finished electrode

Q_v^o = 18.2 ampere-hours/inch³ for this electrode as previously derived

Equation 3 is applicable to the three basic types of electrode configurations and can be used to estimate the corresponding energy density of each structure.

ELECTRODE CONFIGURATIONS

Planar Electrodes

As discussed in Section 2 of this report, planar electrodes are the simplest type of electrode structure and provide a convenient means for performing x-ray, microscopic, crystalographic, voltametric, or chemical analyses

of the active material. Methods for preparing such electrodes can be classified according to the following five categories:

- Anodic oxidation of nickel metal
- Chemical attack of nickel metal
- Cathodic or chemical precipitation of nickelous hydroxide
- Mechanical "pasting" with various binders and additives
- Electrophoretic or electroplated deposits

Briggs, et al (Ref. 50) prepared electrode samples by the first two methods in which uneven and nonadherent deposits of up to 1 ma hour/cm^2 were obtained. Henderson, et al (Ref. 55) found that when the nickel surface is first coated with a hydrophobic layer, anodic oxidation occurs rapidly and uniformly in KOH/KCl solutions, resulting in reversible electrochemical capacities of up to 2.5 ma hours/cm^2. Further oxidation of the substrate resulted in nonadherent or electrochemically inactive additional deposit. If it is assumed that Henderson's value of 2.5 ma hours/cm^2 corresponds to the maximum effective loading of active material on foil substrates, that the deposit is void free, and that it can be cycled at 100% utilization, the thickness of this deposit would be about 20 microns. If it is further assumed that both sides of a foil substrate of thickness t_s are activated with these 20μ deposits, Equation 3 reduces to the following expression for such an electrode:

$$Q_v = 18.2\left(1 - \frac{t_s}{t_s + 40(0.03937)}\right) \qquad (4)$$

where t_s is the substrate foil thickness expressed in "mils." Table 18 shows the values of Q_v for various foil thicknesses computed on the basis of this result.

Table 18

THEORETICAL ENERGY DENSITY OF PLANAR ELECTRODES
(20μ Active Material Deposit -- Two Sides)

t_s (mils)	Q_v (amp-hrs/in.^{3})
0.0	18.2
0.5	13.8
1.0	11.1
1.5	9.28
2.0	8.00
2.5	7.00
3.0	6.25
3.5	5.65
4.0	5.10

Thus, under the most optimistic conditions foils of less than about 2.5-mil thickness would be required to achieve the energy density goal. In addition, over eight square feet of active area (four square feet of electrode) would be required for a single 20-ampere-hour cell.

In an attempt to increase the surface area of smooth planar substrates in order to enhance the volumetric capacity of the resulting secondary electrode, Henderson developed a method (Ref. 56) whereby adherent deposits of nickel sponge were electrolytically "sintered" to foil substrates by a nickel plating solution containing suspended nickel powder. The resulting substrate was found to be similar to conventional sintered nickel plaque. When this substrate was anodically oxidized to form a nickel hydroxide surface, it had a volumetric capacity comparable with but not exceeding that of commercial plates (< 5 ampere-hours/inch^3).

Blaek, Pentecost, and Moore (Ref. 57) were able to deposit up to 0.75 ampere-hour/feet^2 of active nickel on a three-mil metallized nonwoven Dynel* fabric by means of a modified electroplating technique which resulted in electrodes with only about 2 ampere-hours/inch^3 volumetric capacity. These electrodes were developed for use in flexible, thin-film, sealed nickel-cadmium cells and were not necessarily designed for maximum volumetric energy density. Nevertheless, it was decided that the high-energy density goal could not be achieved by any reasonable variation of the above approaches.

Plaque Electrodes

It was concluded from the above analysis that $Ni(OH)_2$ is nonconductive and that only relatively thin, active material deposits adjacent to the electronically conductive substrate would be "active" (the local active material utilization would be expected to diminish with increasing distance from the substrate). Ideally, the optimum electrode configuration for energy density would, therefore, be one which provides for a maximum volume of active material dispersed on a large area of conductive support. Since all commercially prepared nickel hydroxide electrodes begin with some form of porous nickel substrate, this is consistent with the postulation made.

For this analysis, plaque-type substrates can be assumed to be inert, electronically conductive matrices with uniform cylindrical pores of a diameter D, and a length L. The length also corresponds to the thickness of the substrate. The active mass can be assumed to occupy a portion of the void volume in the form of a uniform, thin deposit on the walls of each pore such that the final, or residual, porosity of the electrode, θ, corresponds to a void-pore diameter, d. The degree to which the substrate is loaded with active material can then be defined in terms of a pore utilization factor, E, as follows:

$$E = \frac{\text{Volume of active material}}{\text{Total pore volume}} = \frac{(\pi/4)(D^2 - d^2)}{(\pi/4)(D^2)} = 1 - \left(\frac{d}{D}\right)^2 \qquad (5)$$

*Trademark

Assuming that the active material loading, the substrate thickness, L, and the porosity, θ_s, of the substrate are held constant, the total active mass surface area, A, in the electrode can be calculated as follows, letting:

V_T = Total electrode volume

N = Number of pores

V_p = Total pore volume - $NL\pi D^2/4$

$A = NL\pi d$

Therefore:

$$\theta_s = \frac{V_p}{V_t} = \frac{NL\pi D^2}{4V_T} \qquad (6)$$

Solving Equation 6 for N and Equation 5 for D^2, then substituting the results in the expression for A, gives

$$A = \frac{4V_T\,\theta\sqrt{(1 - E)}}{D} = \frac{K}{D} \qquad (7)$$

This result shows that the surface area of the active material in contact with either the electrolyte or the pore walls (provided the pores are not completely filled) is inversely proportional to the substrate pore diameter under the assumed conditions. Therefore, considering planar electrodes, the use of smaller-pore substrates appears to be advantageous, because a specified electrode capacity could be achieved with proportionately thinner active material deposits. All other things being equal, the thinner active material layer should lead to lower ohmic losses in the electrode. The higher surface area of active material afforded by smaller pores is also advantageous from the standpoint of current density on the active material -- the lower the current density, the lower the overpotential of the electrode. In addition, Milner and Thomas (Ref. 1) have shown that the overall active material utilization increases with decreasing active material thickness.

Still another agrument can be made in favor of smaller pores. In a collection of small pores having the same total cross-sectional area as one large pore, the concentration gradients in the radial direction are smaller, leading to lower concentration polarization effects. Since the substrate pore volume ($NL\pi D^2/4$) and the electrode thickness have been held constant in the above analysis, the cross-sectional area for ionic diffusion or migration from the bulk electrolyte has not been changed. However, as the pore utilization is increased for any given pore size (increased active mass loadings) this cross-sectional area is decreased (reduced residual porosity), thereby reducing the rate capability of the electrode. Thus, a trade-off between the energy density and the rate capability of the electrode occurs as the residual porosity or active mass loading is varied.

Equation 3 can be used to show the dependence of electrode energy density on this residual porosity for the "idealized" plaque electrode. In this case, Equation 3 reduces to:

$$Q_V = 18.2\,\eta(\theta_s - \theta) \qquad (8)$$

Figure 23 shows the computed energy density as a function of residual porosity for several initial plaque porosity values (current collector included), assuming 80% active mass utilization for such electrodes. This figure shows that in order to achieve an energy density of 8 ampere-hours/inch^3 with an 80% porous plaque (typical value of a standard sintered nickel battery plaque), the residual porosity cannot exceed about 32%.

It should be remembered that the active material was assumed to be "ideally" deposited in the plaque. In actual practice, some pores will be plugged with the active material while in other electrodes the active material itself may be quite porous. Both of these nonideal conditions can be expected to result in pores operating at extremely low utilizations. For this reason, the cathodic deposition process (Ref. 37) was selected as the most promising method for loading the plaque-type structures for the fabrication task. A full discussion of this choice over conventional chemical impregnation will be presented in Section 5 of this report.

In further attempts to determine the effects of residual porosity and other structural properties on the rate capability and the active mass utilization of plaque-type structures, the continuum or one dimensional electrode analysis of Grens and Tobias (Ref. 58) was analyzed. This electrode model is relatively simple in that variations in electrolyte composition and conductivity are considered only with respect to the depth of the pores (direction normal to the plane of the electrode). In spite of this and several other simplifying assumptions, the solution to the system of resulting differential equations required numerical techniques employing a digital computer to perform the complex, finite-difference analysis. The assumption that the properties of the porous electrode's solid phase are unaffected by the passage of current caused the greatest concern about the applicability of the analyses' results to the $Ni(OH)_2$ electrode.

Nevertheless, the qualitative results obtained in applying the continuum model to relatively simple electrode systems (cadmium oxide anodes and ferri-ferrocyanide cathodes) are consistent with the conclusions derived from the initial model of the $Ni(OH)_2$ electrode and the general behavior demonstrated by many other porous electrode systems. The key elements of these results follow.

1. The local current density on the active mass is higher at the electrode/electrolyte interface than it is in the deeper regions of the pores.
2. This gradient of "reactivity" with respect to pore depth increases with current drain, pore tortuosity, electrode thickness, and reduced porosity.

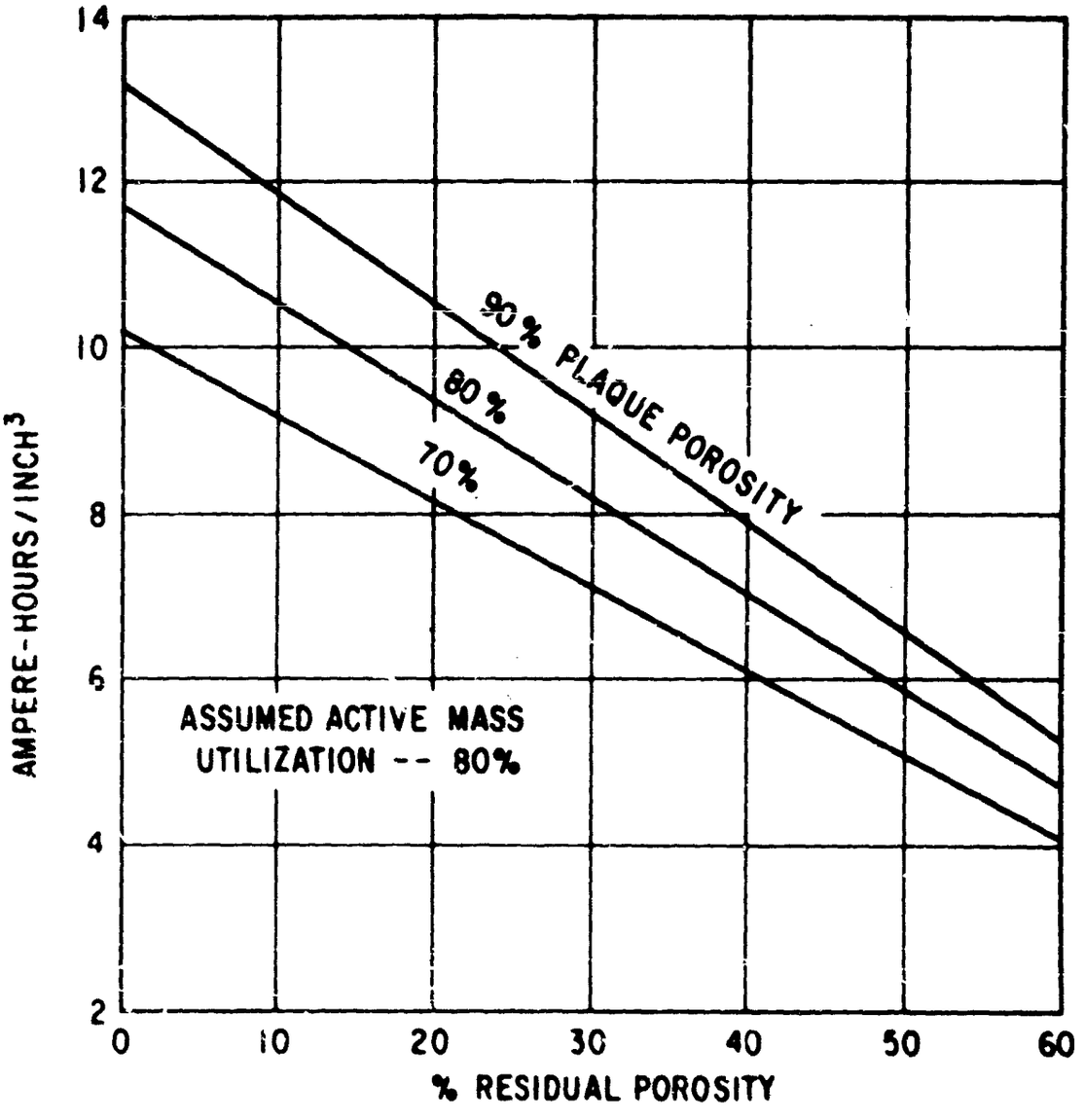

Figure 23. Theoretical Energy Density of Plaque Electrodes

3. At constant porosity, changes in pore size have no direct bearing on the transport phenomena between the free electrolyte and the porous electrode. Pore size merely dictates the specific surface (cm^2 of reactant surface per cm^3 of electrode volume) available for the active mass. This affects the current distribution in the structure only as a consequence of changes in the electrode overpotential (for constant active mass loading).

Thus, the continuum model describes the expected $Ni(OH)_2$ electrode behavior and shows the qualitative effects of the major electrode parameters on this behavior for steady- state or short-term discharges.

It was decided that an experimental program, rather than a continuation of the above involved mathematical analysis, would be a more efficient means for determining the effects of plaque structure at practical performance levels and depths of discharge. This experimental program was aimed specifically at determining the effects of pore size and plate structure on the active mass utilization and the corresponding electrode energy density at approximately the C/5 discharge rate.

In the first test, four samples of identical, sintered-nickel battery plaque were first compressed to varying degrees and then loaded by cathodically precipitating active material to an extent proportional to the unfilled, compressed sinter porosity, i.e., to the same pore utilization factors for each electrode. These plates were then cycled at the C/5 rate based on their respective weight gains. After the tenth cycle, capacities were determined, the electrodes were chemically analyzed for active material content and level of cobalt additive, and the corresponding active material utilizations were computed. The pertinent results of these analyses are shown in Table 19.

Table 19

ACTIVE MATERIAL UTILIZATION
AS A FUNCTION OF PLAQUE COMPRESSION

Final Thickness (Inch)	Cobalt* in Active Material (%)	Initial Weight of Sinter (g/dm^2)	Final Weight of Sinter (g/dm^2)	Weight of $Ni(OH)_2$ +$Co(OH)_2$ (g/dm^2)	Tenth-cycle Active Mass Utilization (%)
0.0223 (standard)	12	6.8	6.8	5.84	98
0.0182 (compressed)	12	6.8	6.8	5.03	86
0.0135 (compressed)	11	6.8	6.9	2.73	75
0.0110 (compressed)	10	6.8	6.9	2.16	71

*All the solutions used for electrochemical precipitation contained 10 mole % cobalt. Because of limitations in the chemical analyses, the differences in cobalt levels are not considered significant.

These results show that the active mass utilization decreases with increasing compression of the plaque prior to loading. The ideal structure analysis predicted that, all other things being equal, smaller pores would lead to higher utilizations. Since some uncontrolled effects, such as blockage of the surface pores by compression of the sinter or by active material, might account for this unexpected result, microsections of the four test electrodes were prepared. Figure 24 shows the cross sections of the two more-highly compressed structures of this test. The white areas in these photographs are metallic nickel, and the black areas are the pores containing the active material. An examination of these cross sections shows that the surface of the plaque material did tend to compress to a greater extent than the interior. The resulting smaller pores at the surface could reduce electrolyte access to the bulk of the active material, thereby producing the inverse relationship between active mass utilization and average pore size.

Because of these inconclusive experiments, a second series of tests was undertaken to establish the effect of substrate configuration on the active material utilization. Nine different samples of various porous nickel materials, ranging from ultrafine pore plaque (3 to 7μ pores) to Foametal* material (> 100μ pores) were loaded with active material to approximately the same pore utilization factor. The three materials with the largest pores were unsatisfactory because of their inability to retain the active material. The resulting electrodes were given twelve total-discharge cycles in flooded cells at approximately the C/5 rate. The porosity and pore size distribution of the unloaded plaque material were determined by conventional mercury intrusion methods. The average pore size of the Foametal samples was greater than 100 microns, so the intrusion method was not suitable for these materials. As a result, a microscopic examination was used to estimate the average pore size of these samples. These pore-size data are useful in ranking or classifying the various substrate materials. The experimental data from the above tests are shown in Table 20.

Figure 25 shows the active material utilization and the corresponding energy density as a function of the average pore size of the various substrate materials. The spuriously high value for the active material utilization for the 500μ-pore size material occurred because most of the active material did not adhere firmly to the substrate and was lost. The firmly adherent material had a high utilization.

These results suggest that a high interfacial contact area between the conductor and the active material is important in achieving high active mass utilization and electrode energy density. On this basis, it appears that the pore size of conventional, sintered battery plaque is about at the optimum value and that relatively little improvement in the $Ni(OH)_2$ electrode can be expected to result from further alterations in the physical properties of the plaque-type structure. Efforts to achieve an improved plaque electrode should therefore be aimed at developing better active material loading techniques and methods

*Registered U. S. Trademark of the General Electric Company

Electrode No. 16 (150X)

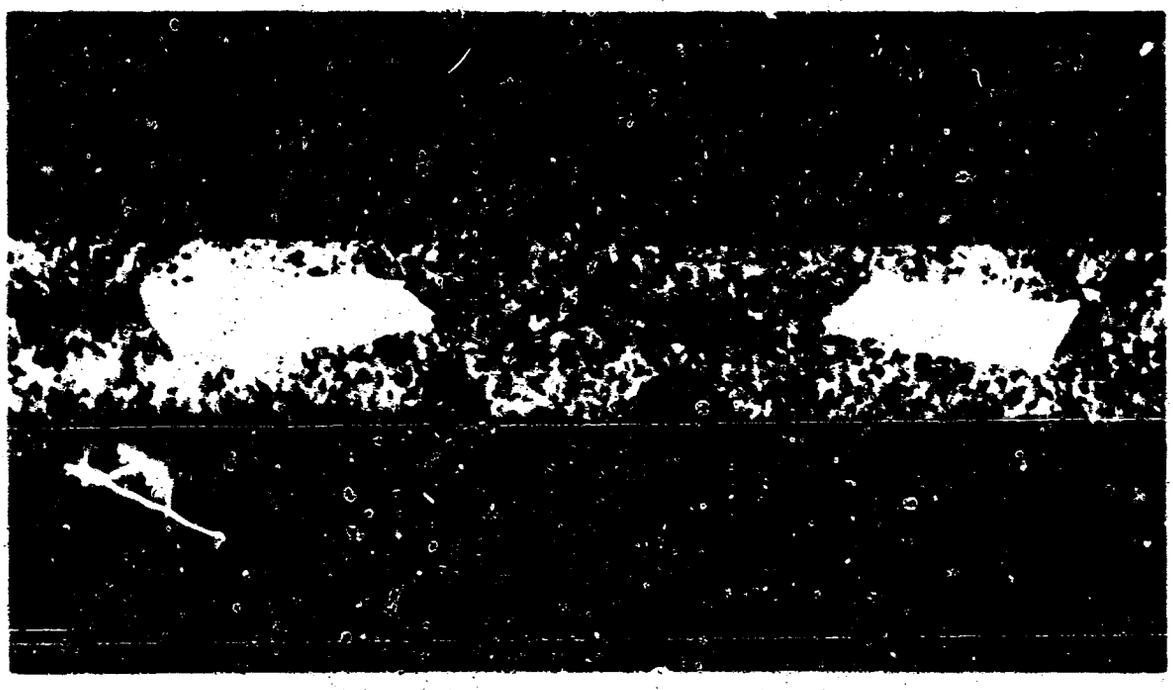

Electrode No. 18 (150X)

Figure 24. Microsections of Compressed Plaque (Compressed before Loading)

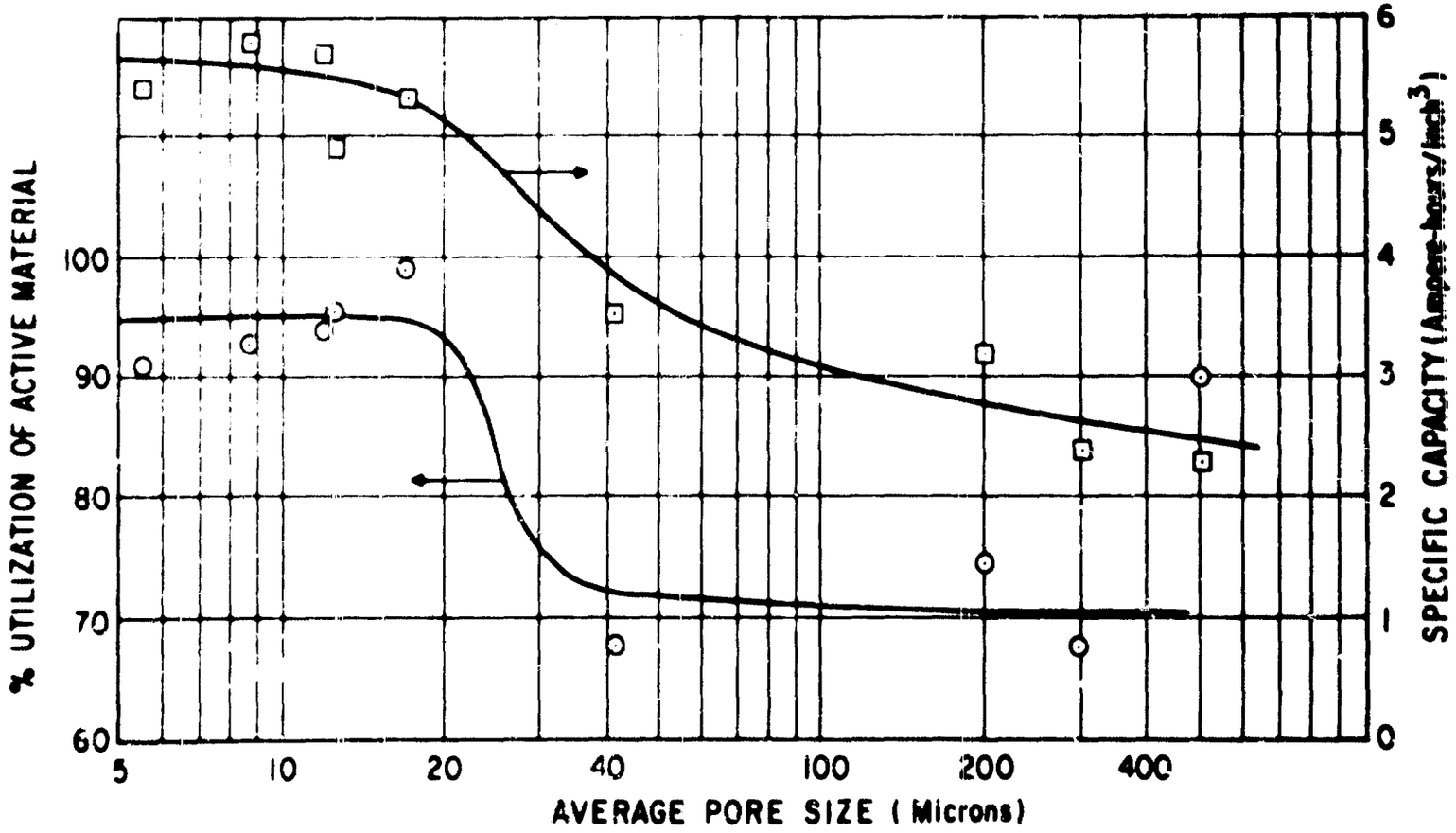

Figure 25. Active Material Utilization and Specific Capacity as a Function of Substrate Pore Size

Table 20

ACTIVE MATERIAL UTILIZATION AS A FUNCTION OF SUBSTRATE PORE SIZE
(1.25-inch by 1.50-inch Electrodes)

	Substrate Material	Average Pore Size (microns)	Porosity (%)	Thickness (ins.)	Weight Gain (g/cm^3 of (pore volume)	Cobalt (%)	Capacity at C/5 (amp.-hrs)	Utilization[1] (%)	Energy Density (amp-hrs/$in.^3$)
1.	Foametal[2]	~200	82	0.0275	1.18	5.7	0.183	75	3.2
2.	Foametal[2]	~300	81	0.0208	0.98	6.5	0.102	68	2.4
3.	Foametal[2]	~500	86	0.0187	0.73	8.5	0.090	90	2.3
4.	Feltmetal (Huyck)	40 - 43	80	0.0193	1.42	5.7	0.138	68	3.5
5.	Plaque -- clevite[3]	12.5	78	0.0300	1.38	5.1	0.304	96	4.9
6.	Plaque[4]	12	77	0.0238	1.69	7.2	0.282	94	5.7
7.	Plaque[4]	8.8	79	0.0254	1.76	7.0	0.304	93	5.8
8.	Plaque[5]	5.5	81	0.0251	1.41	7.0	0.283	91	5.4
9.	Plaque[3]	17	81	0.0253	1.34	4.8	0.282	89	5.3

1) Based on chemical analysis of cycled electrodes

2) General Electric Company Metallurgical Products Department, Detroit, Michigan

3) 20 by 20 mesh nickel screen current collector, sintered carbonyl nickel powder

4) Nickel-plated steel foil current collector, sintered carbonyl nickel powder, General Electric Company, Battery Business Section, Gainesville, Florida

5) 30 by 30 mesh nickel screen current collector, sintered hydrogen-reduced $NiCl_3$, General Electric Company, Research and Development Center, Schenectady, New York

for achieving full utilization of the benefits to be derived from the use of additives.

Pasted Electrodes

Pasted, or polymer-bonded, structures offer an additional degree of freedom in electrode design over plaque structures. That is, the active mass-conductor interfacial area in these structures can be adjusted by variations in the physical properties of the conductor alone, while all other parameters (conductor-active mass ratio, residual porosity, volume of conductor, etc.) are held constant. Since each individual conductive particle can be surrounded (ideally) with active material in the pasted structure, it may be expected that for a given electrode volume the pasted structure provides a greater interfacial area than possible with a plaque substrate. On the other hand, the discontinuity of conductive particles in the pasted structure can be expected to result in a lower overall electronic conductivity when compared with the plaque-based electrode. Thus, the optimization of pasted structures must first be concerned with the trade-off between electronic conductivity on the one hand and active mass utilization on the other, while interactions between the electrode and the electrolyte appear to play only a secondary role.

Since little literature exists on pasted $Ni(OH)_2$ electrodes and a great deal of "art" would probably be required in the fabrication of such electrodes, it was decided that an experimental rather than an analytical approach would best determine the feasibility of pasted structures. Equation 3 can be used directly to predict the available energy density of pasted electrodes under ideal conditions. Figure 26 shows the relationship between this energy density and residual electrode porosity for various levels of conductor, assuming 80% active mass utilization and 10 weight % of a binder having a density of 1 g/cm^3. Further discussion of the lasted nickel hydroxide electrode is presented in Section 5 of this report.

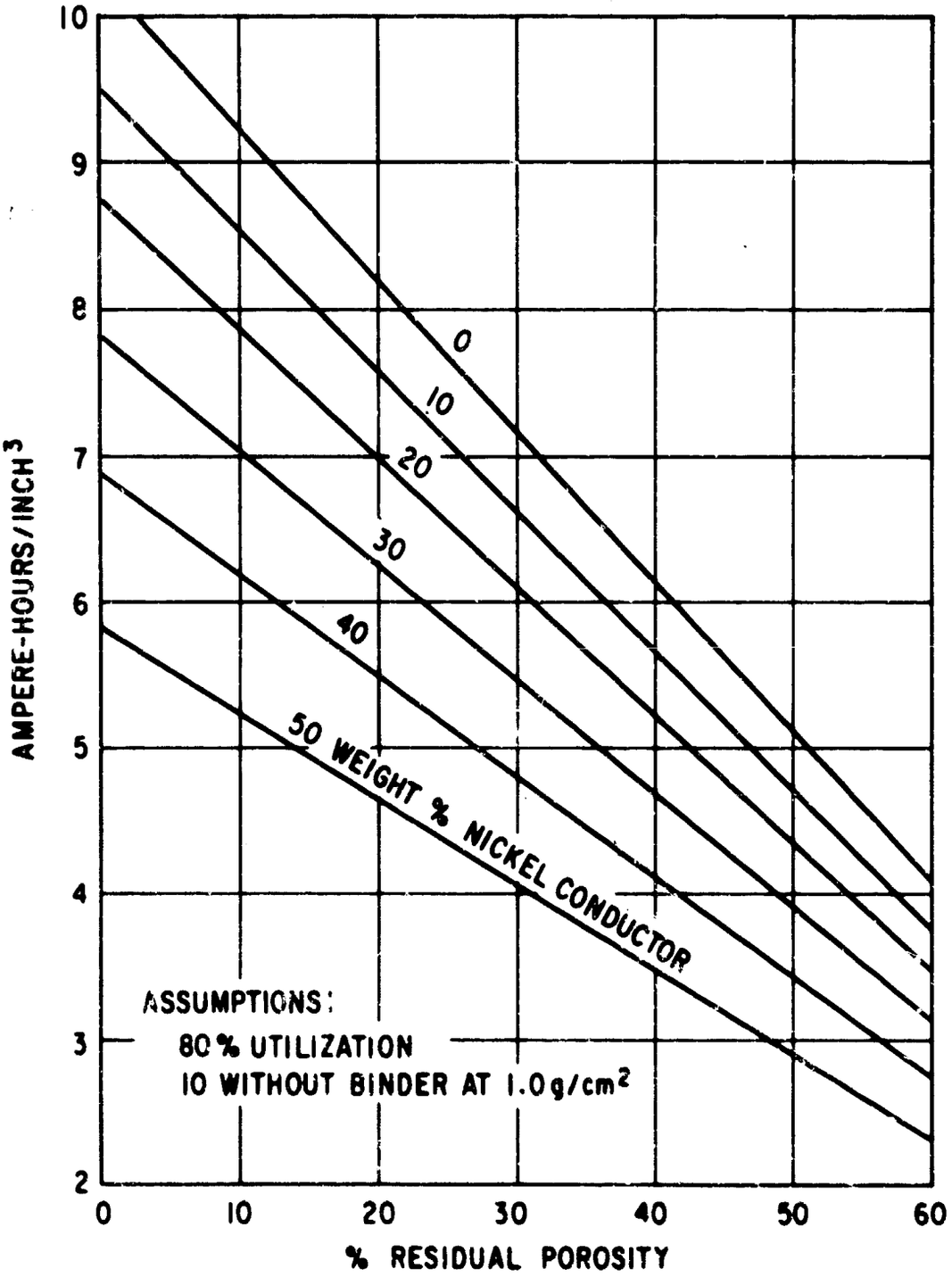

Figure 26. Theoretical Energy Density of Pasted or Polymer-bonded Electrodes

Section 5

PLATE FABRICATION

SINTERED STRUCTURES

Introduction

A survey of available literature revealed several procedures for activating sintered structures with $Ni(OH)_2$. The various methods fall into three basic categories:

- Impregnation with solutions of nickel salts followed by conversion of the salts to hydroxide
- Oxidation of metallic nickel to electrochemically active $Ni(OH)_2$
- Electrochemical precipitation of $Ni(OH)_2$ from nickel salt solution

There is some overlapping between the first two categories.

Impregnation Methods

The commercial impregnation process most commonly used for preparing nickel hydroxide electrodes is described by Milner and Thomas in Reference 1. As described in Reference 1, the process involves the vacuum impregnation of the plaque with concentrated nickel nitrate solution. A slight excess of nitric acid is added, and subsequent precipitation of the hydroxide is accomplished by imersion in a hot alkali solution. Five to seven such vacuum impregnation cycles are usually required to load the desired amount of active material in the plates.

A significant portion of the resulting electrode capacity is derived from the corrosion of the sintered nickel structure during this vacuum impregnation process. Plates can be designed to have specific capacities from 5.5 to 7 ampere hours/inch^3. This depends on the type of plate and the number of impregnation cycles the plate is subjected to.

Belove et al (Ref. 59) report specific capacities of impregnation-activated $Ni(OH)_2$ electrodes of up to 8.6 ampere-hours/inch^3. However, this was obtained after ten 100% depth-of-discharge cycles in excess electrolyte and was based on the initial electrode thickness. Initial specific capacity was less than 5.0 ampere-hours/inch^3. Popat et al (Ref. 60) report first-cycle specific capacities as high as 11 ampere-hours/inch^3 for impregnated electrodes. As

much as 55% of the sinter was corroded during activation. It was stated that plates thicker than 0.035 inch warped during formation and cracked under restraint. Behavior of this type of heavily loaded plate during cycling had not yet been established. Rampel (Ref. 61) patented a method for impregnating porous plaques with nickel salts dissolved in low surface-tension organic solvents. In one example cited, active material weight gain in four impregnation cycles was 1.8 g/cm^3 of pore volume.

A variation on the impregnation process is the addition of a step in which the nickel nitrate is thermally decomposed to some degree before being converted to $Ni(OH)_2$ in caustic. Bourgault et al in Reference 62 claim that heat-impregnated plaque from 180° to 220°C improves the electrochemical utilization of the active material. Part of the active material in their electrodes was derived from corrosion of the sinter. Plates given a single impregnation-thermal decomposition cycle have up to 4.3 ampere-hours/inch^3 in capacity at a C/20 discharge rate. Plates given two cycles have shown capacities up to 7.5 ampere-hours/inch^3 at a 1 ma/cm^2 discharge rate. The doubly-impregnated plates had a relatively short life and disintegrated on cycling.

Menard (Ref. 63) patented a claimed improvement on the method of Bourgault et al. Menard claimed up to 8 ampere-hours/inch^3 specific capacity. Part of the electrode capacity was derived from corrosion of the sinter.

Oxidation or Corrosion Methods

Several methods have been reported for activating or increasing the capacities of $Ni(OH)_2$ electrodes by deliberate corrosion of the nickel sinter. Both chemical and electrochemical methods have been used. Ackermann et al (Refs. 64 and 65) have patented methods for corroding sintered nickel by wetting the plaque with a solution of corrosive salts and exposing it to moist air or to steam. The nickel salts produced by the corrosion were then converted to $Ni(OH)_2$ by immersing the electrode in hot caustic solution. A specific capacity of 4.5 ampere-hours/inch^3 is reported. If the electrode prepared as described above is then given an impregnation cycle, the specific capacity is increased to 7.4 ampere-hours/inch^3.

Henderson et al (Ref. 55) studied the production of $Ni(OH)_2$ on nickel foils by anodization in KOH/KCl solutions. They found that coating the nickel with a hydrophobic layer promoted production of nickel hydroxide. Cleaned nickel surfaces tended to evolve oxygen without being attacked. Schneider (Refs. 66 and 67) developed a method of anodically corroding sintered nickel in a sodium bicarbonate solution. He produced 1-mm thick electrodes with a maximum specific capacity of 4.9 ampere-hours/inch^3 and 3-mm thick plaque with a maximum specific capacity of 3.0 ampere-hours/inch^3. Okinaka and Turner (Ref. 68) patented a method of increasing the capacities of previously activated $Ni(OH)_2$ electrodes by cycling them in 6.9N K_2CO_3. The presence of the carbonate ions promoted the anodic corrosion of the metallic nickel. They claim a specific capacity of 5.8 ampere-hours/inch^3.

Electrochemical Precipitation Methods

Electrochemical precipitation methods for forming active material in the pores of porous structures fall into two categories -- anodic and cathodic.

Kober (Ref. 69) reported on a method of depositing nickel hydroxide by anodizing porous sintered nickel plaque in a 28% ammonium hydroxide solution containing nickel formate. The mechanism is not known, but the nickel ions from the solution are deposited as hydroxide in the pore structure of the plaque. Plates with specific capacities from 5.8 to 6.2 ampere-hours/inch^3 have been produced, using a 12-hour deposition time. Briggs et al (Ref. 70) reported on the preparation of foil electrodes by anodic deposition from a bath containing nickel and sodium acetates acidified to a pH of 4.8. The mechanism for this process is not clearly understood.

Kandler (Ref. 39) and others (Refs. 37 and 38) have worked on a cathodic electrochemical process for depositing nickel hydroxide from nickel nitrate solutions without additives. The mechanism is fairly well established. The nitrate ions are electrochemically reduced to ammonium hydroxide at the test electrode according to the following formula:

$$NO_3^- + 10\ H^+ + 8\ e = 2\ NH_4^+ + 3\ H_2O\ .$$

The consumption of hydrogen ions raises the pH locally to a sufficiently high value to cause the nickel ions to precipitate as nickel hydroxide. The process is then a balance between the rate of consumption of hydrogen ions (or the generation of hydroxyl ions), the rate of diffusion of nickel ions into the porous electrode structure, and the rate of diffusion of hydrogen ions from the bulk solution into the electrode (or the rate of diffusion of hydroxyl ions out of the electrode structure). With proper selection of solution concentration, temperature, and current density, the precipitation of nickel hydroxide into the porous plaque structure can be made to begin at the center of the plaque structure and proceed outward as the inner pores become filled. The proper conditions will vary with plaque porosity, thickness, and pore geometry.

McHenry (Ref. 38) made a series of electrodes using solutions of 0.2M, 1.0M, and 4.0M nickel nitrate, current densities of 45, 220, and 1110 ma/inch^2/side, and temperatures of 25, 50, and 75°C. At each solution concentration and temperature, he found a best current density. There appeared to be no significant advantage in using either high temperature or low solution concentration. He chose, for convenience and speed of preparation, the conditions of 25°C, 4.0 molar solution, and 1110 ma/inch^2/side current density. Häusler (Ref 37) and McHenry (Ref. 38) have produced electrodes by this method giving 2.4 to 5.1 ampere-hours/inch^3 in flooded electrolyte.

The electrochemical precipitation process was chosen as the most promising activation method from the standpoint of the goals of this study. Porous

plaque structures can be activated without corrosion, and some additives can be co-precipitated with the nickel hydroxide and uniformly distributed throughout the active material. It was felt that it would be difficult to produce electrodes with reproducible capacities using activation techniques that depend at least in part on corrosion of the sintered nickel for the active material.

Development of Electrode Activation Method

Several preliminary test electrodes were prepared by the above process, using various nickel nitrate solution concentrations and current densities. Cobalt nitrate was included in all of the solutions in the ratio nickel-to-cobalt of 9 to 1. The electrochemical precipitations were done in Lucite* plastic cells constructed so as to minimize current density variations across the faces of the test electrodes. One test electrode was mounted vertically between two sheet nickel counter electrodes spaced 3/16 of an inch from it. The sides and bottoms of the electrodes touched the sides and bottom of the cell. The cells were filled with just sufficient solution to cover the top of the test electrode. The test electrode had 1.75 inches by 3.0 inches of active area with a tab connected to one short edge. The plaque material consisted of carbonyl nickel powder sintered to a nickel mesh or screen. The porosity of the sinter was about 85% and of the unimpregnated electrode, including the mesh, about 80%.

After the electrochemical precipitation was complete, the test electrode was immersed in hot (60 to 70°) 31% KOH for about one hour then washed and dried. Capacity of the electrode was determined by charging and discharging it twice in 31% KOH in a flooded cell. The electrodes were discharged at a convenient current between the C and C/5 rate. The second-cycle discharge capacity and the initial plaque thickness were used to calculate specific capacity. Table 21 summarizes the results of the first series of electrodes made.

These results and those of McHenry (Ref. 38) show that a given solution concentration there is an optimum current for electrochemical precipitation. For instance, for a 0.1-molar solution, 9.6 ma/cm^2 was too high a current. The precipitated material formed on the surface of the electrode and flaked off. For a 2.5-molar solution, 4.8 ma/cm^2 was too low a current. The diffusion of hydrogen ions from the bulk solution was sufficiently high to prevent the pH increase necessary to precipitate the nickel hydroxide. Because the optimum current increases with increasing concentration and the amount of material deposited in the plaque does not appear to depend on solution concentration, a 4.0-molar solution was chosen for subsequent experiments. Higher concentrations of the solution would have been more nearly saturated and not as easily prepared. The use of high concentrations and high currents is advantageous from a processing standpoint -- less time is required for electrode preparation.

*Trademark

Table 21

ELECTRODES IMPREGNATED BY ELECTROCHEMICAL PRECIPITATION

Concentration of Ni (10% Co) $(NO_3)_2$ (moles/ℓ)	Electrode Thickness (mils)	Current Density (ma/cm²/side)	Charge Input (amp-min)	Weight Pickup (g/in³)	Specific Capacity (amp-hrs/in.³)**
0.1	22	9.6	102	small	small
0.3	22	9.6	140	18.5	3.7
0.3	22	4.8	120	16.1	4.5
2.5	22	4.8	120	small	small
4.0	30	150	183	20.4	4.9
4.0	22	*	170	20.8	6.0
4.0	30	*	170	19.0	5.3

*15 ma/cm² for 20 minutes plus 75 ma/cm² for 10 minutes plus 150 ma/cm² for 10 minutes.

**Based on initial thickness and second cycle discharge capacity.

A second series of electrodes was made to determine the optimum current and precipitation time for a 4.0-molar nickel (10% cobalt) nitrate solution. The plaques used were 1.75 inches by 3.0 inches by 0.0255 inch and 81% porous.

The following method was selected as being suitable for electrode preparation:

1. Add 4.0-molar mixed nickel and cobalt nitrates to the test cell containing the test electrode and the two sheet nickel counter electrodes. The counter electrodes are spaced 5/16 of an inch from the test electrode.
2. Connect the power supply within two minutes after filling the cell in order to minimize plaque corrosion. Connect the negative of the power supply to the test electrode.
3. Within two minutes after disconnecting the power supply, remove the electrode from the solution and immerse it in hot 31% KOH, at 55 to 65°C, for one hour.
4. Rinse thoroughly with distilled water and scrub the active material from the surface of the electrode with a nylon bristle brush.
5. Dry in the air for one hour at 65°C. This step could be eliminated between precipitations if intermediate weight gains were not needed.

Table 22 shows the weight gains for one precipitation cycle at various currents and charge inputs.

Table 22

EFFECT OF CURRENT AND CHARGE INPUT ON ACTIVE MATERIAL PICKUP

	Charge Input	
	(60 Ampere-minutes)	(120 Ampere-minutes)
Amperes	(g/inch^3)	(g/inch^3)
2*	12.3	18.0
6	13.8	17.4
10	14.7	17.0
2 + 4**	12.5	18.6
2 + 1**	13.2	18.2

*Equivalent to 190 ma/inch^3/ side

**One-half of charge input at each current

For the 60-ampere-minutes charge input, the efficiency of precipitation increased with increasing current, but the opposite was true for the 120 ampere-minutes charge input. Inspection of the electrodes showed that at the higher currents the precipitated material tended to build up on the electrode surface rather than in the pores. At the higher charge input, the electrodes warped, and a large excess of material formed on the surface. This excess was later scrubbed off.

At the lower current densities, small lumps of active material about 1 mm in diameter formed on the surface of the test electrode. At all current densities at the higher charge inputs, the surface (where not speckled) was coated with a film of dark green deposit. When scraped loose, this deposit had the consistency of paste.

Because the amount of active material precipitated into the plaque structure was considerably less than theoretically expected, electrodes were prepared which were given three precipitation cycles. On the basis of the above tests, the method chosen for the first cycle was 2 amperes for 50 ampere-minutes plus 4 amperes for 50 ampere-minutes. The charge input was reduced from 120 to 100 ampere-minutes to reduce both the warping of the electrodes and the deposition of excess surface material. The precipitation cycles were carried out as outlined previously. Table 23 shows the currents, the charge inputs, and the weights gained for each of the cycles.

Table 23

ACTIVE MATERIAL LOADING OF 5.25-INCH² ELECTRODES

Electrode No.	Weight Gain First Precip.* (g/in²)	Second Precipitation				Third Precipitation			
		Current (amp)	Charge Input (amp-min)	Weight Gain (g/in.²)	Total Weight Gain (g/in.²)	Current (amp)	Charge Input (amp-min)	Weight Gain (g/in.²)	Total Weight Gain (g/in.²)
49	16.9	1**	85	8.2	25.1	0.5	35	3.4	28.6
50	17.0	2	58	7.2	24.2	0.25	11	2.2	26.4
51	17.3	0.5	40	7.9	25.2	0.5	52	4.5	29.7
52	17.7	3	45	6.1	23.8	0.25	29	3.3	26.1

* All weight gains are based on initial plaque thickness

** [illegible] side

The results of the second cycle weight determinations show that the corresponding optimum current is 0.5 to 1 ampere less than the optimum current for the first precipitation cycle. The reason for this is that the porosity and the pore size have been reduced and less current is required to maintain the proper rise in pH within the electrode structure. The charge inputs for the second cycle were all greater than necessary, the excess charge produced surface material which was brushed off during washing. The data from the third precipitation cycle are more ambiguous because of the differences in the previous weight gains and because one of the charge inputs, 11 ampere-minutes at 0.25 ampere, was too low. All of the other charge inputs produced considerable excess surface material.

The four electrodes described above were tested for capacity by cycling them in 31% KOH in flooded cells. Each positive electrode was placed between two commercial cadmium anodes, using one layer of Pellon 2505 ML* nonwoven nylon as the separator. Each electrode pack was held under light compression between Lucite plastic plates in order to prevent flexing and bending of the electrodes. The test cells were given 24 100% depth-of-discharge cycles at 200 ma (at approximately the C/4 to C/5 rate). The charge period was 6 hours at 200 ma, about 20% excess.

Because of malfunctions in the cyclers and some of the recorders, the capacity change during cycling could not be determined exactly, but it averaged about a 20% increase during 24 cycles. The malfunctions also resulted in Electrode 52 being cycled 14 times. The capacity increase can be ascribed to two sources: improvement in utilization of the active material; and corrosion of the substrate. What fraction to assign to each mode is uncertain. If all of the increase were caused by corrosion, 13% of the sinter would be corroded, corresponding to a weight gain (assuming $Ni(OH)_2$ as the product) of 190 mg. The largest measured weight gain was 60 mg. Subsequent chemical analysis of the

*Trademark

cycled electrodes indicated an average of 4% corrosion of the sinter. This corresponds to an average increase in capacity of about 0.05 ampere-hour, or about 6% of the initial capacity.

Table 24

CYCLING TESTS OF 5.25-INCH^3 ELECTRODES

Electrode No.	Initial Electrode Thickness	Increase in Thickness During Cycling (%)	Final Capacity (amp-hrs)	Final Specific Capacity (1 (amp-hrs/in.^{3})
49	23.7(2	28	0.99	6.3
50	22.6(3	26	1.02	6.7
51	25.9	20	1.01	6.3
52(4	25.2	14	0.97	6.4

1) Based on electrode volume after cycling

2) Compressed dry under 19,000 psi after activation

3) Rolled dry after activation. Elongated by 3% during rolling

4) Given 14 cycles. Other electrodes given 24 cycles

Table 24 lists the results of the cycling tests and the measurements of electrode thickness after cycling. The increase in thickness of the electrode during cycling indicates that the active material density varies with the state-of-charge and exerts considerable pressure on the sintered structure. Assuming a density of 3.85 g/cm^3 for $Ni(OH)_2$ (Ref. 7), Electrode 52 was about 34% porous after activation, corresponding to about 58% filling of the pore volume. Swelling of the cycled plates resulted in a considerable reduction in specific capacity. It is interesting to note that, although specific capacities based on inital electrode thicknesses and last-cycle capacities ranged from 7.3 to 8.4 ampere-hours/inch^3, the specific capacities based on final thickness ranged from 6.3 to 6.7 ampere-hours/inch^3.

Samples were cut from Electrodes 49 to 52 for chemical analysis and for microsectioning. Using a method developed by Kroger (Ref. 71), samples were leached to remove the oxidized nickel and cobalt without dissolving the metallic nickel sinter. Analysis was then made for Ni^{++}, Co^{++}, and nickel (metal) per unit volume of electrode. Table 25 summarizes the results of the analyses. Utilization of the active material (ampere-hour/g) was calculated, assuming that the cobalt contributes to the electrode capacity.

The microsections of Electrodes 49 to 52 were examined and no significant differences in appearance between the electrodes could be seen. Photo-

micrographs were taken of a cross section of Electrode 50 at magnifications of 100X, 250X, and 500X and are shown in Figures 27, 28, and 29. The white areas are metallic nickel, the black areas are active material, and the gray areas are epoxy. It appears that a significant part of the void volume consisted of areas not filled because of gas pockets trapped during the electrochemical precipitation process.

Table 25

CHEMICAL ANALYSIS OF CYCLED ELECTRODES

Electrode No.	$Ni^{++} + Co^{++}$ (moles/in.^{3})	Mole % Co^{++} in Active Material	Mole % K^+ in Active Material*	Utilization** (%)	Corrosion of Ni Sinter (%)
49	0.230	11	1.4	102	2
50	0.226	9	1.6	111	6
51	0.223	8	1.7	105	3
52	0.236	9	1.0	101	4

*Excluding screen current collector

**Based on last cycle capacity and on moles $Ni^{++} + Co^{++}$/in.^{3}

Sealed Cell Testing.

In order to test sintered electrodes of the size used in 20-ampere-hour sealed cells, electrodes 2.75 inches by 5.4 inches were fabricated, cycling apparatus was assembled and sealed test cells were designed and built. Four electrodes were activated using the electrochemical precipitation method described, each with a different nickel hydroxide-to-cobalt hydroxide ratio. These four electrodes and two commercially sintered nickel positive plates were cycled 100 times to about 70% depth of discharge at approximately the C/4 rate. Full discharge cycles were taken at three points to determine capacity maintenance. Another set of partial charge and discharge cycles were taken to measure electrode charge acceptance efficiency.

Electrode Fabrication. Using the electrochemical precipitation method discussed on page 80, four 2.75-inch by 5.4-inch electrodes were prepared, using 4.0-molar solutions containing nickel nitrate and 0-, 5-, 10-, and 15-mole % cobalt nitrate. The currents and precipitation times used were 170 ma/inch^2/side for 70 minutes, 95 ma/inch^2/side for 60 minutes, and 48 ma/inch^2/side for 70 minutes for the first, second, and third precipitation cycles, respectively. To insure maximum pore filling, sufficient times were used to produce excess material on the surface of the test electrodes, an excess that was later removed. The plaque used was 26.3 mils thick, weighed 755 mg/inch^2, and contained a 20 by 20 mesh, 7-mil wire screen as a current collector. The plaque was initially about 82% porous, including the current collector.

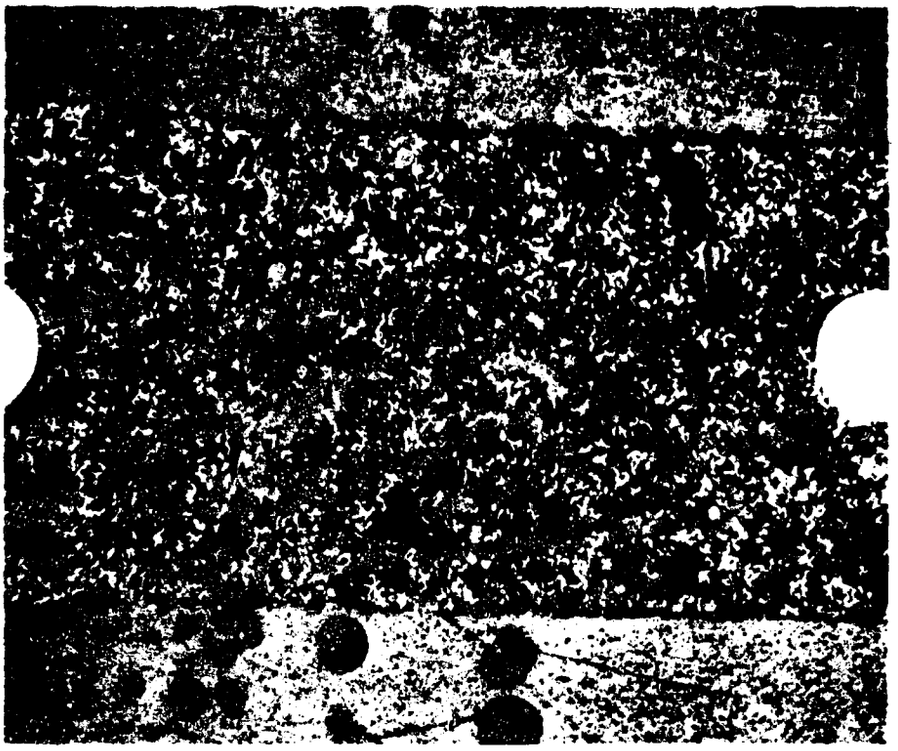

Figure 27. Cross Section of Electrode 50 (Magnified 100X)

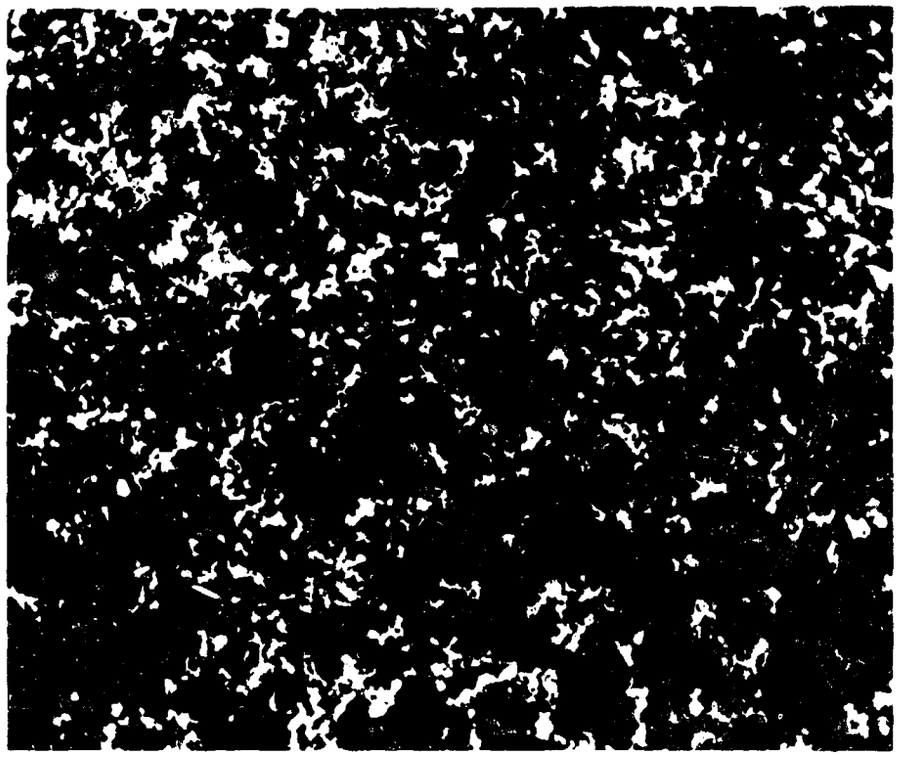

Figure 28. Cross Section of Electrode 50 (Magnified 250X)

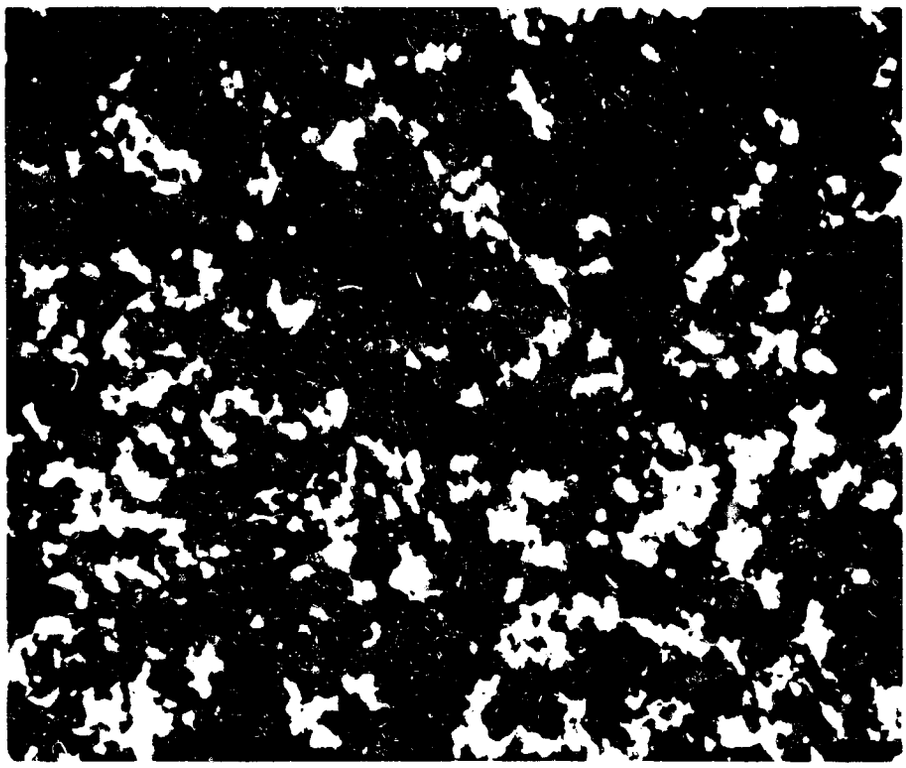

Figure 29. Cross Section of Electrode 50 (Magnified 500X)

Table 26 summarizes the results of the activation by electrochemical precipitation. The weight gains are slightly less than those obtained for the smaller electrodes. After the third precipitation cycle, the electrodes were compressed by rolling them between chrome-plated rollers and then formed in excess 31% KOH by charging them completely, overcharging for about 15 minutes at 3 amperes, discharging completely, and overdischarging for about one hour at 200 ma. After being washed and dried, the electrodes were ready for assembly into the test cells.

Table 26

PREPARATION OF 2.75-INCH BY 5.4-INCH ELECTRODES BY ELECTROCHEMICAL PRECIPITATION

Electrode No.	T_i[1] (mil)	Mole Cobalt in Solution (%)	First Precipitation Weight Gain[2] (g/in^2)	Second Precipitation Weight Gain[3] (g/in^2)	Third Precipitation Weight Gain[4] (g/in^2)	Total Weight Gain (g/in^2)	Total Weight Gain per Electrode (g)	T_f[5] (mil)
59	26.3	10	16.7	6.1	3.6	26.4	10.05	24.8
60	26.4	0	16.9	6.6	3.2	26.7	10.31	25.3
61	26.3	5	15.8	7.7	3.8	27.3	10.44	25.0
62	26.3	15	16.0	8.3	3.8	28.1	10.83	25.0

1) Unactivated plaque thickness

2) 5 amperes for 70 minutes. Weight gains based on T_i

3) 2.8 amperes for 60 minutes

4) 1.4 amperes for 70 minutes

5) After actuation compression and electrochemical formation

After the testing in sealed cells was complete, the electrodes were chemically analyzed to determine the amounts of nickel ions, cobalt ions, potassium ions, and metallic nickel. The results of these analyses are shown in Table 27. The analyses of metallic nickel agreed within ± 1.3% with the original sinter weight, indicating little, if any, corrosion of the sinter during activation and testing. Comparison between the weight gained during activation and the amount of active material, determined by chemical analysis, agreed within ± 1%, except for Electrode 62. The discrepancy with this electrode was 27%. Because the other results for active material and all of the results for metallic nickel agreed so closely, it is assumed that a weighing or calculation error was responsible for the discrepancy. The weight gained during activation was used for utilization calculations for Electrode 62.

Cycling Apparatus. The apparatus used for testing electrode performance during cycling was designed to be adaptable to a wide range of test conditions. From one to ten cells could be cycled in series. By proper choice of the timer motor and gear assembly, the cycle length could be varied from a few seconds

Table 27

CHEMICAL ANALYSES OF 2.75-INCH BY 5.4-INCH ELECTRODES

Electrode No.	Mole Cobalt in Active Material (%)	Mole K^+ in Active Material* (%)	Theoretical Capacity (amp-hrs)**	Final Electrode Thickness (mils)	Increase in Thickness*** (%)	Final Electrode Volume (in^3)
59	8.0	1.7	2.91	30.4	23	0.448
60	0.03	0.7	2.98	31.1	23	0.458
61	2.3	1.3	3.02	29.8	19	0.439
62	12.9	2.0	2.31	30.0	20	0.446
BBS-1	3.0	1.0	3.60	32.1	17	0.472
BBS-2	3.5	1.0	3.48	31.6	15	0.464

*In the fully discharged state

**Assuming 0.289 ampere-hour/g of $Ni(OH)_2$

***Based on thicknesses after formation and after testing

to several days. The ratio of the charge period to the discharge period could be varied from 0 to 1 to 1 to 0. The charge and discharge currents could be made equal by the use of one power supply, or they could be made two values by the use of two power supplies. Charge and discharge currents up to about 10 amperes could be used. Voltage-versus-time curves were recorded for each cell on a Rustrak recorder. The use of one-megohm impedance amplifiers allowed the recording of either cell voltage or the voltage between a reference and one of the other electrodes. Controllers were included in the circuit so that each cell could individually be put on open circuit and by-passed if the voltage being recorded reached either an upper or a lower preset level. Figure 30 is a photograph of the cycling apparatus and six test cells.

Sealed Test Cells. The test cells were constructed of three pieces of Lucite plastic, solvent-bonded during final assembly. One outer piece was a block 4.3 inches by 8 inches by 1 inch. A small well was bored from the inside surface partway through the block and contained a Hg/HgO reference electrode. The reference was positioned at the center of one 2.75-inch by 5.4-inch face of the electrode pack. A pressure gage was threaded into the top 1-inch by 4.3-inch edge of the block. A small hole from the inside surface of the block to the pressure gage hole served to admit gas pressure to the gage and also served as an electrolyte filler hole.

Figure 30. Ten-station Cycling Apparatus and Six Test Cells

The other outer piece of a Lucite plastic block 4.3 inches by 8 inches by 1/2 inch in size. The cell terminals consisted of No. 6-32 stainless-steel screws bolted into the block with the head on the inside. A nylon washer compressed under the head of each screw sealed against leakage. The electrode tabs were welded to the heads of the screws. The third Lucite plastic piece was a frame 3/16-inch thick with 4.3-inch by 8-inch outside dimensions and 2.9-inch by 6.5-inch inside dimensions. This piece was sandwiched between the two outer blocks. Because the electrode packs were generally thinner than 3/16 of an inch, Lucite plastic and fluorocarbon shims were used to fill the excess space.

The electrode pack consisted of one positive test electrode, two commercial cadmium negative electrodes, and four layers of separator. The separator was 37 mg/inch^2, Pellon, nonwoven nylon. One layer of the nylon was placed between the positive electrodes and each of the negative electrodes, and one layer was placed on the outside of the pack. The negative plates had been decarbonated by charging and discharging them in excess 31% KOH, after which they were washed and dried. The separator material had been washed thoroughly in distilled water and was dried before use. The assembled electrode pack was compressed in the cell so that the separator thickness was about 9 mils per layer.

The two commercial positive electrodes, labeled BBS-1 and BBS-2 in subsequent tables, were of the sintered-nickel type used in aircraft batteries. They measured 2.75 inches by 5.34 inches and were coined 0.1 inch along the top and sides. The current collector was nickel-plated, perforated steel. The initial thickness was 27.5 mils. Their nominal capacity in flooded electrolyte was stated to be 3.4 ampere-hours/dm^2 or 7.9 ampere-hours/inch^3 at the C/2 rate.

After the cells were assembled, the electrolyte was added, 11.4 ml of 31% KOH per cell. The pressure gages were firmly threaded into the cells using Teflon* pipe tape on the threads. The cells were then clamped between 3/8-inch thick aluminum plates to help prevent bulging and rupturing of the cells. On one occasion, the internal pressure of one cell exceeded 50 psig, with no leakage. Figure 31 is a photograph of three assembled cells.

Tests of Capacity Maintenance During Cycling. The test cells with the electrodes described in the two previous subsections were given 102 cycles according to the following regime:

1. Cycles 1 and 2. Charged for 6.2 hours at 600 ma and discharged at 600 ma to zero v between the positive and the Hg/HgO reference electrode
2. Cycles 3 to 49. Charged for 3.1 hours at 600 ma and discharged for 2.9 hours. Any cell whose positive-to-reference voltage dropped to

*Trademark

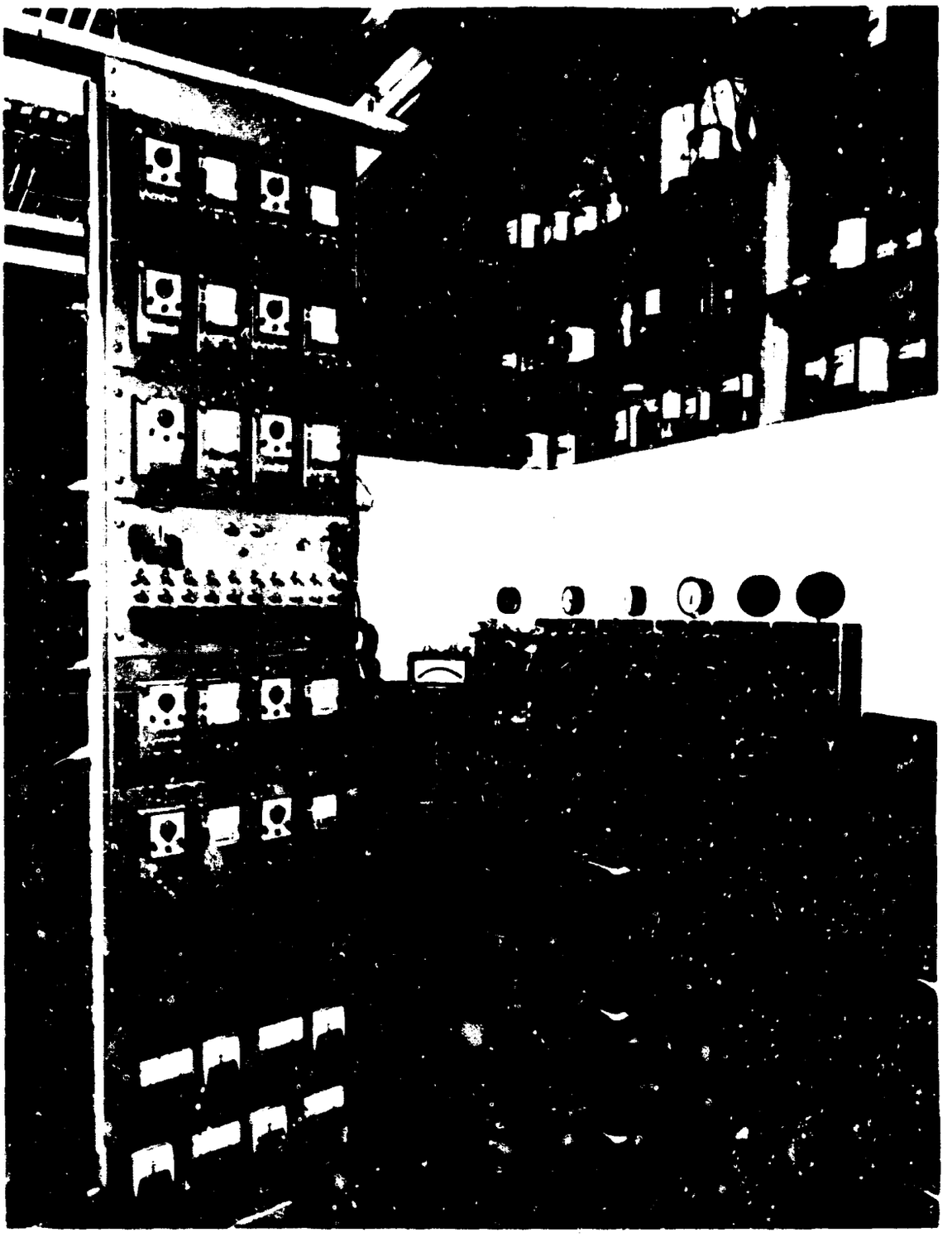

Figure 31. Sealed Test Cells

zero during discharge was returned to open circuit until the start of the next charge

3. Cycles 50 and 51. The same as Cycles 1 and 2
4. Cycles 52 to 99. The same as Cycles 3 to 49
5. Cycles 100 to 102. The same as Cycles 1 and 2

The discharge capacities of the six test electrodes for Cycles 1, 2, 50, 51, 100, 101, and 102 and the final specific capacities are shown in Table 28. The reason for the jump in capacities from Cycles 50 to 51 and Cycles 100 to 101 was that, during the previous 70% depth-of-discharge cycles, the approximate 7% overcharge was insufficient to overcome the inefficient charge acceptance of some of the electrodes and keep them fully charged. Also, a cycler malfunction caused Cell 59 to discharge completely at Cycle 48. The complete discharges of Cycles 50 and 100 and substantial overcharges during Cycles 51 and 101 essentially returned the electrodes to the fully charged state.

Table 28

DISCHARGE CAPACITIES IN AMPERE-HOURS OF 2.75-INCH BY 5.4-INCH ELECTRODES

Electrode No.	Cycle Number							Specific Capacity Cycle 102 (amp-hrs/in.^{3})
	1	2	50	51	100	101	102	
59	2.31	2.30	1.94	2.34	2.06	2.32	2.30	5.12
60	2.46	2.39	1.85	2.29	1.79	2.19	2.19	4.77
61	2.42	2.34	2.00	2.27	1.72	2.33	2.25	5.12
62	2.56	2.58	2.42	2.45	2.31	2.41	2.40	5.38
BBS-1	2.79	2.85	2.25	2.56	1.73	2.45	2.46	5.21
BBS-2	2.80	2.84	2.13	2.58	1.93	2.50	2.51	5.40

Based on final electrode volume. See Table 27

It is tempting to base specific capacities on the thicknesses of the electrodes as they were assembled into the cells. On this basis, the specific capacities based on the Cycle 102 capacity would range from 5.9 to 6.5 ampere-hours/inch^3 for the electrochemically impregnated electrodes and 6.1 to 6.2 ampere-hours/inch^3 for the commercial electrodes.

Figure 32 shows the percent of the first-cycle capacity delivered during Cycles 2, 51, and 102. Electrode 59, with 8% cobalt, maintained its first cycle capacity within 2%. Electrodes 61 and 62, with 2.3 and 12.9% cobalt, respec-

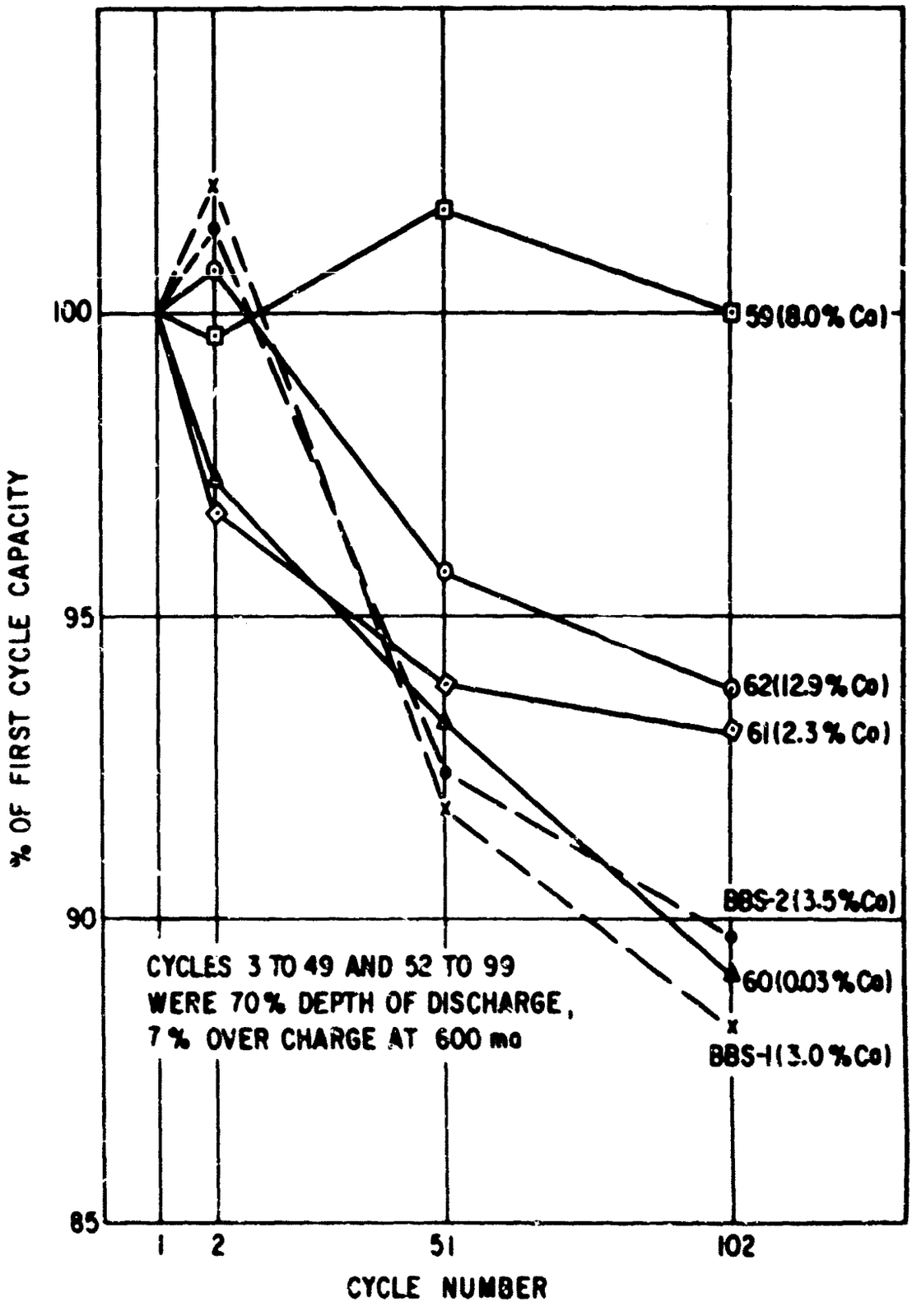

Figure 32. Capacity Maintenance of 2.75-inch by 5.4-inch Electrodes

tively, showed a 6 to 7% capacity loss at Cycle 102. Although the number of electrodes tested were too few to draw hard conclusions, there appears to be an optimum cobalt loading of about 8% for capacity maintenance. Electrode 60, with about 0.3% cobalt, and the two BBS electrodes showed 10 to 12% capacity loss at Cycle 102.

The active material utilization for each electrode for Cycles 51 to 102 is shown in Figure 33. The utilization is calculated using the discharge capacity C and the amount of active material, M, according to:

$$\% \text{ Utilization} = (C \times 92.7 \times 100)/(M \times 26.8)$$

The optimum cobalt level appears to be in the range of 8%. Figures 32 and 33 both show that the BBS electrodes displayed lower capacity maintenance and active material utilization than would be expected on the basis of the levels of cobalt in the active material.

Figure 35 shows charge and discharge voltages at the C/5 rate as a function of cobalt level. The charge voltages were taken at the midpoint of the charge in the sealed test cells and the discharge voltages were taken at the midpoint of the discharge in the flooded test cells. For the electrochemically-activated electrodes, both the charge and discharge voltages decreased with increasing cobalt level. However, the BBS electrodes have higher discharge voltages and lower charge voltages than the electrochemically-activated electrodes with the same cobalt loading.

Tests of Electrode Charging Efficiencies. After completion of the capacity maintenance tests, an additional series of partial charge and discharge cycles were run to determine the charge acceptance efficiency of the electrodes. $Ni(OH)_2$ electrodes evolve oxygen during charge, and the fraction of the charging current producing oxygen increases as the electrode approaches the fully charged state. Because of the tendency to evolve oxygen, the fraction, discharge capacity/charge input, is usually less than one.

The electrodes were tested by charging at 500 ma for a given time then discharging to a cell voltage of 0.9 v. At least two cycles were obtained at each charge input to minimize the effects of previous history. The percentage efficiency, (100 x discharge capacity)/(charge input), was determined for the last cycle at each charge input. The results are shown in Figure 35. The abscissa is the percent of the Cycle 102 capacity (refer to Table 28) delivered for a given charge input. Small variations in the power supply output account for the 101 and 100.5% efficiencies. The order of determination of the points is shown by the numbers in parentheses in Figure 35.

Electrodes 59 and 62, with 8 and 12.9% cobalt in the active material, show significantly better charge acceptance efficiency than the others. The BBS electrodes appear to be less efficient at high states of charge than the electrochemically activated electrodes with 0.03% and 2.3% cobalt.

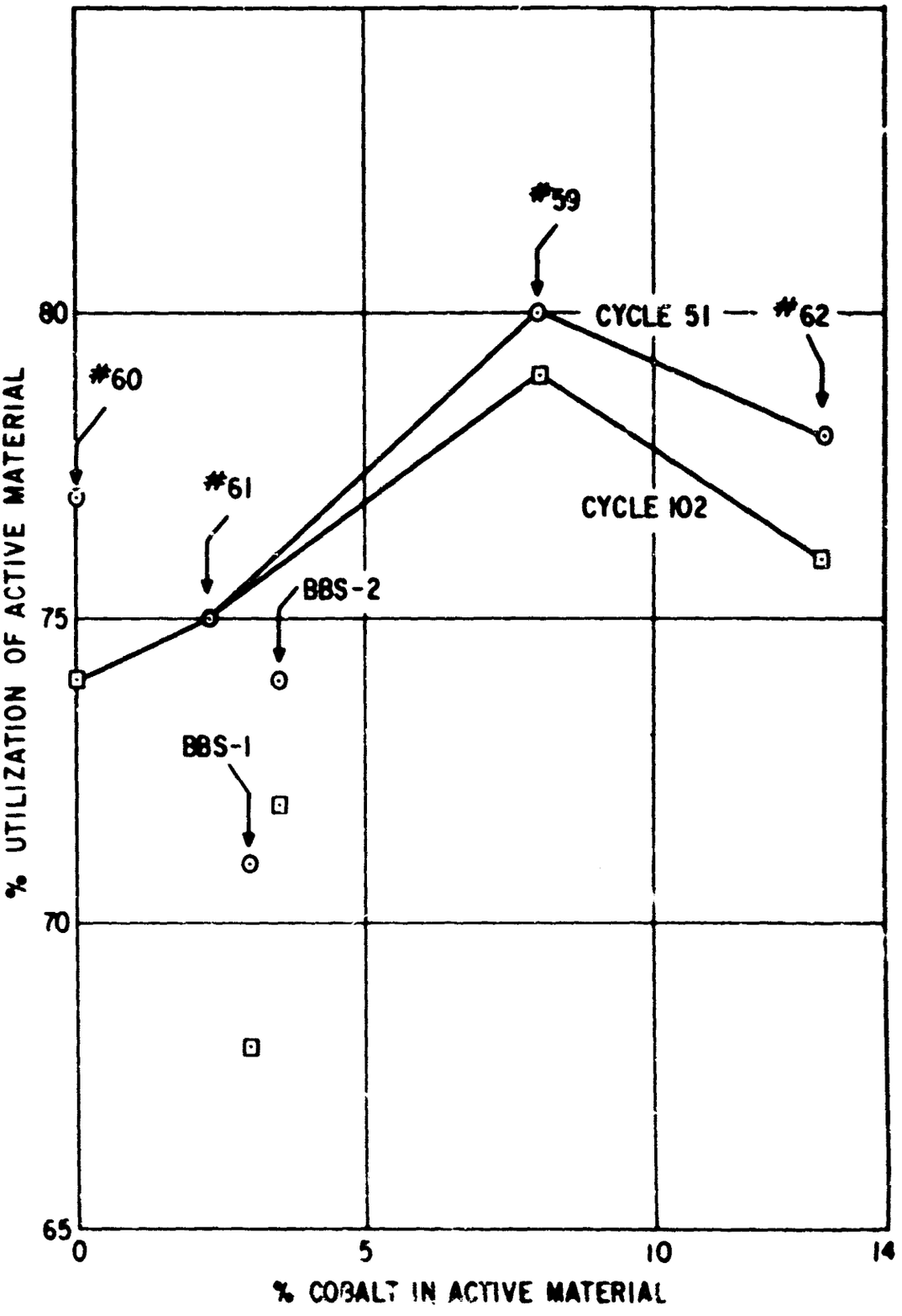

Figure 33. Active Material Utilization as a Function of Cobalt Level

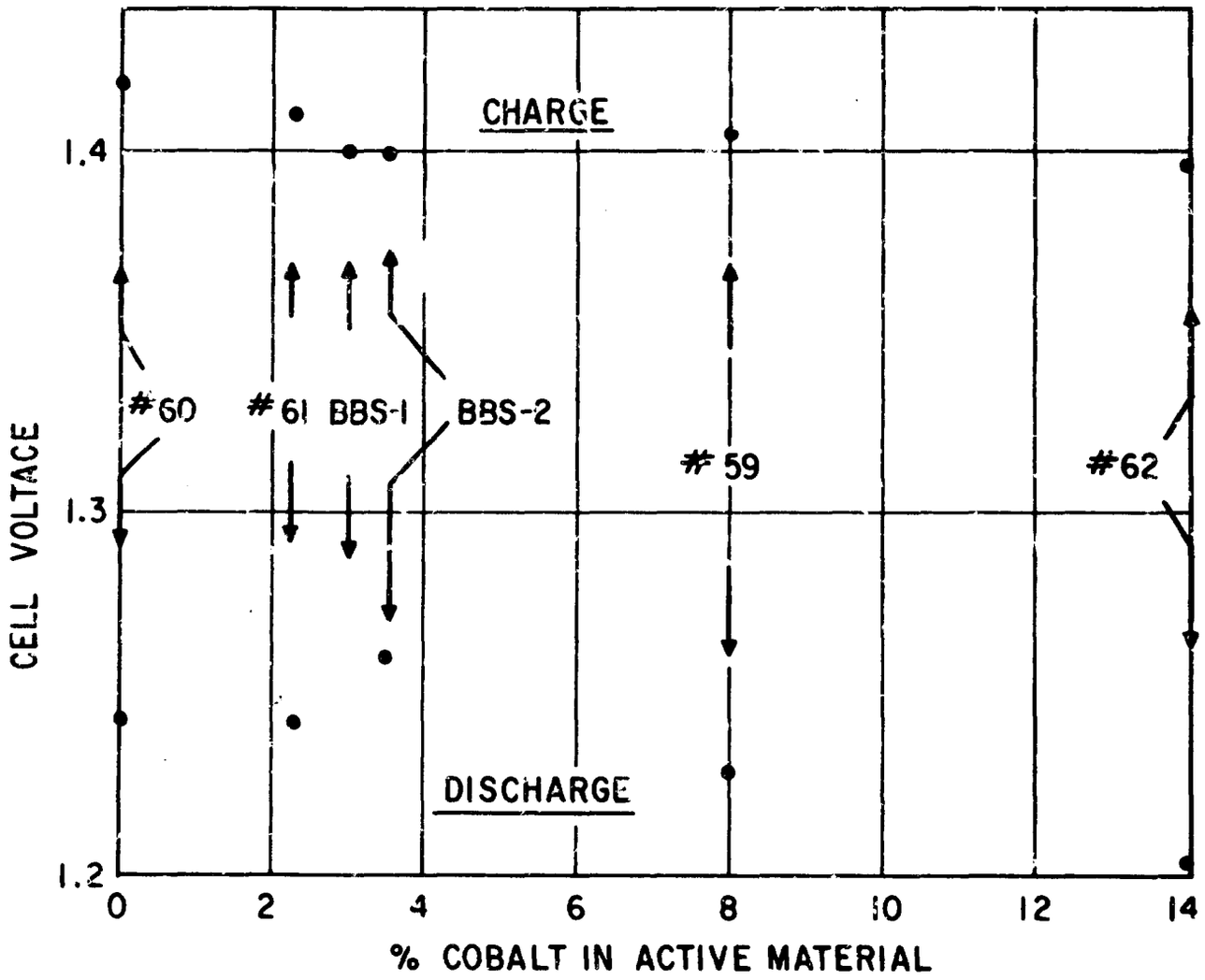

Figure 34. Charge and Discharge Voltages as a Function of Cobalt Level in the Active Material

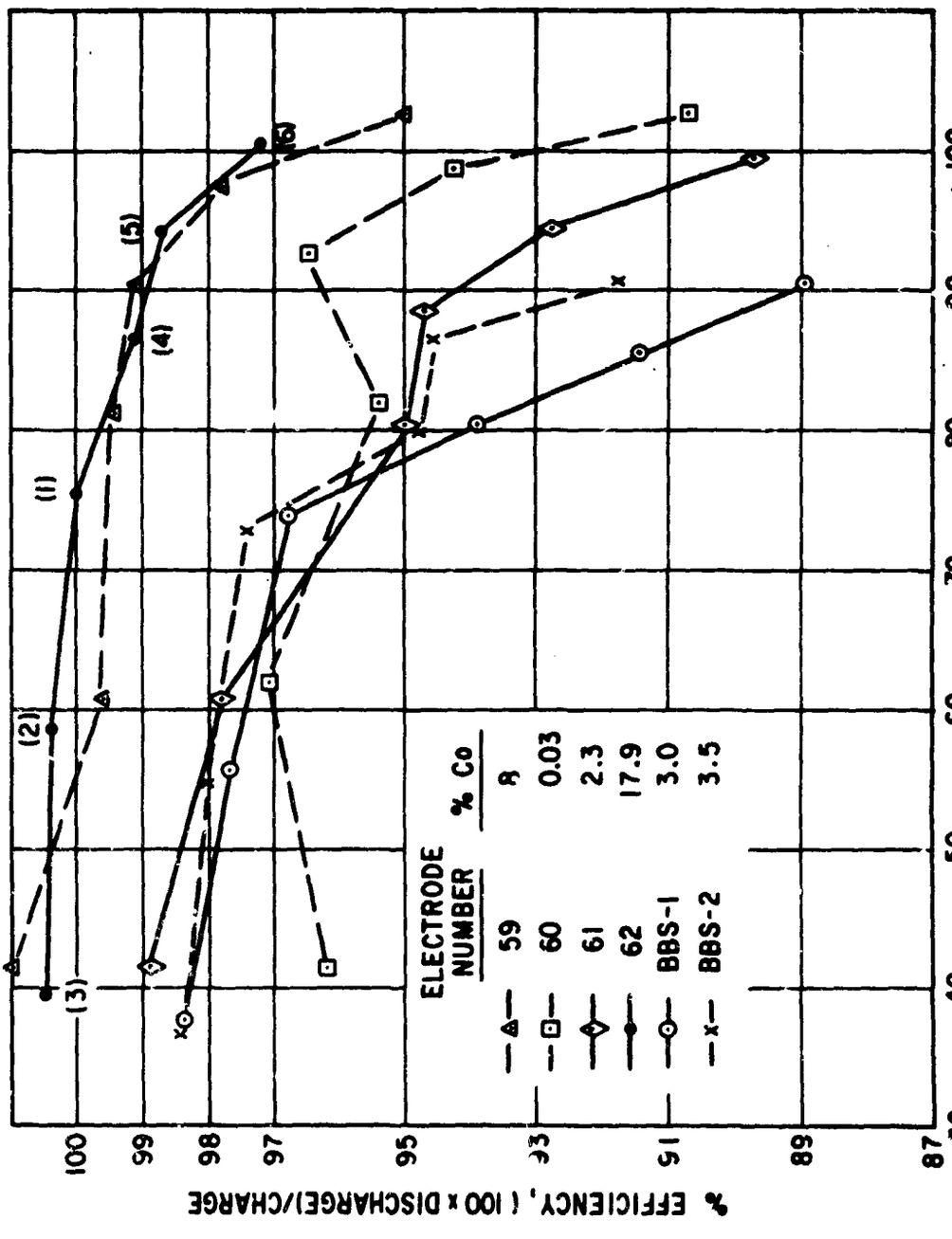

Figure 35. Charge Acceptance Efficiency of 2.75-inch by 5.4-inch Electrodes

Summary

It has been shown that $Ni(OH)_2$ electrodes with about the same specific capacities as commercial aircraft battery positives can be produced by an electrochemical precipitation technique. Electrodes with about 8 mole % $Co(OH)_2$ in the active material showed better capacity maintenance and higher charge acceptance efficiency than the commercial positive plates tested.

The electrochemical precipitation process presents two distinct advantages over the standard impregnation process. The first is reduction of processing time. Three electrochemical precipitation cycles are sufficient to produce active material loadings comparable to those attained in five to eight impregnation cycles. An electrochemical precipitation cycle requires about one hour for the precipitation, a one-hour soak in caustic, and about one hour for washing. If intermediate weight determinations are required, a one-hour drying step would be included. An impregnation cycle requires about the same length of time. The final drying step cannot be dispensed with. The second advantage is that the distribution of additives in the active material is more uniform than in impregnated plates. The active material derived from corrosion in impregnated plates has, if any, very small amounts of the additives included in the impregnation solution.

The 5.1 to 5.4 ampere-hour/inch^3 specific capacity obtained for the electrodes tested in sealed cells is well below the contract goal of 8.0 ampere-hours/inch^3. Some of the results of the tests indicate that the maximum capacity attainable for sealed cells may not be much higher than this. One such result is the swelling of cycled plates indicating that the active material has a much lower density in the charged state and can exert considerable force on the sinter structure of heavily loaded plates. The density of the charged active material, at present unknown, will determine the maximum attainable specific capacity. Another result is that there is considerably less utilization of the active material in the limited electrolyte of sealed cells than there is in flooded cells. Figure 33 shows that active material utilization in sealed cells in 80% at best, and Table 25 shows active material utilizations of about 100% in flooded cells. If the flooded-cell specific capacities shown in Table 24 are reduced by 80%, values from 5 to 5.4 ampere-hours/inch^3, are obtained. These are the same range of values as shown for sealed cells in Table 28.

There is the possibility of improvement of the specific capacities of electrodes activated by electrochemical precipitation. Further refinement of current densities used for precipitation (including experimentation with pulsed currents), the application of vacuum to remove gas trapped in the pores, or the use of surfactants to improve wetting of the plaque structure might improve the distribution and degree of filling of the plaque pore structure.

With respect to the other goals of a 98% charge and of uniform capacity of ± 1% for 200 cycles at 50% depth of discharge, the following have been

demonstrated: charge efficiency of better than 98 to 95% state-of-charge and better than 96 to 100% state-of-charge; and capacity maintenance of ± 1% for 100 cycles at 70% depth-of-discharge.

PASTED ELECTRODES

Introduction

If it were possible to substitute a pasted plate for the use of sintered plate in the fabrication of $Ni(OH)_2$ electrodes and at the same time maintain the energy density, the plate manufacturing process could be substantially improved i.e., by decreasing the number of operations, decreasing production costs, and improving the uniformity of the product. Unfortunately, a viable substitute is not presently available. Furthermore, there is no reason to believe that the sintered structure corresponds to an optimum design so as to preclude all other structures. Consequently, an investigation was conducted on the development of an alternative structure with the intention of either constructing at least a comparably performing electrode, or showning definitively that it is impossible to match the performance of sintered plate.

The pasted structure was selected for study because it is ideally suited for simple, rapid, and economical fabrication. Also, the physical characteristics of the plate and the formulation of the active materials can be altered by minor adjustments in the process steps.

The literature on the fabrication techniques of pasted nickel electrodes is rather meager. The patent literature does describe the various methods for making pasted structures (Ref. 72 through 78). Essentially, they all describe various ways of mixing $Ni(OH)_2$ with a conductive diluent and a binder, activating the binder, and preparing the plate. Another such method is discussed in this report. The differences between the method discussed here and those already patented seem to differ sufficiently so as to suggest a possible patent position on the method. From the point of view of a disclosure of information, the presentation here not only describes the preparation but also presents test data to support the performance claims and gives insights into those critical factors that determine performance.

Experimentation

The active materials to be used in pasted electrodes were prepared in the following manner : 327 grams of $Ni(NO_3)_2 \cdot 6H_2O$ and 36.4 grams of $Co(NO_3)_2 \cdot 6H_2O$ were dissolved and diluted to exactly one liter with distilled water. Then 250 ml of this solution had 240 ml of 22.5% KOH (45% KOH diluted one to one with distilled water) rapidly stirred into it. The result was centrifuged, the supernatent was removed, and the precipitate was washed by stirring with distilled water. This latter sequence was repeated until the pH of the supernatent was about eight. About five washings were required. The collected

precipitate was dried at 150° F, pulverized in a motar, sieved through a 125-micron screen and stored under vacuum. By virtue of the method of preparation, the composition of the active material was 90 mole % $Ni(OH)_2$ and 10 mole % $Co(OH)_2$.

The binder in the pasting process was GAF Ganex* V816 polyvinyl pyrrolodone resin at a 2-weight-%-concentration level. Nickel powder of various sizes and various concentration levels was used as the conductive diluent. The binder and the nickel powder were dispersed in the active material by ball milling.

The preliminary cycling tests were performed at ambient temperature under flooded conditions and in a CO_2-free environment. The cycles were determined by a voltage cutoff established by the oxygen evolutionary reaction during the charging process and selected as 0.10 v versus Hg/HgO during discharge. The charging voltage cutoff was carefully selected to correspond to a stablized condition of overcharge wherein any further oxidation of $Ni(OH)_2$ is insignificant. The pasted electrodes in these tests were prepared on 7-mil, 20-mesh nickel screens having a geometric area (bounded by the edges) of 19.7 cm^2 (1 3/4 inches by 1 3/4 inches) with a tab for electrical connections. They were designed so as to correspond to the specific capacity of 3.75 ampere hours/dm^2 (theoretical; i.e., 0.739 ampere-hour per electrode).

The carefully weighed dry mixes were spread on the nickel screens which in turn were resting on a nonwoven nylon separator material. The electrode material was then wet-mixed to form a paste and spread into a screen. The actual pasting was done on a hot surface (about 160° F) using TFE liners. The hot surface served to increase the rate of evaporation of the water from the paste. This, together with the periodic additions of water, provided a convenient means for maintaining the paste at a workable consistency. At this point, a pressing step was employed as needed. The pressure used was an experimental parameter that is discussed fully in the following subsection. Essentially, the pressing procedure involved: a) a prepressing of the wet-pasted electrode between stainless steel plates (excess water was thereby squeezed out of the matrix); b) drying overnight at 150° F (caution); and c) a final pressing between stainless steel plates to achieve maximum densities (up to 7000 to 8000 psi pressure). The drying step must be done with some caution in that severe dehydration causes the plates to crack and become separated from the screen. Constraining Lucite plastic plates (sandwiching the electrode) were beneficial in maintaining the integrity of the plates during the drying step. When cracking did occur, water was added to the plate and the pasting was repeated. The electrodes were double-wrapped with nonwoven nylon, and sintered cadmium electrodes were used as a counter. Voltage measurements were made versus a Hg/HgO reference electrode.

*Trademark

The experimental method used for the pretest phase was identical with that of the sintered electrode, which is presented earlier in this report. The cathode preparation is the only difference in the method. It involved a pasting, which used a mix containing 50% INCO 255* nickel powder, 2% binder, and 48% active materials spread on a 2.75-inch by 5.34-inch screen (94.8 cm^2) in the manner described above. The amount of actual material used was determined by the theoretical capacity designed into the plate. The pressing procedure is described above.

Discussion

The primary objective of this study on $Ni(OH)_2$ pasted plates was to achieve an energy density comparable to that of a sintered electrode. If this cannot be achieved, the other objectives under the contract would be of no significance as applied to pasted electrodes.

The measurement of utilization as defined here is the ratio of the discharged capacity divided by the theoretical capacity of the plate. The discharged capacity is understood here to be that deliverable capacity resulting after a full charge terminated by a voltage cutoff signal and indicating an inflection in the charge curve. For the purposes of the utilization measurement, the discharge capacity is taken to be the capacity resulting from the reduction of Ni(III) and Co(III) mixture and taken that no contribution was made by oxidation of any of the metallic nickel found in the plate. The values given for utilization must be understood in this context. However, the experimental measurement of the plate energy density is not directly dependent on these assumptions, since the value presumes all available sources of energy. Unless noted otherwise, all utilizations were measured on the tenth cycle of the plate.

It must be pointed out that energy density measurements are based on the initial projected volumes of the electrodes tested. This was done as a matter of convenience in testing; and, in view of the nature of the testing performed, it was also a satisfactory approximation.

As the first step in the experimental program, a series of pasted electrodes was tested at a constant porosity (i.e., 72%) to determine the effect of nickel powder concentration on the utilization of the active material. The porosity in this case was that which ordinarily existed after pasting. The INCO 255 nickel powder used is a product of the International Nickel Corporation having a particle size of about 3 microns. The cycling rate was held at C/15. Table 29 demonstrates that a pasted electrode having a naturally occurring porosity is of no value. The utilizations were so poor that they correspond to energy density in the range 0.14 to 0.33 ampere-hour/$inch^3$.

*Trademark

Table 29

PASTED ELECTRODES -- POROSITY 72%

Electrode No.	Nickel Powder (weight %)	Utilization (%)
1	2	0
2	5	7
3	10	5
4	20	5
5	30	9

Postmortem failure mode analysis showed that the only areas where reaction had taken place was in the immediate vicinity of the nickel wires of the screen substrate. This observation is consistent with the fact that $Ni(OH)_2$ had a high electrical resistivity. The need for a highly conductive matrix was evident. Two ways of achieving this were considered: a) increasing the nickel particle size so as to provide an extension to the nickel screen, and b) compressing the matrix in order to link up the nickel particles already present. Table 30 shows the effect of particle size at constant porosity, and Table 31 shows the effect of porosity at constant nickel concentration and particle size with everything else being equal. In Table 31 the choice of 30 weight % nickel was based solely on the observation that the constant current data showed the lowest resistance overpotential losses. The data to this point was unambiguous in that it demonstrated that the use of large particles in the form of filaments and matrix compression resulted in substantially im-

Table 30

EFFECT OF NICKEL PARTICLE SIZE AT CONSTANT POROSITY (72%) AND CONSTANT NICKEL POWDER CONCENTRATION (30 WEIGHT %)

Electrode No.	Particle Characteristics	Utilization at C/15 (%)
5	INCO 255 nickel powder; ~3μ size	9
8	Metals Disintegrating Company Type 202; 30μ size	9
9	Fiberfil Corporation, "Filamets"* nickel fibers; 0.0015-inch by 0.0015-inch by 0.250-inch filaments	30

*Trademark

Table 31

EFFECT OF COMPRESSION AT CONSTANT NICKEL POWDER PARTICLE SIZE (~3μ) AND CONSTANT CONCENTRATION (30 WEIGHT %) AT C/15 RATE

Electrode No.	Porosity (%)	Utilization (%)
5	72	9
7	38	29

proved utilizations. Unfortunately, further compression was not feasible in either case. Obtaining a porosity significantly less than 72% for the plates containing the nickel filaments was the maximum achievable with the presses available.

Cycling tests of this electrode were disappointing. This was attributed to a decompression of the plate which took place after pressing. This would be analogous to the manner in which a compressed spring returns to its equilibrium position when the restraining force is gradually released. For the electrode, it resulted in a poorly adherent structure. The utilization decreased rapidly with cycle number. Consequently, the use of filaments was eliminated from further consideration. On the other hand, consideration was given to nickel structures that are compressible but would not require restraining forces to maintain stability, i. e., Foametal porous nickel. More will be said about this later.

The general trend of the results obtained up to this point was the apparent need for intimate nickel hydroxide-nickel metal interfacial contact. A further illustration of this is the well-known observation that dry-pressed $Ni(OH)_2$ electrodes are of no value. The attempt during this program to produce such a dry-pressed electrode (having 30% INCO 255 nickel powder concentration) gave a 5% utilization. This can be compared with the 29% utilization of the pasted-then-pressed electrode of the same composition. It is difficult at this stage to even speculate on the nature of the interfacial interaction. However, it is this interaction which is the essence of producing a workable $Ni(OH)_2$ electrode, whether pasted or sintered. It is disclosed here that to produce a pasted $Ni(OH)_2$ electrode, the structure must be compressed after pasting. It must be pointed out that the low utilization observed with the dry-pressed electrode tested may have been caused by the failure of the binder to "set" when placed in the electrolyte. This amounts to a trivial example of a lack of intimate contract between particles.

In order to pursue this idea of intimate active material-to-nickel metal contact, studies of the effect of nickel powder concentrations above 30% were performed. The results were wholly consistent with the hypothesis shown in Table 32. The utilizations and the observed plate energy densities were

encouraging. At this time in the program a decision was necessary as to the composition of the pretest electrodes. On the basis of the data available, the electrode containing 50% nickel powder was selected because of its high energy density.

Table 32

EFFECT OF INCREASED NICKEL POWDER (INCO 255) CONCENTRATION ON COMPRESSED PASTED ELECTRODES AT C/5 RATE

Electrode No.	INCO 255 Nickel Powder (%)	Utilization (%)	Energy Density (amp-hrs/in^3)
7	30	29	1.81
19	40	43	3.06
15	50	58	3.51
16	70	77	2.86

As a parallel effort with the pretest preparation and execution, a Foametal porous nickel substrate having 45 pores per linear inch was impregnated with a mixture of 40% INCO 255 powder and then crushed with a pressure of 20,000 psi. The results were as anticipated. The energy density amounted to 5.07 ampere-hours/inch^3. In fact, it was the best pasted electrode tested so far. A pictorial summary of the results is given in Figures 36, 37, and 38. Pertinent information supplimenting the figures is given in Table 33.

Table 33

REVIEW OF SIGNIFICANT DATA
(All Electrodes: Theoretical Capacity = 0.739 Ampere-hour)
(Electrodes Cycled at C/5 Rate, 0.150 Ampere)

Electrode No.	Substrate	Description*	Thickness (inch)	Porosity (%)	Maximum Discharge Utilization at C/5 Rate (%)	Energy Density (ampere-hours/inch^3)
7	20-mesh, 7-mil nickel screen	30% INCO 255 powder	0.098 (8000 psi)	38	29	1.81
14	20-mesh, 7-mil nickel screen	30% INCO 255 powder; electrode pressed from dry powder	0.024 (8000 psi)	28	Falls apart in KOH; utilization - 5%	Maximum
15	20-mesh, 7-mil nickel screen	50% INCO 255 powder	0.040 (8000 psi)	41	58	3.51
16	20-mesh, 7-mil nickel screen	70% INCO 255 powder	0.085 (8000 psi)	49	77	2.86
18	100-mil thick, 97% porous (45 pore) nickel Foametal	60% INCO 255 powder	0.030 (20,000 psi)	29	67	5.09
19	20-mesh, 7-mil nickel screen	60% INCO 255 powder	0.034	38	43	3.06

* nickel additive + 2% binder + active material = 100%

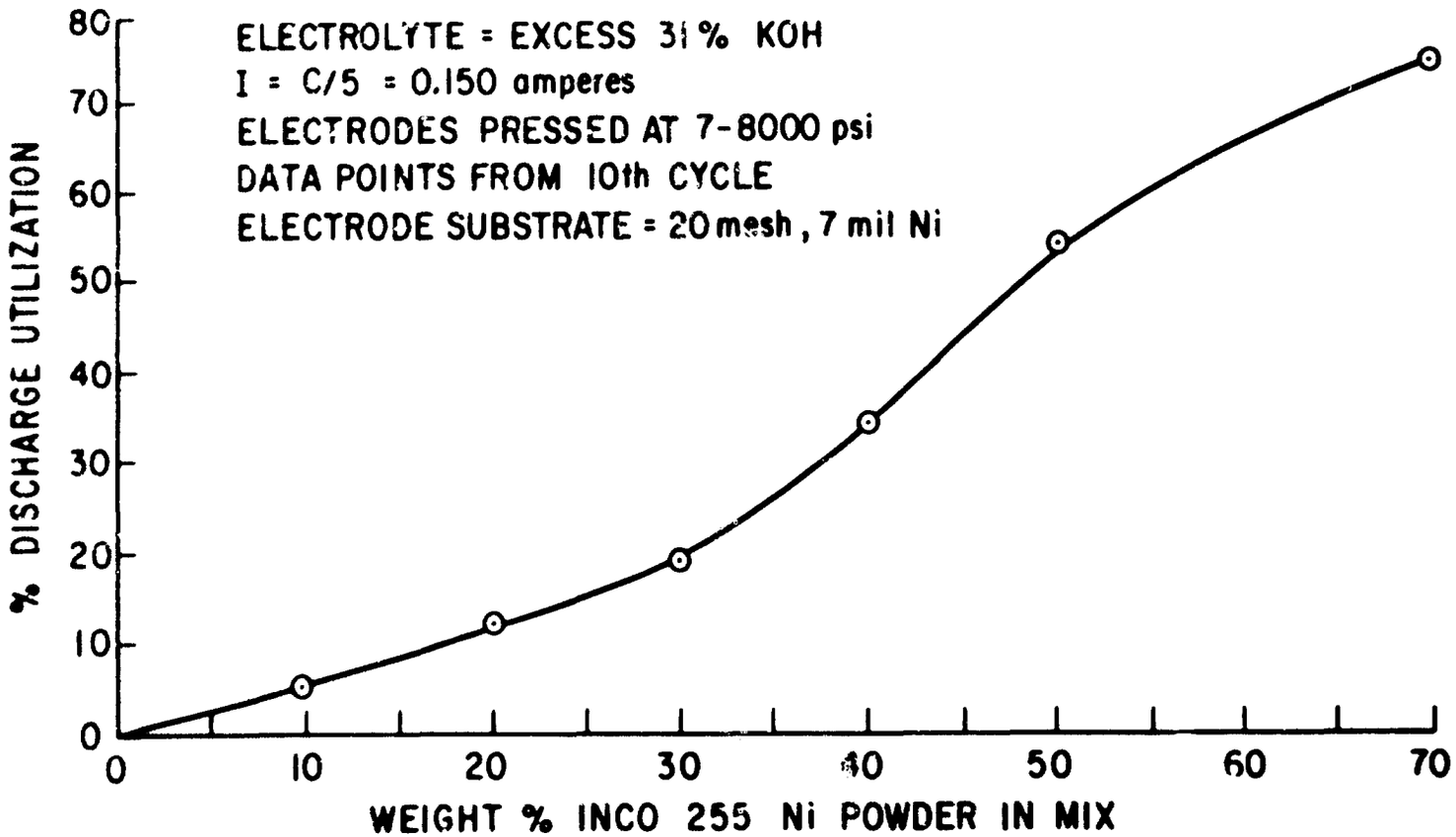

Figure 36. Pasted Electrode Discharge Utilization Versus Weight % INCO 255 Nickel Powder in Mix

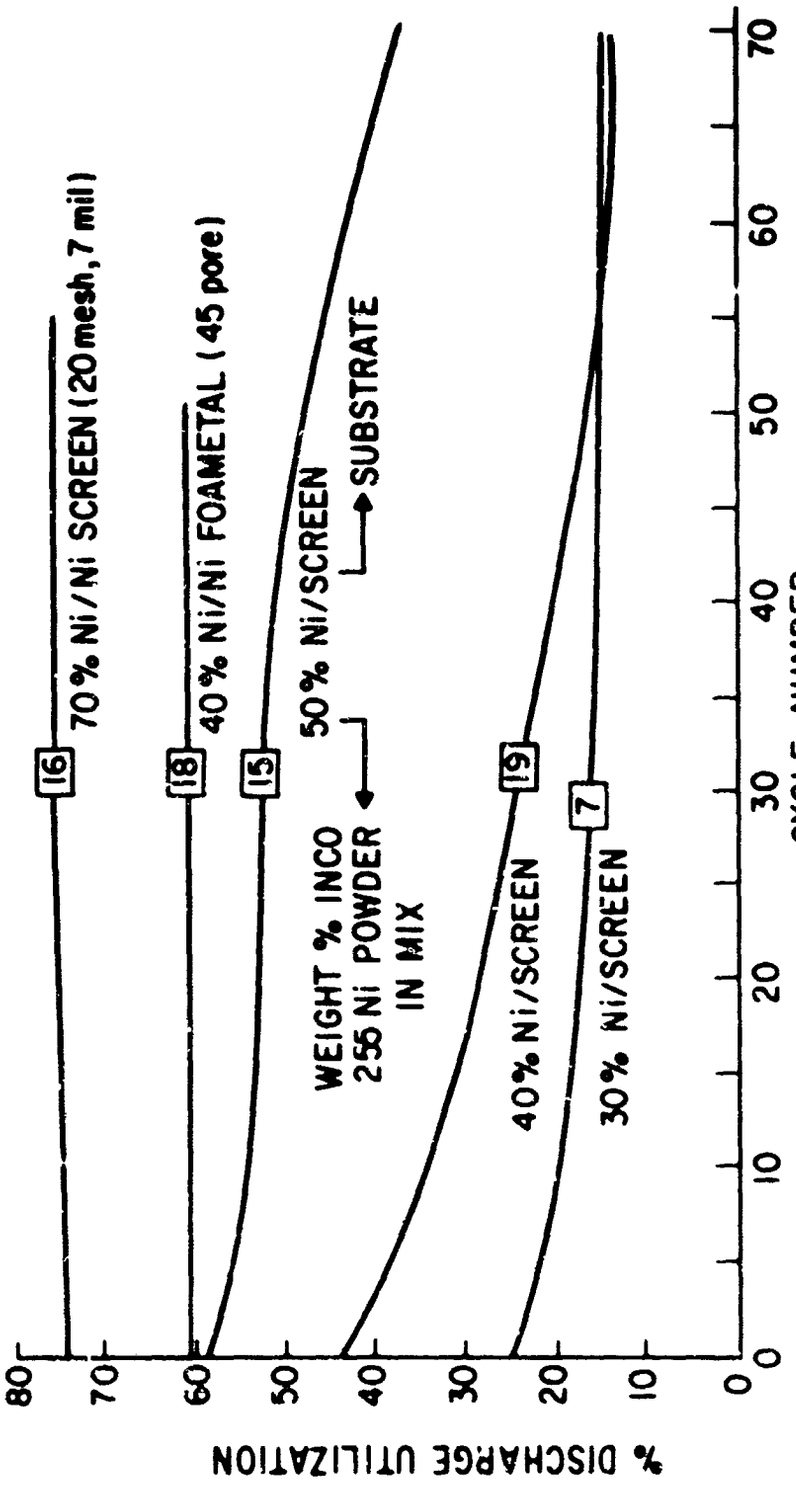

Figure 37. Pasted Electrode Discharge Utilization Versus Cycle Number at C/5 Rate

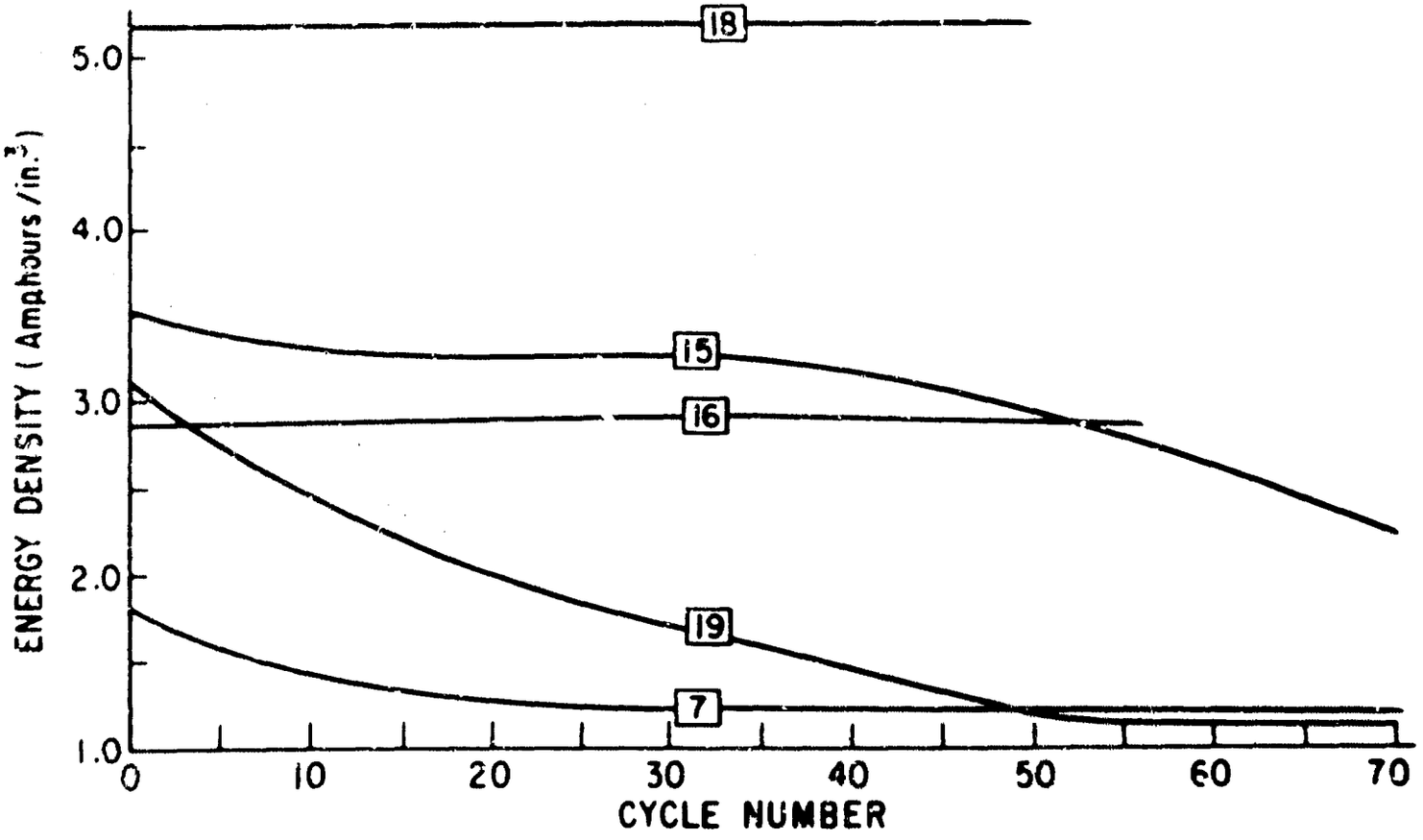

Figure 38. Pasted Electrode Energy Density Versus Cycle Number C/5 Rate

From the flooded cell experiments, it is easily conceivable that a reactive layer exists around each nickel particle. An attempt to assign a layer thickness can be arrived at from geometric considerations. It can be shown as a first order approximation that the reactant layer thickness, t, can be given as

$$t = r_3 \frac{PW_{Ni(II)}\rho_{Ni}}{\rho_{Ni(II)}W_{Ni}}$$

where P is the porosity, ρ is the density of the subscripted species, W is the weight of the subscripted species, and r is the radius of the nickel particle. The obvious conclusion is that a much greater dependence exists on the radius of the nickel particle than on the ratio of the weight of nickel powder to nickel hydroxide. A substantial increase in energy density can be predicted by using smaller particle size together with a decrease in the weight of nickel powder.

With reference to substrate corrosion, the data show nothing. That is, either no significant corrosion is taking place, or it exactly compensates for a loss in capacity on cycling (refer to Figures 37 and 38, Electrodes 16 and 18).

Two sealed pretest cells were prepared. The results obtained to date are given in Table 34. It is readily apparent that the starved electrode in the pretest behaved in a manner almost identical to that studied under flooded conditions. Measurements of capacity uniformity and charge efficiency over 200 cycles await the completion of the test. A postmortem plate inspection will be performed at that time.

Conclusions

The objective of this study on pasted structures was either to prepare pasted nickel electrodes having comparable performance to the sintered electrodes or to demonstrate that this is impossible to achieve. The objective is not yet fully achieved. The results secured so far indicate that a pressed-pasted structure containing substantial amounts of nickel powder (greater than 30%) can, at least under experimental conditions, approach the performance of sintered electrodes (e.g., 5.0 ampere-hours/inch^3). Of course, the proof lies in testing actual cells in the manner of a "head" test. Critical data obtained under these conditions would be definitive.

In lieu of the original objective, it appears highly probable that a pasted $Ni(OH)_2$ electrode can be developed that will match the best performance achievable with sinters.

Table 34

PRETEST DATA AND RESULTS
(Electrode Dimensions: 2.75 inches by 5.34 inches)
(Geometric Area: 14.69 inches^2: 94.75 cm^2)
(Electrodes Pressed at 7000 psi)

Electrode No.	Theoretical Specific Capacity (ampere-hours/dm^3)	Theoretical Capacity (ampere-hours)	Required Amount Active Material (grams)	Amount of 50% Nickel Mix (grams)	Thickness (inch)	Volume (inch^3)
1	3.75	3.55	12.28	25.58	0.046	0.676
2	4.25	4.03	13.94	29.04	0.052	0.764

I = C/5 (Based on Cell No. 1) = 0.70 Ampere
Cycles 1-4: Charge for 6 hours
Discharge 6 hours or to electrode voltage of 0.00 versus Hg/HgO
Subsequent Cycles: 3.2 hours charge
2.8 hours discharge or to voltage cutoff

Cycle No.	Cell No. 1 Ampere-hours Discharge	Utilization (%)	Cell No. 2 Ampere-hours Discharge	Utilization (%)
1	1.54	43	1.50	37
2	1.95	55	1.91	47
5	1.88	53	1.86	46
10	1.81	51	1.85	46
15	1.74	49	1.86	46
20	1.69	48	1.86	46
24	1.69	48	1.84	46

Section 6

MEMORY ANALYSIS

INTRODUCTION

This analysis was undertaken to investigate the type of electrode(s) that contribute to the phenomenon known as memory and the extent of their contribution. In this context, the memory is defined as the temporary loss of capacity delivered above a set cutoff voltage. This loss arises on prolonged highly repetitive cycling at less than 100% depth of discharge. The continuation of discharge beyond the voltage cutoff point gives little or no additional discharge capacity. The end of the discharge voltage at the assigned depth of discharge tends to fall with each successive cycle.

The currently prevailing opinion in the available literature is that the positive nickel electrode is largely responsible for the effects defined above. In order to solve this problem, a combination of electrochemical and wet-chemical analytical methods was selected under the assumption that the appearance of a memory effect somehow also must be reflected in the chemical composition of the electrodes involved.

EXPERIMENTAL APPROACH

Initial Plan

The test cells used were cylindrical, sealed, nickel-cadmium cells with a standard wound construction and a metal cell case. As C_s cells, they had a nominal discharge capacity of one ampere-hour and were built from well-characterized positive nickel and negative cadmium electrode material of porous nickel-sinter construction. Nonwoven nylon was used as the separator, and the electrolyte was 31% (by weight) aqueous KOH solution.

Each cell was equipped with a centrally located reference electrode, consisting of a partially charged piece of positive electrode material. The proper functioning of the reference electrode was monitored at regular intervals. This reference electrode, its conducting wire to the outside, and the epoxy closing of the top section of the cell were deviations from normal factory construction.

Following assembly, the cells were submitted to two charge/discharge cycles for formation and the determination of individual cell discharge capacities.

Cycle 1. Charge for 20 hours at the nominal five-hour rate (C/5) of 200 ma. The average end-of-charge voltage (EOCV) was 1.436 v with a $\pm 1\sigma$ limit of 0.002 v. Discharge at the same nominal rate to 1 v resulted in an average capacity of 1.14 ampere-hours with a $\pm 1\sigma$ limit of 0.007 ampere-hour.

Cycle 2. Charge for 16 hours at 200 ma with an average EOCV of 1.439 and a ± 1 σ limit of 0.002 v. Discharge at 200 ma to a 1.0 v cutoff point yielded an average capacity of 1.14 ampere-hours with a ± 1 σ limit of 0.011 ampere-hour.

The cells were then put on 16 hours of charge at the adjusted five-hour rate (C/5) of 228 ma in preparation for the first cycle discharge with the same current. At repetitive cycle conditions, a three-hour cycle consisted of 72 minutes of charge, 38 minutes of rest, and 60 minutes of discharge, thus providing a depth of discharge of 20% of the average cell capacity and an overcharge factor of 1.2 of the capacity removed.

Fifty-six cycles were acquired per week, and at those time intervals the cells were removed from the test and submitted to analyses. For the first four weeks of testing four cells were taken every time, and from weeks 5 to 10 only two were scheduled for inspection.* Four different cell treatments were executed:

Type A. Monitored discharge of 228 ma to zero v with determination of the discharge limiting electrode. Disassembly of cell in preparation for chemical analysis

Type B. Discharged as with Type A followed by rejuvenation consisting of a 16-hour stand in externally shorted condition and a 16-hour charge at the true ten-hour rate (C/10) of 114 ma. Then nominal discharge and disassembly for chemical analysis

Type C. Monitored discharge as usual. Rejuvenated and returned to repetitive cycling one week later for another group of 57 cycles. Discharge and chemical analysis

Type D. Same as with Type C, however, the second group of repetitive cycling lasted four weeks, or for 225 cycles

Modified Plan

When it became apparent that the repetitive cycling regime failed to induce the memory as expected, two changes were made:

1. After five weeks of repetitive cycling, the weekly sampling of cells for Type A and B treatments was abolished and replaced by monitoring the end-of-discharge voltages. Sampling is scheduled to begin again as soon as significant changes in the end-of-discharge voltage can be detected.
2. After a total of 402 cycles, half of the remaining cells were switched to a ten-hour rate (C/10) regime with a cycle length

*In addition, two cells each were analyzed chemically after closing and after formation discharge.

of six hours, but under continuation of the depth of discharge and overcharge factors as before.

At reporting time, the cells are still on test with 764 five-hour rate cycles and 402 C/5 plus 181 ten-hour rate cycles, respectively.

Chemical Analyses Methods

The chemical methods applied in the analyses of the composition and for the examination of the state of charge of the electrodes were developed in the Battery Business Section laboratories prior to the contract work. They are described in General Electric Company Report No. P3C-PB-105, Test Methods. A brief outline of the methods is given in the following paragraphs.

Sample Preparation. The discharged cells were opened, and all of the parts were removed from the can to be extracted several times with hot distilled water. The extracts were collected and aliquots were used for analysis of the electrolyte. After vacuum drying, the roll was unwound and three samples were cut from each electrode. The locations of the sample-taking were always the same, i.e., at the start of the roll winding, at the middle portion of the electrode length, and at the end of the electrode length. Active material and nickel sinter were removed from the nickel-plated steel substrate, finely ground and stored under exclusion of air. Aliquot parts of about 0.3 to 0.5 g were then used in the subsequent analyses. The respective results were then calculated on a defined area basis.

Total Capacities. Nickel sinter and positive active material were separated by means of a leaching process which only removed the nonmetallic components. In aliquot parts of the extract, the nickel ions were then determined by a conventional complexometric titration. A negative electrode sample was completely dissolved in nitric acid and, in aliquot parts, the cadmium was also determined by a complexometric titration after a masking of the interfering nickel ions. The amounts of positive and negative active material were then calculated as total theoretical electrode capacities.

Residual Electrode Charge. A sample of positive electrode material was reacted with a known amount of ferrous ammonium sulfate in an acetic acid medium. The higher-than-2+ valency nickel components oxidized an equivalent amount of the ferrous ions, while the unreacted portion was back-titrated with permanganate. The difference between the ferrous ions given and back-titrated was then calculated as a residual charge of the positive.

A sample of the negative electrode material was reacted with an excess of ferric sulfate in an acetic acid medium. The metallic cadmium reduced an equivalent amount of ferric ions, which could then be determined by a permanganate titration and calculated as a residual charge of the negative electrode.

Uncharged Electrode Capacity. This is defined for both electrode types as the difference between the total electrode capacity found in earlier chemical analysis and the sum of the electrochemical discharge capacity and the residual electrode capacity found in the residual electrode charge tests.

RESULTS AND DISCUSSION

Discharge Capacities and Voltages

In Figures 39 and 40, typical cell voltages versus time curves for the complete discharge of cells with 228 ma (C/5) are presented. In addition, the discharge curve from the second formation cycle is given, with a mark indicating the formation discharge capacity corrected for the higher current used at the repetitive cycling regime. The time for the regular end of discharge at a 20% depth and the area of halftime through a complete discharge are also marked and serve as control points.

Figure 39 shows the discharge curve of Cell 118 after 281 repetitive cycles and after a rejuvenation process as described above. As can be seen, after 281 cycles the cell voltages were slightly depressed at both control points to approximately 40 and 50 mv, respectively. The discharge capacity to 1 v was about 5% lower than obtained at the second formation cycle. The rejuvenation completely eliminated those differences. The remaining difference in cell voltage between formation and discharge after rejuvenation is caused by the two different discharge currents applied.

Figure 40 shows the situation for Cell 116, which was cycled for 225 times, rejuvenated, and recycled for another 225 times. As can be seen, the depression in cell voltage was identical at the two control points for the two discharge runs, namely, 40 mv at the normal end of discharge and 50 mv at the halftime point. Capacity loss at the first complete discharge was 4%, and 12% of formation capacity after the second sequence of repetitive cycles.

Table 35 contains respective data of all of the complete discharges performed to date. The cell identification number and the number of cycles acquired prior to the first discharge are given. Between the values for the two discharges involved, the cell treatment is also indicated, i.e., rejuvenation R and the number of repetitive cycles of the second regime. This form of coding is also used in the subsequent tables. The column marked "Change in V_{60}" contains the cell voltage drops in mv at the regular end of the discharge, while the column marked "Change in V_{HT}" comprises the corresponding value at the halftime point of the complete discharge.

In the column marked "Change in Capacity," the losses in discharge capacity to 1 v are expressed in percent of the formation discharge value and are sorted for the different treatment conditions. The last line of the table contains some pertinent group averages.

As can be seen, the average of the voltage loss for V_{60} at the normal end-of-discharge was 38 mv and had a $\pm 1\,\sigma$ limit of 6 mv. A comparison with the individual values shows that the treatment conditions did not affect this term. The average voltage loss for V_{HT} at the halftime of a complete

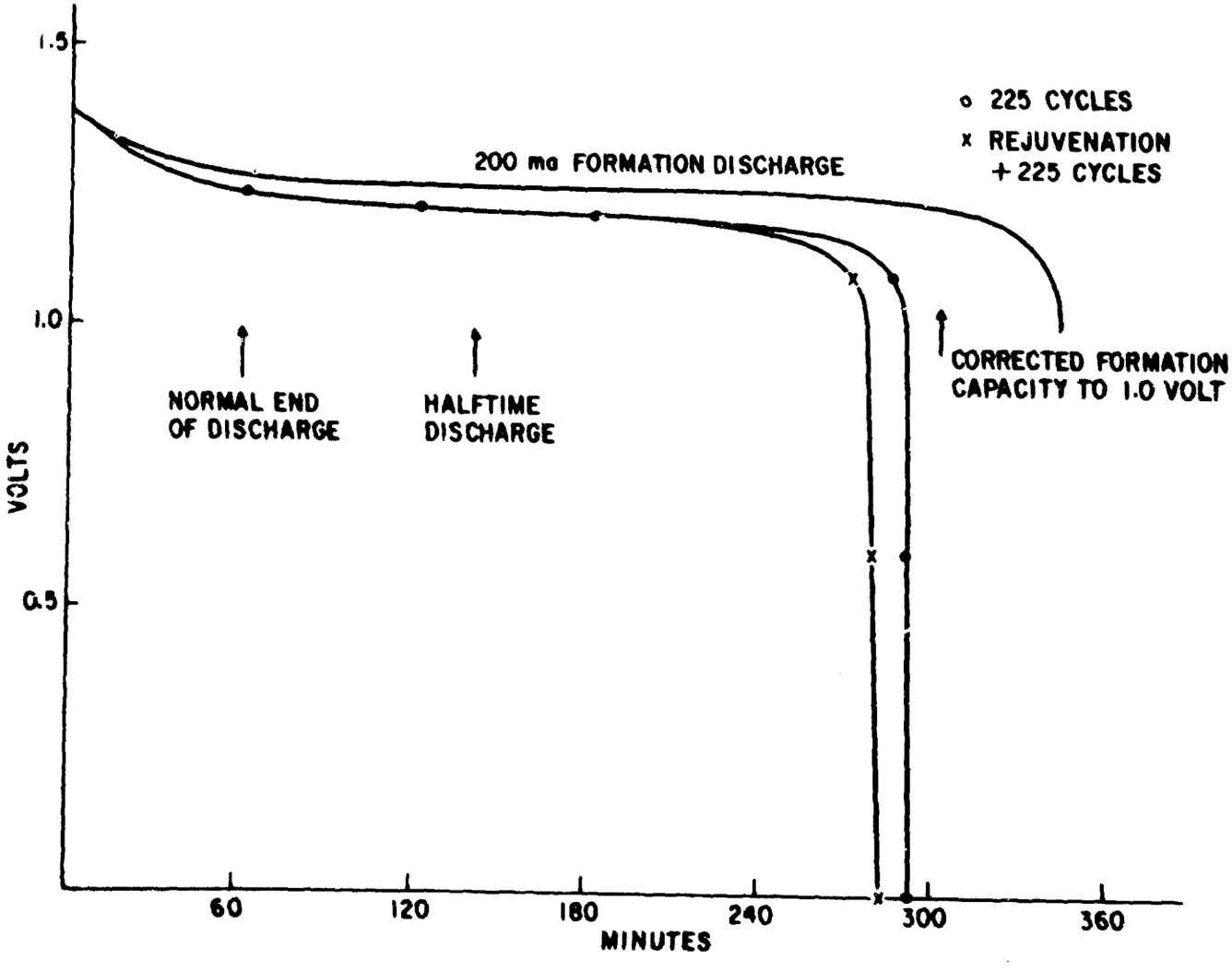

Figure 39. Cell Voltages Versus Time (C/5 Rate and Room Temperature)

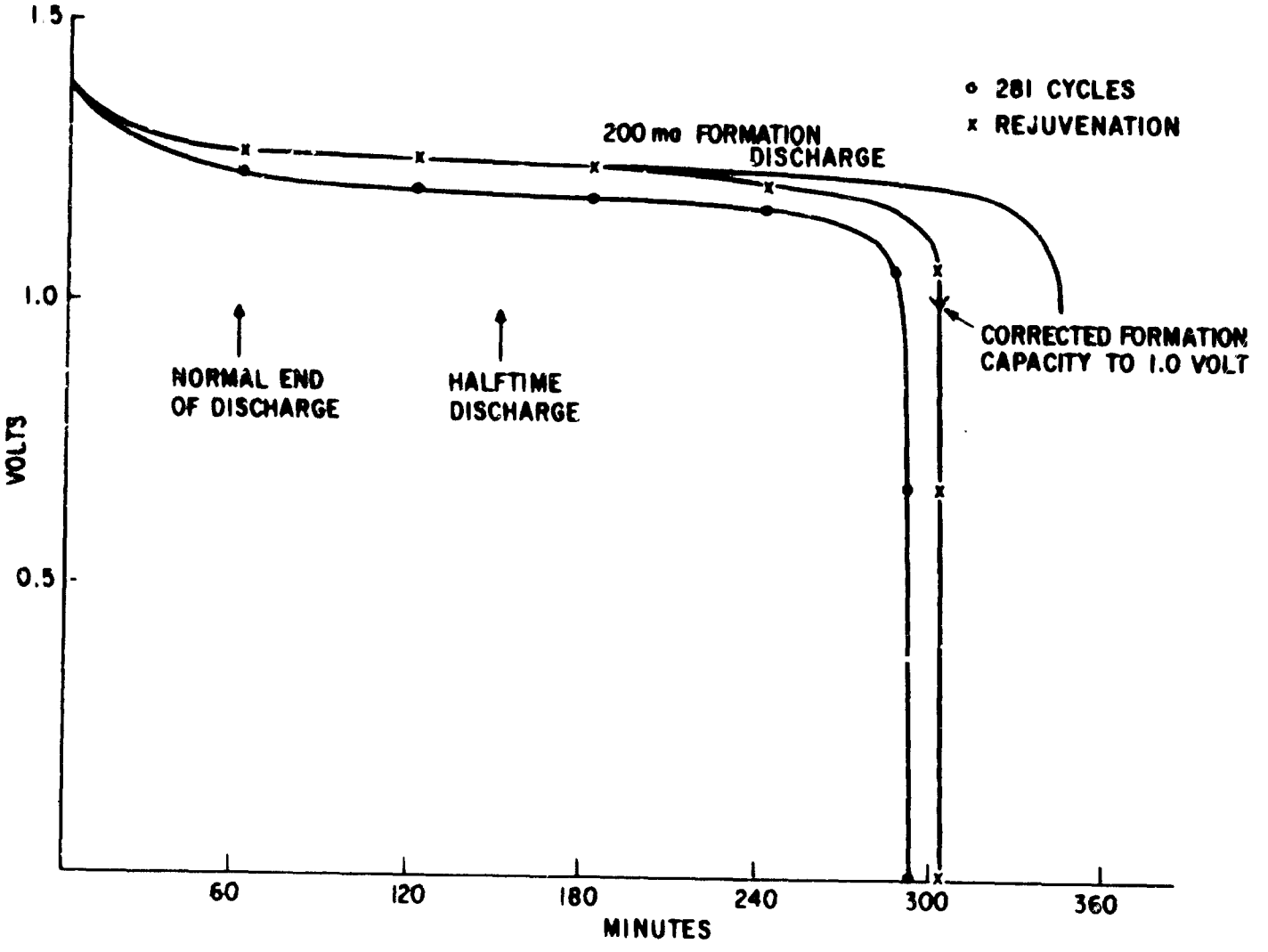

Figure 40. Cell Voltages Versus Time (C/5 Rate and Room Temperature)

Table 35

SUMMARY OF VOLTAGE DROPS AND CAPACITY LOSSES

Cell No.	Cycle No.	First Discharge: Change in V 60 (mv)	First Discharge: Change in V_{HT} (mv)	First Discharge: Change in Capacity (%)	Treatment	Second Discharge: Change in V 60 (mv)	Second Discharge: Change in V_{HT} (mv)	Second Discharge: Change in Capacity (%)
	Close	--	--	--				
	Form	0	0	0				
101	57	30	30	5				
102		30	30	7	R	0	0	2
103		30	40	6	R 57	30	40	7
104		30	40	6	R 225	40	50	12
105	113	40	50	7				
106		40	50	8	R	0	0	0
107		40	50	7	R 57	40	50	9
108		40	40	7	R 225	40	50	13
109	169	40	50	4				
110		40	50	6	R	0	0	1
111		30	50	4	R 57	30	50	6
112		40	50	5	R 225	40	50	13
113	225	40	50	6				
114		50	60	5	R	0	0	1
115		40	50	5	R 57	40	50	8
116		40	50	4	R 225	40	50	9
117	281	30	50	5				
118		30	50	4	R	0	0	0
119	402	40	50	3				
151	402+52*	50	50	7				
	Group Average	38	48	5				1 8 14

*Cycles at C 10 rate

discharge to 1 v was 48 mv and had a ± 1σ limit of 6 mv. A slight increase from an initial value of 30 mv was detected after one week of cycling to 50 mv; however, beyond that no further changes with time occurred. When the rejuvenation treatment was immediately followed by a complete discharge, the cell voltages at the two control points did not differ from the values originally obtained at the formation process.

It should be noted here that in all cases the differences in voltages were caused by the positive electrode and that under the conditions applied this electrode always was the discharge-limiting one. The losses in discharge capacity at a complete discharge were affected both by the rejuvenation process and by the number of subsequent cycles. However, the number of repetitive cycles accumulated prior to the rejuvenation did not influence the dischargeable capacity.

The average capacity loss of 6% after any number of cycles was reduced to about 1% at a discharge immediately following the rejuvenation procedure. The average loss after 57 repetitive cycles following the process was, at 8%, slightly higher than that for untreated cells, but significantly lower than the average of 12% observed for cells with 225 cycles in the second cycle sequence.

Having evaluated the capacities dischargeable to 1 v, capacities dischargeable to less than 1 v were investigated. Table 36 presents the results of these analyses. Column C_{Do} contains the total capacity discharged to zero cell voltage. This is followed by the discharge capacity to 1 v discussed above. The two values given in columns "0.6" and "0.0" are incremental capacities obtained in the ranges 1 to 0.6 and 0.6 to 0.0 v, respectively. The cells were then rejuvenated (R) and recycled for 57 and 225 more repetitive cycles.

As can be seen, there were also losses in the total capacity to zero at the first discharge, but they were apparently independent from the number of cycles obtained. In all cases, the incremental capacities became greater than at formation, but not to such an extent as to compensate for the overall decline in capacity.

At discharges immediately following rejuvenation, not only the capacity to 1 v was improved, as mentioned previously, but also the incremental capacities were reduced towards their initial values at formation. Renewed repetitive cycling after rejuvenation let the incremental capacities grow again with a pronounced effect on the number of cycles of that second sequence.

The following conclusions can be drawn following these investigations.

- Under the conditions applied, the test cells failed to memorize in the assumed sense of the definition, i.e., neither drops in discharge voltages nor losses in dischargeable capacity were significant.

Table 36

TOTAL AND INCREMENTAL DISCHARGE CAPACITIES
(All Values in Ampere-hours/Cell)

Cell No.	Cycle No.	First Discharge C_{Do}	1.0	0.6	0.0	Treatment	Second Discharge C_{Do}	1.0	0.6	0.0
	Close	0.0	0.0	0.0	0.0					
	Form	1.15	1.14	0.003	0.003					
101	57	1.10	1.08	0.013	0.008					
102		1.08	1.06	0.013	0.008	R	1.13	1.11	0.006	0.009
103		1.09	1.07	0.0[illegible]	0.011	R 57	1.08	1.06	0.011	0.011
104		1.09	1.07	0.010	0.013	R 225	1.03	1.00	0.015	0.011
105	113	1.09	1.06	0.008	0.021					
106		1.08	1.05	0.016	0.016	R	1.15	1.13	0.008	0.010
107		1.09	1.05	0.022	0.021	R 57	1.05	1.03	0.008	0.011
108		1.09	1.05	0.020	0.021	R 225	1.03	0.98	0.023	0.023
109	169	1.12	1.09	0.010	0.017					
110		1.11	1.06	0.022	0.027	R	1.14	1.12	0.010	0.009
111		1.13	1.10	0.010	0.015	R 57	1.08	1.05	0.015	0.015
112		1.12	1.08	0.014	0.021	R 225	1.03	0.99	0.021	0.021
113	225	1.10	1.07	0.019	0.011					
114		1.11	1.08	0.015	0.015	R	1.15	1.13	0.008	0.009
115		1.11	1.09	0.011	0.008	R 57	1.08	1.05	0.013	0.014
116		1.12	1.09	0.008	0.023	R 225	1.07	1.04	0.015	0.019
117	281	1.10	1.08	0.011	0.011					
118		1.12	1.10	0.008	0.011	R	1.16	1.14	0.006	0.009
119	402	1.13	1.11	0.010	0.009					
151	402+52*	1.09	1.05	0.022	0.018					

*Cycles at C/10 rate

- The rejuvenation process restored the initial cell performance but only on a temporary basis.
- When repetitive cycling was resumed after rejuvenation, the losses in discharge capacity observed were greater than before and obviously increased with growing number of cycles in the second sequence.
- The so-called incremental capacities of repetitively cycled cells increased considerably over their values at formation and could not be brought back to those initial values by means of rejuvenation.

Chemical Analysis

In Tables 37 and 38, the composition of the positive and negative electrodes is expressed on an ampere-hour-per-electrode area basis. The samples for analysis were always taken from the same locations of the electrodes and were only 10 cm^2 in size. However, the results were scaled-up to the respective electrode size so each sample would represent the whole electrode. The description of the samples on top of Table 37 refers to their relative positions in the wound-electrode pack, with the inside label coinciding with the beginning of the winding.

The column marked "C_{TH}" contains theoretical capacities of the active materials. The capacities were arrived at on the basis of 1×26.8 ampere-hours/mole for positive electrodes and 2×26.8 ampere-hours/mole for negative electrodes. In the column marked "C_R", the residually charged capacities after the discharge to zero volt are found. Inasmuch as those levels were determined by means of well-known chemical redox reactions, no unknown conversion factors were involved in the calculations. Finally, in column "C_u" the portions of the active materials which remained uncharged at the end of the preceding charge period are found. They are calculated by definition as the difference between C_{TH} and the sum of C_{Do} and C_R.

In some of the positive electrodes, a number of cases of negative values for the uncharged portion are observed which naturally have no significance. These negative values can be eliminated when a slightly greater conversion factor than 26.8 mole, or more than one electron involved in the charge transfer, is assumed.

On the other hand, it is interesting to note that negative values are only detectable at the end of cycling and after rejuvenation, but never after recycling. This could support the idea that structural changes are encountered in the active material that affect the efficiency of the leaching process and consequently the values of C_{TH}.

Other observations that can be made are that the level of residual charge was always the highest at the end of normal cycling and declined with rejuvenation. It is difficult to see any influence of the subsequent recycling. Also the

Table 37

POSITIVE ELECTRODE COMPOSITION
(All Values in Ampere-hours/Electrode Area)

Cell No.	Cycle No.	Treatment	C_{Do}	Inside C_{TH}	Inside C_R	Inside C_u	Middle C_{TH}	Middle C_R	Middle C_u	Outside C_{TH}	Outside C_R	Outside C_u
	Close		- -	1.41	0.16	1.25	1.42	0.15	1.27	1.42	0.15	1.27
	Form		1.15	1.40	0.32	-0.07	1.43	0.33	-0.05	1.42	0.40	-0.13
101	57		1.10	1.28	0.33	-0.15	1.29	0.34	-0.15	1.39	0.41	-0.12
102		R	1.13	1.33	0.27	-0.07	1.37	0.28	-0.04	Sample Lost		
103		R 57	1.06	1.32	0.24	±0.00	1.38	0.24	0.06	1.42	0.28	0.06
104		R 225	1.03	1.43	0.22	0.18	1.41	0.23	0.15	1.47	0.22	0.22
105	113		1.09	1.29	0.35	-0.15	1.35	0.34	-0.08	1.30	0.39	-0.18
106		R	1.15	1.25	0.21	-0.11	1.29	0.23	-0.09	1.31	0.24	-0.08
107		R 57	1.05	1.37	0.25	0.07	1.35	0.29	0.01	1.38	0.31	0.02
108		R 225	1.03	1.34	0.22	0.09	1.39	0.21	0.15	1.33	0.21	0.09
109	169		1.12	1.39	0.35	-0.08	1.37	0.36	-0.11	1.39	0.40	-0.13
110		R	1.14	1.29	0.25	-0.10	1.29	0.27	-0.12	1.32	0.29	-0.11
111		R 57	1.08	1.52	0.24	0.20	1.51	0.23	0.20	1.48	0.26	0.14
112		R 225	1.03	1.37	0.23	0.11	1.37	0.24	0.10	1.41	0.24	0.14
113	225		1.10	1.35	0.33	-0.08	1.35	0.35	-0.10	1.38	0.39	-0.11
114		R	1.15	1.32	0.24	-0.07	1.39	0.26	-0.02	1.38	0.29	-0.06
115		R 57	1.08	1.41	0.24	0.09	1.41	0.24	0.09	1.40	0.23	0.14
116		R 225	1.07	1.47	0.28	0.12	1.46	0.24	0.15	1.44	0.24	0.13
117	28*		1.10	1.42	0.30	0.02	1.40	0.34	-0.04	1.45	0.37	-0.02
118		R	1.16	1.45	0.23	0.06	1.42	0.26	0.00	1.44	0.26	0.02
119	402		1.13	1.46	0.29	0.04	1.46	0.31	0.02	1.44	0.35	-0.04
151	402+52*		1.09	1.44	0.26	0.09	1.46	0.29	0.06	1.45	0.33	0.03

*Cycles at C/10 rate

Table 38

NEGATIVE ELECTRODE COMPOSITION
(All Values in Ampere-hours/Electrode Area)

Cell No.	Cycle No.	Treatment	C_{Do}	Inside			Middle			Outside		
				C_{TH}	C_R	C_u	C_{TH}	C_R	C_u	C_{TH}	C_R	C_u
	Close		--	3.10	0.70	2.40	3.13	0.64	2.49	3.08	0.70	2.38
	Form		1.15	3.06	1.27	0.64	3.14	0.99	1.15	3.03	0.75	1.13
101	57		1.10	3.04	1.06	0.86	3.09	0.92	1.07	3.04	0.99	0.95
102		R	1.13	3.26	1.14	0.99	3.04	0.95	0.96	2.15	0.78	1.04
103		R 57	1.08	3.08	1.08	0.92	2.90	0.95	0.87	2.89	0.95	0.86
104		R 225	1.03	3.25	0.82	1.40	3.03	0.87	1.13	3.03	1.48	0.52
105	113		1.09	2.91	1.16	0.66	3.03	0.92	1.02	2.90	0.99	0.82
106		R	1.15	3.05	1.08	0.82	3.05	1.06	0.84	3.04	0.83	1.06
107		R 57	1.05	3.14	0.99	1.10	3.14	1.03	1.06	3.25	1.15	1.05
108		R 225	1.03	2.92	0.85	1.04	2.94	0.84	1.07	2.92	1.22	0.67
109	169		1.12	2.78	1.07	0.59	2.89	0.91	0.86	2.89	1.39	0.38
110		R	1.14	2.81	1.08	0.59	2.81	0.86	0.81	2.88	1.15	0.59
111		R 57	1.08	2.91	1.01	0.82	2.91	0.88	0.95	3.08	1.27	0.73
112		R225	1.03	2.86	0.95	0.88	2.53	0.85	0.95	3.00	1.37	0.60
113	225		1.10	3.06	1.12	0.84	3.07	0.98	0.99	3.14	1.25	0.79
114		R	1.15	2.93	1.01	0.77	3.00	0.91	0.94	3.02	1.47	0.40
115		R 57	1.08	2.73	0.94	0.71	2.84	0.84	0.93	2.84	1.10	0.66
116		R 225	1.07	2.91	1.04	0.80	2.89	0.89	0.93	2.78	1.33	0.38
117	281		1.10	2.90	0.97	0.83	3.00	1.00	0.90	3.04	1.29	0.65
118		R	1.16	2.96	0.97	0.83	2.97	0.88	0.93	3.01	1.29	0.56
119	402		1.13	2.83	0.97	0.73	2.81	0.86	0.82	2.87	1.30	0.44
151	402+52*		1.09	2.81	0.92	0.80	2.78	0.87	0.82	2.77	1.22	0.46

*Cycles at C/10 rate

amount of material with residual charge was apparently enriched towards the outside of the electrode roll. The corresponding analytical results for the negative electrodes are presented in Table 38.

At the moment of closing, the electrode composition was rather uniform with respect to the total amount of the active materials and the charged and uncharged portions thereof. The formation process increased the level of residual charge by almost a factor of two at the inside and by about 50% in the middle portion, while the outside section remained virtually unchanged.

While repetitive cycling apparently leads to stabilization at slightly lower or the same levels in the first two portions, the amount of residual charge in the outside zone increases to such an extent that after 169 cycles the charge distribution in the electrode is the absolute opposite of the stage attained after formation. Rejuvenation generally lowers the numerical values, however, without destroying the respective charge distribution.

Resumption of cycling brings some further reduction at the inside and middle section, while at the outside the trend to imbalance appears more pronounced. Naturally, the changes in residually charged capacity are reflected in the amount of uncharged material available. The latter is also referred to as the charge reserve of the negative electrode. In some instances, this term drops to about one-third of its initial value at formation.

In conclusion, even if changes in electrode composition could be found, they were not severe enough to induce memory. They merely led to insignificant losses in capacity and voltage performance.

CONCLUSIONS

1. Under the test conditions applied, i.e., 20% depth of discharge and 120% overcharge at both the five- and ten-hour rate, the cells did not exhibit any signs of memory even after more than 700 repetitive cycles.
2. Temporary losses and changes in discharge voltages and capacities were almost insignificant and could be eliminated by a single rejuvenation procedure, consisting of external short circuiting and subsequent full charging.
3. All cells tested were positive-electrode-discharge limiting.
4. The residual charge in the positive electrodes increased during the formation process, and its level in the outside portions was slightly higher than in other sections.
5. Negative values for uncharged positive material, arrived at by the defined mode of calculation, disappeared during the second sequence of repetitive cycling, thus indicating a possible change in the composition of the active material.

6. The state-of-charge-distribution of the negative electrodes underwent a marked change, inasmuch as the initially high level of residual charge moved from the inside portions to the outside. This was accomplished between Cycles 113 and 169.

Section 7

CONCLUSIONS AND RECOMMENDATIONS

The major conclusions and corresponding recommendations based on the results of this study are listed below.

1. Additives -- General

Voltametric cycling studies have shown that all deliberate additions of cations (cobalt, zinc, cadmium, aluminum, and lithium) to the active material have a beneficial effect on the performance of the $Ni(OH)_2$ electrode. None of these additives showed any negative effects. Cobalt and zinc were the most effective with regard to high active mass utilization, capacity maintenance with cycling, and charge efficiency, especially at higher temperatures (45°C).

2. Cobalt Additive

The optimum amount of cobalt appears to be between 8 and 10% of the active material. Uniform additive distribution in the active material is essential for maximum efficiency of the additive. Such homogeneity cannot be achieved in commercially impregnated plates which derive a significant portion of their available capacity from corrosion of the nickel substrate. It is recommended that all future electrode preparations in this program be designed to insure an 8 to 10% cobalt addition as standard practice.

3. Zinc Additive

The extent of zinc absorption in the positive plate during operation of a nickel-zinc cell amounts to about 20% of the "active" cation content after about 400 hours of cell operation. This absorption has no detrimental effect on the performance of the nickel electrode. In fact, the voltametric performance of $Ni(OH)_2$ electrodes appears to be enhanced by the presence of ZnO dissolved in the electrolyte.

4. Voltametric Cycling

Voltametric cycling of planar electrodes offers a convenient method for studying the electrochemical aspects of the electrode mechanism. Further experimental work is required to fully interpret the voltametric results obtained from porous electrode structures in terms of actual battery usage. It is felt that such work could lead to useful correlations with more conventional battery tests and that modified voltametric test methods could be successfully used for accelerated life testing or for rapidly evaluating transient effects in electrode processes such as memory.

5. Substrate Material

From technical considerations alone, platinum represents the best possible substrate material for the $Ni(OH)_2$ electrode because of its high oxygen overvoltage and chemical stability. From economical considerations, however, nickel appears to be the only suitable choice of a substrate material. The additional cost associated with the search for other alloys or surface treatments in lieu of nickel is not warrented at this time. If, in the course of the next phase of this program, it is concluded that the rate of nickel substrate corrosion with cycling represents a major obstacle to achieving an improved $Ni(OH)_2$ electrode, this additional cost may be justified.

6. Substrate Interface and Porosity

A high active mass/conductor interfacial area and maximum substrate porosity are the primary requisites for achieving good active mass utilization and high electrode energy density in sintered structures. The physical properties of presently available sintered nickel battery plaque appear to be optimum with respect to these criteria. Little or no improvement in electrode performance is expected to result from any modification in such plaque material or from the use of other forms of porous substrates. The highest electrode energy densities were obtained with sintered substrates having an average pore diameter of about 8 to 12 microns (all other things being equal).

7. Precipitation Technique

The electrochemical precipitation technique developed in this program can be used to produce electrodes with about the same specific capacity as that of commercial aircraft battery plates. The electrochemical technique offers two distinct advantages over the commercial process:

- Three electrochemical precipitation cycles requiring a total of about nine hours versus five to eight chemical impregnation cycles at about three hours per cycle will mean reduction in processing time.
- Distribution of additives in the active material will be improved and little, if any, corrosion of the sinter will occur during activation.

8. Electrode Capacities

Based on initial electrode thicknesses, measured specific electrode capacities obtained in this program were as high as 6.5 ampere-hours/inch^3. The fact that the thickness of all heavily loaded sintered plates increased by about 20% during cycling suggests that the active material has a much lower density in the charged state and that the above value may therefore be near the maximum attainable energy density with sintered structures under sealed-cell conditions.

9. Charge Efficiencies

Charge efficiencies of over 98% were achieved for electrodes charged to 95% of full capacity. When fully charged, efficiencies of over 96% were demonstrated for electrodes containing 8% cobalt additive. Capacity maintenance of ± 1% was demonstrated for 100 cycles at 70% depth of discharge for the electrochemically prepared plates.

10. Sintered Plates

In view of the previous conclusions, it is recommended that work on electrochemically activated sintered plates be continued in order to develop further refinements in this promising fabrication process. These efforts should be aimed at examining in greater detail the effects of other precipitation current densities and conditions, such as pulsed currents, the application of vacuum to remove extrapped gas during precipitation, and the use of surfactants and other additives to the impregnating solution.

11. Pasted Plates

Pasted plates offer the greatest promise from the standpoint of ease of fabrication, production cost, and capacity uniformity. Moreover, alterations in the physical characteristics of the pasted structure can be effected by only minor adjustments in the fabrication process. While the production of such electrodes presently involves a great deal of art, there appears to be a high probability that pasted plates can match (or perhaps even exceed) the performance capability of sintered structures. Since time did not permit a complete evaluation of these electrodes during the present report period, it is recommended that work on this type of structure be continued in order to permit a full characterization of the pasted $Ni(OH)_2$ electrode. Preliminary testing under sealed-cell conditions is underway at this time. A complete determination of capacity uniformity and charge efficiency with cycling will be made for these electrodes shortly. Postmortem analyses will be made in an effort to predict the primary failure mode of pasted structures.

12. Memory

No evidence for memory was obtained after more than 700 repetitive, partial-depth discharge cycles -- a condition which was thought to induce the memory effect most rapidly. Only small, temporary losses in discharge voltage and capacity were found with repetitive cycling, and these were eliminated by a single rejuvination procedure. It is recommended that the present cycling regime be continued until a significant change in the electrical performance of these test cells is observed. At that time, the scheduled postmortem analyses should be reinstated to determine the cause and origin of memory.

Section 8

REFERENCES

1. P. C. Milner and U. B. Thomas, Advances in Electrochemistry and Electrochemical Engineering, (editor, C. W. Tobias), 5. Interscience, New York, New York (1967).
2. U. Falk and A. J. Salkind, Alkaline Storage Batteries, (Unpublished), Electrochem. Soc., New York, New York (1970).
3. G. W. D. Briggs and W. F. K. Wynne-Jones, Electrochimica Acta, 7, 241 (1962).
4. G. W. D. Briggs, G. W. Scott, and W. F. K. Wynne-Jones, ibid., 7, 249 (1962).
5. H. Bode, Angew. Chemie., 73, 553, (1961).
6. H. Bode, K. Dehmelt, and J. Witte, Chemie-Ingenieur Technik, 36, 671 (1964).
7. H. Bode, K. Dehmelt, and J. Witte, Electrochimica Acta, 11, 1079 (1966).
8. G. T. Croft and D. Tuomi, J. Electrochem. Soc., 108, 915 (1961).
9. D. Tuomi, ibid., 112, 1 (1965).
10. D. Tuomi and G. J. B. Crawford, ibid, 115, 450 (1968).
11. D. Tuomi, "Extended Abstract No. 2," Battery Div., Electrochem. Soc. Mtg., Detroit, Mich. (October 1969), p. 12.
12. P. D. Lukovtsev, Soviet Electrochem., Proc. Fourth Conf. Electrochem., Acad. Sci. Moscow, 1956, Consultants Bureau Translation, Plenum Press, New York, New York (1966), p. 156.
13. P.D. Lukovtsev and C. J. Slaidin, Electrochim. Acta, 6, 17 (1962).
14. P. D. Lukovtsev, Elektrokhima, 4, Consultants Bureau Translation, Plenum Press, New York, New York (1968), p. 337.
15. B. E. Conway and P. L. Bourgault, Can. J. Chem., 37, 292 (1959).
16. B. E. Conway and P. L. Bourgault, ibid., 38, 1557 (1960).
17. B. E. Conway and P. L. Bourgault, ibid., 40, 1690 (1962).
18. B. E. Conway and P. L. Bourgault, ibid., 40, 1933 (1962).
19. B. E. Conway, M. A. Sattar, and D. Gilroy, Electrochim. Acta, 14, 677 (1969).
20. M. A. Sattar and B. E. Conway, ibid., 14, 695 (1969).

21. B. E. Conway, M. A. Sattar, and D. Gilroy, ibid., 14, 711 (1969).

22. B. E. Conway and M. A. Sattar, Electroanal. and Interfacial Electrochem., 19, 351 (1968).

23. M. F. Scarr, J. Electrochem. Soc., 116, 1528 (1969).

24. D. M. MacArthur, Electrochem. Soc. Battery Div. Mtg., Abstract No. 253, New York (May 1969).

25. R. J. Doran, Proc. Internat. Symp. on Batteries, Paper (y), Christchurch, 1958.

26. R. J. Doran, Second Internat. Symp. on Batteries, Paper 26, Bournemouth, 1960.

27. R. J. Doran, "Batteries" (editor, D. H. Collins), Third Internat. Symp. on Batteries, Bournemouth, 1962, Pergamon Press, New York, New York (1963), p. 105.

28. E. J. Case, A. R. Bubois, P. E. Lake, and W. J. Moroz, J. Electrochem. Soc., 112, 371 (1965).

29. J. P. Harivel and J. F. Laurent, Electrochim. Acta, 9, 703 (1964).

30. J. P. Harivel, B. Morognat, and J. Migeon, "Extended Abstract No. 164," Battery Div., Electrochem. Soc. Mtg., Buffalo, New York (1965), p. 109.

31. J. P. Harivel, B. Morognat, J. Labat, and J. F. Laurent, "Power Sources 1966," (editor, D. H. Collins), Fifth Internat. Symp. on Batteries, Brighton, 1966, Pergamon Press, New York, New York (1967), p. 239.

32. J. P. Harivel, Thesis, Univ. Strasbourg (February 1969).

33. J. L. Weininger and M. W. Breiter, J. Electrochem. Soc., 110, 484 (1963).

34. J. L. Weininger and M. W. Breiter, ibid., 111, 707 (1964).

35. A. T. Vagramyan and T. A. Fatueva, Zhur. Neorg. Khim., 4, 1959; Chem. Soc. Translation, New York, New York (1960), p. 577.

36. M. Hansen, Constitution of Binary Alloys, Second edition, McGraw Hill Book Company, New York, New York (1958), p. 485.

37. E. Häusler, "Power Sources 1966," (editor, D. H. Collins), Fifth Internatl. Symp. on Power Sources, Brighton, 1966, Pergamon Press, New York, New York (1967), p. 287.

38. E. J. McHenry, Electrochem. Technology, 5, 275 (1967).

39. L. Kandler, U. S. Patent No. 3, 214, 355 (1965).

40. N. G. Klyukina, Zhur. Prikl. Khim., 33, Consultants Bureau Translation, Plenum Press, New York, New York (1960), p. 73.

41. N.G. Klyukina and G.M. Kudryashova, ibid., 36, Consultants Bureau Translation, Plenum Press, New York, New York (1963), p. 475.

42. V.N. Flerov, ibid., 40, Consultants Bureau Translation, Plenum Press, New York, New York (1967), p. 65.

43. P.D. Lukovtsev and G.Y. Slaidin, Zhur. Fiz. Khim., 36, Chem. Soc. Translation, New York, New York (1962), p. 1227.

44. P.D. Lukovtsev and G.Y. Slaidin, ibid., 38, Chem. Soc. Translation, New York, New York (1964), p. 299.

45. B. Cupp, Seventeenth Ann. Power Sources Conf., Atlantic City, New Jersey (1963), p. 106.

46. T.F. Sharpe, J. Electrochem. Soc., 116, 1639 (1969).

47. S. Januszkiewicz, Thirteenth Annual Power Source Conf., Atlantic City, New Jersey (1959), p. 75.

48. G. Feuillade and R. Jacoud, Electrochim Acta, 14, 1297 (1969).

49. P.V. Popat, et al, "Heat Sterilizable and Impact Resistant Ni-Cd Battery Development," Quarterly Report, Jan-March, 1969, Contract NAS-7-100, Texas Instruments, Inc., Dallas, Texas (1969).

50. G.W.D. Briggs, E. Jones and W.F.K. Wynne-Jones, Trans. Faraday Soc., 51, 1433 (1955).

51. Chemical Engineers' Handbook, (editor, J.H. Perry), Third Edition, McGraw-Hill Book Company, New York, New York (1950).

52. F.T. Bacon and P.W. Jones, U.S. Patent No. 3, 167, 457 (to National Research and Development Corporation) (1965).

53. M. Garfinkel and J.L. Weininger, U.S. Patent No. 3, 429, 831 (to General Electric Company) (1969).

54. R.J. Brodd and N. Hackerman, J. Electrochem. Soc., 104, 704 (1957).

55. I.H.S. Henderson, S.G. Ladan, P.L. Bourgault, and B.E. Glover, Defense Chemical Biological and Radiational Establishment Report No. D53-80-08, (Part III), Ontario, Canada (1966).

56. I.H.S. Henderson and S.G. Ladan, Defense Chemical Biological and Radiational Establishment, Report No. D53-80-08, (Part IV), Ontario, Canada (1966).

57. R.G. Black, J.L. Pentecost, and H.S. Moore, Electrochem. Technology, 6, No. 1-2 (1968), p. 20.

58. E.A. Grens and C.W. Tobias, Electrochim. Acta, 10, 761 (1965).

59. L. Belove et al, Final Report No. ECOM02361-F, Contract No. DA 28-043-AMC-02361(E), Sonotone Corporation, Elmsford, New York (1969).

60. P.V. Popat, et al, Seventh Quarterly Report, Jet Propulsion Laboratory, Contract No. 951972, Modification No. 8, Texas Instruments, Inc., Dallas, Texas (1969).

61. G. Rampel, U.S. Patent No. 3,248,266 (1966).

62. P.L. Bourgault, et al, Can. J. of Tech., 34, 495 (1957).

63. C.J. Menard, U.S. Patent No. 3,442,710 (1969).

64. K. Ackermann, et al, U.S. Patent No. 3,281,272 (1966).

65. K. Ackermann and L. Schlecht, U.S. Patent No. 3,269,864 (1966).

66. F.A. Schneider, U.S. Patent No. 3,455,741 (1969).

67. F.A. Schneider, "Power Sources 1966" (editor, D.H. Collins), Fifth Internatl. Symp. on Power Sources, Brighton, 1966, Pergamon Press, New York, New York (1967), p. 309.

68. Y. Okinaka and D.R. Turner, U.S. Patent No. 3,274,028 (1966).

69. F.P. Kober, Electrochem. Tech., 4, 423 (1966).

70. G.W.D. Briggs and M. Fleischmann, Trans. Faraday Soc., 62, 3217 (1966).

71. H.H. Kröger, private communication.

72. F.C. Arrance, U.S. Patent No. 3,287,166 (1966).

73. E.L. Adler, U.S. Patent No. 3,024,296 (1962).

74. S.O. Aulin, U.S. Patent No. 3,305,401 (1967).

75. J.J. Coleman, M.E. Wilke, and C.J. Vander Yacht, U.S. Patent No. 3,317,347 (1967).

76. S.A. Corren, A.S. Louis, and M.A. Coler, U.S. Patent No. 3,009,979 (1961).

77. G.B. Ellis, U.S. Patent No. 3,184,339 (1965).

78. R.A. Herold, U.S. Patent No. 3,108,910 (1963).

Appendix I

BIBLIOGRAPHY

PHYSICAL AND CHEMICAL PROPERTIES OF $Ni(OH)_2$ -- METHODS OF PREPARATION OF ELECTRODE MATERIALS

Bipolar nickel-cadmium cells for high-energy pulses. CA*, 68, 26177s.

Change in the conductivity of $Ni(OH)_2$ and CdO through neutron irradiation. CA, 65, 8128g.

Characterization by optical and electron microscopy techiques of oxidation products formed on dual porosity sintered nickel electrodes. CA, 65, 14836b.

Determination of the solubility of nickel oxide and nickel hydroxide using ^{63}Ni in water, dimethylformamide, and acetonitrile. CA, 67, 68124f.

Effect of the conditions of preparation of the active part of a positive electrode (for accumulator without a commutator segment) on its initial electrical properties. CA, 62, 12745h.

The effect of the electrolyte concentration and the nature of the cation on the behavior of the nickel-oxide electrode. CA, 64, 18953e.

Electrical conductivity of nickel hydroxide. CA, 67, 68434h.

Electrochemical behavior of cobalt oxides in a concentrated alkali solution. CA, 68. 35241k.

An electrochemical method for producing nickel electrodes for storage batteries. CA, 66, 91031n.

Electrochemical sources of pulse power. CA, 69, 102321x.

Electrochemical surface determination on porous electrodes comparison with the Brunauer-Emmet-Teller (BET) surface determination on sintered nickel electrodes. CA, 64, 289e.

An electrolytic impregnation method: Nickel hydroxide electrode. CA, 65, 8325b.

Electron-microscopic and x-ray diffraction study of nickel(II) hydroxide formation during precipitation. CA, 68, 6867p.

Electrophoretic deposition of inorganic substances from organic media. CA, 64, 55f.

Hydrothermal studies of the system $NiO-H_2O$. CA, 65, 14526f.

*Chemical Abstracts, American Chemical Society, Columbus, Ohio.

Infrared spectroscopic investigation of charged nickel hydroxide electrodes. CA, 66, 70791v.

Magnetochemical study of nickel hydroxides. CA, 61, 6516a.

Methods for determining the structural and stoichiometric changes of $Ni(OH)_2$ electrodes during polarization in alkaline electrolyte. CA, 66, 110973q.

Nickel hydroxides. CA, 62, 6114b.

Nickel-oxide electrode of nonlaminated type made by using plastics as binder. CA, 66, 15882a.

Potassium distribution in nickel oxide electrodes. CA, 64, 18953f.

Nonlamellar nickel oxide electrode. CA, 64, 1638g.

Preparation of highly dispersed nickel hydroxide. CA, 67, 67946q.

Production of porous Ni for alkaline-battery and fuel-cell electrodes: practical and economic considerations. CA, 64, 283b.

Properties and some applications of carbonyl Ni powders. CA, 65, 5136g.

Quantitative evaluation of the effect of an acoustical field on the particle size composition of nickel hydroxide. CA, 64, 15007b.

Rapid determination of the nickel content in nickel hydroxide from its moisture content. CA, 68, 9064k.

Rapid method for x-ray determination of the crystal size dispersity of nickel hydroxide. CA, 69, 55094p.

Reaction of copper, zinc, cadmium, and nickel hydroxides with the corresponding metal sulfates, chlorides, nitrates, and perchlorates. CA, 62, 11409b.

Reaction of hydrazine with nickel(II) hydroxide. CA, 66, 111177v.

Semiconducting electrode catalysts. IV. Dependence of the activity of oxygen electrodes based on variable-valence metals on the nature of the promoter ions of alkali metals. CA, 65, 13215g.

Sintered plate-type nickel-cadmium alkaline batteries. VIII. Discharge performance of sintered plate-type alkaline batteries. CA, 69, 64034w.

Solubility of heavy metal hydroxides in water, sewage, and sewage sludge. CA, 62, 7494d.

Solubility of nickel(II) hydroxides in ammonia solutions of ammonium chloride. CA, 69, 80881a.

Structure of porous Ni electrodes manufactured by the method of powder metallurgy. CA, 65, 5136e.

The thermal decomposition of iron(II), cobalt(II), and nickel(II) hydroxides. CA, 65, 1444e.

Thermal decomposition of some metal oxychlorides and hydroxides. CA, 65, 14823c.

Use of freezing in the production of the active material for alkaline batteries. CA, 67, 104511s.

MECHANISM OF Ni(OH)$_2$ ELECTRODE REACTION

Analysis of the charge-discharge characteristics of nickel-oxide electrodes by infrared spectroscopy. CA, 63, 15851g.

Anodic deposition of NiOOH from nickel acetate solutions at constant potential. CA, 66, 15949c.

Characterization of nickel-cadmium electrodes. CA, 66, 91131v.

Charge and discharge mechanism of a nickel hydroxide electrode. CA, 66, 81803b.

Effect of concentration of electrolyte on the behavior of a nickel oxide electrode. I. Physiochemical properties of the nickel oxides-oxygen system. CA, 63, 5229a.

Effects of high-energy protons on selected cells. CA, 68, 26140z.

Effect of inclusion of nickel hydroxide in the active material of the negative plate of a sintered type nickel cadmium battery. CA, 65, 13205c.

The electrochemistry of oxygen on nickel oxide. CA, 63, 10997b.

Electrodes and electrode reactions. II. Relation of the energy necessary to remove an oxygen molecule from charged nickel oxide electrodes in a vacuum and solutions of potassium hydroxide. CA, 66, 81872y.

Electrode potentials and thermodynamic data for aqueous ions. Copper, zinc, cadmium, iron, cobalt, and nickel. CA, 69, 64069m.

Experimental study of the swelling of a lamellar nickel-oxide electrode in a battery. CA, 67, 78351t.

Hydrogen electrode reaction on nickel in alkaline solutions. I. Exchange current of the discharge step. CA, 68, 24036z.

Ionization of hydrogen in porous nickel. II. CA, 69, 7795w.

Mechanism of nickelous oxide electrode reactions. CA, 61, 3914e.

Mechanism of operation of the hydrogen electrode based on Raney nickel catalysts. CA, 68, 92373d.

Mechanism of operation of a nickel hydroxide electrode. CA, 66, 121506r.

Nickel oxide electrode. II. CA, 64, 13755h.

Oxidation of hydrogen on nickel electrodes in sodium hydroxide solution. CA, 64, 3012b.

Oxidation of hydrogen on a partially submerged nickel electrode in the presence of passivation. CA, 64, 291h.

Polarization studies on sintered plate electrodes containing various amounts of $Ni(OH)_2$. CA, 64, 7675h.

Potentiostatic study of surface conditions of nickel electrode in alkaline solution. CA, 66, 61229r.

Properties of the nickel oxide electrode. I. Electrochemical behavior of higher nickel oxides. CA, 67, 49802k.

Properties of a nickel oxide electrode. II. Nature of the phase formed in the charging of nickelous hydroxide in hot concentrated alkali. CA, 67, 70051z.

Reduction of oxygen on rhodium and nickel in concentrated potassium hydroxide. CA, 69, 102443p.

Some chemical factors in the kinetics of processes at electrodes. CA, 67, 69918f.

A study of oxidized surfaces of metals by recording cathode charging curves (copper and nickel). CA, 65, 8328c.

EFFECT OF ADDITIVES ON NICKEL ELECTRODES

Capacity loss of a nickel oxide electrode during continuous operation. CA, 68, 92330n.

Effect of additions of cobalt sulfate on the granulometric composition of nickel hydroxide. CA, 67, 26043z.

Effect of the composition and concentration of the electrolyte on the characteristics of nickel-nickelous oxide electrodes from depleted active masses. CA, 69, 73414x.

The effect of the electrolyte concentration and the nature of the cation on the behavior of the nickel-oxide electrode. CA, 64, 18953e.

Effect of ultrasonics and lithium additives on the particle size of nickel hydroxide. CA, 68, 99030y.

Effects of various additives on the charge and discharge reactions of a nickel hydroxide electrode. CA, 67, 113176p.

Influence of zinc oxide on the polarization of nickel oxide electrode. CA, 69, 73430z.

Lignin as an additive compound to storage batteries. I. Lignin in alkaline storage batteries. CA, 66, 38975x.

Nickel-cadmium batteries. High-temperature effects on sealed Ni-Cd batteries. CA, 66, 110968s.

Potassium distribution in nickel oxide electrodes. CA, 64, 18953f.

Sintered-plate-type nickel-cadmium alkaline batteries. X. Effects of additives on the discharge performance of sintered-plate alkaline batteries charged at various rates. CA, 70, 102392a.

Structure and stoichiometry of nickel hydroxides in sintered nickel positive electrodes. CA, 66, 110891m.

CORROSION OF NICKEL IN CAUSTIC

Cathodic processes during metal corrosion with hydrogen depolarization and continuous renewal of the surface. CA, 68, 45497n.

Construction materials for filtering apparatus in nickel-cobalt production. CA, 67, 35438j.

Electrochemical oxidation at the nickel hydroxide electrode. I. Determination of the rate of oxidation by an electrochemical method. CA, 68, 110781s.

Influence of pH on corrosion and passivation of nickel. CA, 61, 8890b.

Overvoltage on the nickel-hydrogen electrode in alkaline solution. CA, 68, 110801y.

Ni/Cd CELL DESIGN AND ELECTRODE CONSTRUCTION

Additive to the positive electrode in nickel-cadmium batteries. CA, 67, 7522p.

Ambipolar battery including electrodes of identical nickelous composition. CA, 67, 390603g.

Batteries with plastic electrodes. CA, 63, 6615d.

Chemical formation of positive nickel electrodes. CA, 65, 5025d.

Dual purpose electrodes for alkaline storage batteries on polarization cells. CA, 62, 4913g.

Electrodes for secondary storage batteries. CA, 65, 10130c.

Electrodes for electric batteries. CA, 67, 78529g.

Higher oxides of nickel. CA, 64, 17098d.

Improvement in storage batteries. CA, 67, 70072g.

Manufacture of paste containing a metallic powder. CA, 63, 2211f.

Method for increasing the porosity of a predominantly nickel-containing porous electrode. CA, 68, 45613x.

Method of preparing an electrode structure. CA, 65, 3353h.

Method of producing high-porous sinter plates, preferably for alkaline storage batteries. CA, 67, 60356p.

Nickel and nickel-cadmium containing storage battery plates. CA, 67, 60348n.

Nickel cadmium batteries. Performance prediction for Ni-Cd batteries. CA, 66, 91047x.

Nickel-cadmium battery electrode. CA, 67, 17307m.

Nickel-cadmium battery electrodes. CA, 67, 60352j.

Nickel-cadmium battery electrodes. CA, 69, 82942v.

Nickel electrodes for alkaline batteries. CA, 67, 104638p.

Nickel electrode for alkaline batteries. CA, 68, 92479t.

Nickel electrode for electrochemical cell. CA, 64, 1655e.

Oxidation of nickelous hydroxide for alkaline batteries. CA, 66, 71911w.

Paste for the negative electrodes of lead-oxygen storage batteries. CA, 68, 45612w.

Plates for storage batteries. CA, 66, 51684w.

Porous nickel electrodes. CA, 65, 11771b.

Porous nickel plates for batteries. CA, 65, 11771h.

Positive active material for alkaline batteries. CA, 64, 3060b.

Positive active masses for alkaline storage battery cells. CA, 64, 4602f.

Preparation of a compact nickel-cadmium element for electric storage battery cells. CA, 67, 17336v.

Preparation of double-layer electrodes. CA, 69, 32525r.

Process for producing sintered nickel electrode plates. CA, 68, 110854t.

Sealed alkaline battery. CA, 69, 15380x.

Separators for alkaline batteries. CA, 67, 87236m.

Sintered plaques for storage batteries. CA, 67, 87237n.

Sintered plate or sheet for alkaline battery electrodes. CA, 69, 15382z.

Sintered-frame electrodes for alkaline batteries. CA, 66, 91207z.

Storage battery plaques. CA, 67, 7516q.

Zinc anode for alkaline batteries. CA, 67, 78529s.

PATENTS

Rechargeable alkaline cell. Seymour Cherney, Martin G. Klein and Morris Eisenberg (Electrochimica Corp., Menlo Park, Calif.); U.S. Patent No. 3,438,812, April 15, 1969; U.S. Appl. August 25, 1965.

Electrolyte additives for nickel-cadmium cells. Yutaka Okinaka (Bell Telephone Labs, Murray Hill, N.J.); U.S. Patent No. 3,440,099, April 22, 1969; U.S. Appl. November 15, 1966.

Improvements relating to processes for activating the electrodes of alkaline electric accumulators. Hans Winkler (VEB Grubenlampenwerke). British Patent No. 763, 452, December 12, 1956; Appl. October 7, 1963.

Improvements in alkaline type electric accumulators. Montefiore Barak and Harold Britnor Lunn (The Chloride Electrical Storage Company Ltd.) British Patent No. 848, 922, September 21, 1960; Appl. April 2, 1958.

Improvements in or relating to electric batteries. The Electric Storage Battery Company; British Patent No. 870, 697, June 14, 1961; Appl. October 13, 1958.

Improvements of rechargeable Ruben Ni-Zn with porous Ti nitrate battery elements. M. Samuel Ruben (Mallory Batteries Ltd.); French Patent No. 1, 502, 491, November 30, 1966.

Procedure for fabrication of alkaline accumulators (positive electrode). Varta Aktiengesellschaft; French Patent No. 1, 506, 935, December 29, 1966.

Improvements of electrochemical behavior of alkaline accumulators. Varta Aktiengesellschaft; French Patent No. 1, 506, 936, December 29, 1966.

Secondary battery for repeated charge and discharge. M. Harvey Norman Seiger (Gulton Industries, Inc.); French Patent No. 1, 520, 252, April 24, 1967.

Alkaline nickel-cadmium accumulator. Varta Aktiengesellschaft; French Patent No. 1, 533, 613, August 3, 1967.

Electroceposition of sponge nickel. Ian H. S. Henderson and Stephan G. Ladan; Canadian Patent No. 809, 195, March 25, 1969; Appl. June 15, 1965.

Accumulator with alkaline electrolyte. Paul Ruetschi (The Electric Storage Battery Co. Phila. Pa.); German Patent No. 1, 101, 549, March 9, 1961.

Preparation of electrodes for electrochemical use. Gunter Barthel (Pintsch Bamag Aktiengesellschaft); German Patent No. 1, 273, 498, July 25, 1968.

Sealed nickel-cadmium accumulator. Dieter Jander and Manfred Boning (Societe des Accumulateors Fixes et de Traction Soc. An.); German Patent No. 1, 283, 312, November 21, 1968.

Procedure for fabrication of electrodes. J. W. Schuttevaer (N. V. Philips' Gloeilampenfabrieken te Eindhoven); Netherlands Patent No. 6, 613, 587, March 28, 1968.

Preparation by impregnation of active masses into porous nickel oxide electrodes for alkaline accumulators. F. I. Kukoz, Yu. N. Pervushin, and M. F. Skalozubov, Russian Patent No. 223, 862, November 21, 1968.